AMERICAN UNIVERSITY OF BEIRUT

INTEGRATED NUMERICAL MODELLING OF
GROUNDWATER FLOW IN THE UPPER LITANI BASIN:
TESTING THE NEED OF MANAGED AQUIFER RECHARGE

by
REDA ELGHAWI

A thesis
submitted in partial fulfillment of the requirements
for the degree of Master of Science
to the Department of Geology
of the Faculty of Arts and Sciences
at the American University of Beirut
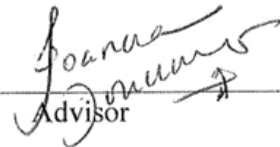
Beirut, Lebanon
June 2020

AMERICAN UNIVERSITY OF BEIRUT

INTEGRATED NUMERICAL MODELLING OF GROUNDWATER FLOW IN THE UPPER LITANI BASIN: TESTING THE NEED OF MANAGED AQUIFER RECHARGE
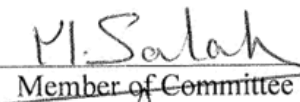
by
REDA ELGHAWI

Approved by:

_____

Dr. Joanna Doummar, Assistant Professor   Advisor
Geology

_____

Dr. Mohamed Salah, Associate Professor   Member of Committee
Geology

_____

Dr. Ibrahim Alameddine, Assistant Professor   Member of Committee
Civil and Environmental Engineering

Date of thesis defense: June 17, 2020

AMERICAN UNIVERSITY OF BEIRUT

THESIS, DISSERTATION, PROJECT RELEASE FORM

Student Name: ___El Ghawi_____Reda_____Marwan___
 Last   First   Middle

⊘ Master's Thesis   ◯ Master's Project   ◯ Doctoral Dissertation

☐   I authorize the American University of Beirut to: (a) reproduce hard or electronic copies of my thesis, dissertation, or project; (b) include such copies in the archives and digital repositories of the University; and (c) make freely available such copies to third parties for research or educational purposes.

☑   I authorize the American University of Beirut, to: (a) reproduce hard or electronic copies of it; (b) include such copies in the archives and digital repositories of the University; and (c) make freely available such copies to third parties for research or educational purposes
after : **One ⸺ year from the date of submission of my thesis, dissertation, or project.**
         Two ----   years from the date of submission of my thesis, dissertation, or project.
         Three ---- years from the date of submission of my thesis, dissertation, or project.

_____   June 30, 2020
Signature   Date

ACKNOWLEDGMENTS

AN ABSTRACT OF THE THESIS OF

Reda ElGhawi   for   Master of Science
                          Major: Geology

Title Integrated Numerical Modelling of Groundwater Flow in the Upper Litani Basin: Testing the Need of Managed Aquifer Recharge

Groundwater resources management has been a growing concern as the consequences of climate change and other anthropogenic forces have heavily impacted freshwater resources, especially in semi-arid regions. The adoptions of managed aquifer recharge (MAR) remains at its earliest stages of assessment in developing countries such as Lebanon. Regional conflicts and the current refugee status have amplified the need for accessible uncontaminated freshwater resources in the semi-arid Bekaa region. At a pilot scale, this thesis investigates the hydraulic properties of a well drilled in the Miocene alluvial consolidated deposits in the Litani Basin, Bekaa in Lebanon, which is devised to store surface runoff during the winter, to be utilized for agricultural irrigation purposes in the summer (Aquifer Storage and Recovery scheme). The small scale subsurface characterization of aquifer properties was done using grain size analysis of borehole cuttings and several pumping tests to assess transmissivity in the recharged aquifer at the borehole scale. In the latter case, water availability poses a challenge on the sustainability of MAR. To answer this question, an integrated hydrological model was constructed and calibrated using MIKE SHE (DHI, 2017a) for the entire Upper Litani Basin (ULB) catchment to simulate flow in steady-state for the years 1970 and 2010 based on existing water level data to evaluate the water balance in the area including lateral and return flow and recharge to groundwater) in comparison to pumping and river exchange. Transient flow was simulated to assess the degree of groundwater depletion, the availability of water resources, and recharge during high flow periods while accounting for the different hydrological components; namely climate, river, saturated and unsaturated zone. The model serves as an integrated decision support tool to predict the change in groundwater levels in the future under climate change scenarios and to ensure proper sustainable water management. Additionally, the testing of the sensitivity of model output to model parameters will help refine model uncertainty and identifies the need for specific additional measurements to be implemented on the ULB.

CONTENTS

ILLUSTRATIONS

TABLES

CHAPTER 1

INTRODUCTION

At present, groundwater resources management has been a growing concern as the consequences of climate change and other anthropogenic forces have heavily impacted freshwater resources (Kløve et al., 2014). These resources play a vital role in sustaining the ecological and agricultural significance in arid and semi-arid regions, therefore impacting the livelihoods of inhabitants in the regions (Sun et al., 2011). As the global population grows, with predictions to reach 9.8 billion by 2050 (UN, 2017), along with economic development and variable consumption patterns, the demand for fresh water is increasing at a rate of 1 % per year and is significantly recognized in countries with developing economies (UNESCO-WWAP, 2019). As such, Lebanon is characterized by the absence of adequate groundwater governance which consequently leads to stress on groundwater resources as a result of the influences pertaining to population growth, urbanization, and climate change on the quality and quantity of water resources in Lebanon (MOE/UNDP/ECODIT, 2011). Lebanon is struggling in managing and sustaining groundwater resources, as described by the renewable resources per capita over 1,100 m^3/capita/year which is severely near the international benchmark of 1,000 m^3/capita/ year (UNICEF WASH Programme in Lebanon, 2017; World Bank Water Sector, 2009). The declining water quality is a result of urbanization and population increase, excess groundwater abstraction for agricultural activities, and pollution. This is particularly prevalent in the Bekaa Valley where groundwater resources are heavily influenced by the

influx of displaced Syrian refugees since 2010, and due to increasing contamination from domestic, industrial, and agricultural point and non-point sources (Chamber of Commerce Industry & Agriculture Zahle & Bekaa (CCIAZ), 2014; Jaafar et al., 2016). The Bekaa Valley accounts for 42% of the total cultivated areas in Lebanon (Food and Agriculture Organization of the United Nations (FAO), 2008) and can be classified into two basins, the Upper Orontes Basin (UOB) and the Upper Litani Basin (ULB), with the latter being the main interest of this research. The largest Lebanese river, the Litani River traverses through the ULB to reach the Qaraoun reservoir. However, 500,000 individuals housed in the ULB depend heavily on well abstraction of groundwater in order to sustain agricultural and food processing activities, especially during dry summer seasons as surface water sources, have been subject to contamination by sources of wastewater, fertilizer applications, and industrial waste that in turn have affected groundwater quality (Assaf & Saadeh, 2006, 2009). Therefore, adequate management and allocation of groundwater resources are needed in order to sustain the livelihood of the local inhabitants, and to protect aquifers from further deterioration and depletion. Previous studies of the water balance of the ULB were conducted in order to show the effect of well abstraction and consumption on the basin's water table focusing on long term monitoring schemes, awareness campaigns and risk assessment (IRG, 2013; Jaafar et al., 2016; USAID-LRBMS, 2014). However, none of the studies proposed the Managed Aquifer Recharge (MAR) scheme as a means to overcome the current deficit and to mitigate future water table decline. Therefore the following research highlights the change in the water balance over the Litani Basin over the years 1970-2013 and shows the impact of MAR on current water governance practices and future management approaches.

1.1 Motivation

Groundwater quality and quantity in Lebanon have been significantly affected by population growth, over-abstraction, and climate change. As such, measures can be taken to overcome and reduce the ensuing consequences by applying Managed Aquifer Recharge Techniques that have become the primary scheme in overcoming the temporary imbalances caused by demand and storage, and countering water quality decline (Ringleb et al., 2016). By applying the MAR scheme at a pilot scale, the changes in water level heads can be monitored with time, providing significant information with regards to the localized water demands and storage which can be then applied on a regional scale. Therefore, such management techniques can be modeled over time to see the impact of applying the MAR scheme on the Upper Litani River Basin. Integrated numerical modeling tools, such as MIKE SHE have been generally used during phases of planning and optimization of MAR systems to provide a comprehensive understanding of the flow system and conditions in the region (Ringleb et al., 2016). As a convention, the main aims of modeling comprise providing a comprehensive insight of the watershed's water balance, the governing physical processes, and the impacts on water quality and quantity (Bachelor et al., 1998). The estimation of the regional water-balance is significant to simulate the major elements governing the water cycle in order to identify the influences of various anthropogenic activities and climate change on the basin's available groundwater resources. The MIKE SHE model will be used to simulate individual components of the water balance of the ULB. Therefore, this research aims to convey the applicability of MIKE SHE on a regional

scale, highlighting the importance of the accurate and representative estimation of the watershed's water balance.

1.2 Research Objectives

The main objective of this thesis research is to quantify and analyze the available groundwater resources in the Upper Litani Basin (ULB) through the use of a fully distributed physically-based hydrological modeling tool in order to assess the sustainable exploitation of the groundwater resources at a regional scale. The evaluation of the applicability of MIKE SHE for simulating hydrological processes in the semi-arid ULB watershed is accomplished by:

1.2.1   Characterization at a pilot-scale (Aana) for the estimation of hydraulic conductivity in a pilot site:

   a) Well drilling and description of cuttings;

   b) Sieve analysis and assessment of grain size distribution in relation to hydrological characteristics;

   c) Well testing for the Neogene via a step drawdown and long term pumping test.

1.2.2   Characterization of flow at a large scale:

   a) Developing a conceptual model for the Upper Litani Basin (ULB).

   b) Constructing a numerical model for the ULB.

c) Calibrating the numerical model at steady-state based on 1970 observation

head measurements and validating the numerical model based on 2010

head observation measurements using standard statistical measures (e.g.

RMSE, ME, MAE, and R^2 values between observed and modeled water

heads).

d) Defining the components of the finalized water balance.

e) Quantifying the response of the water balance dynamics based on the

effects of increased well extractions and climate change based on transient

model simulations.

1.3 Thesis Division

The thesis is divided in such a way that it examines the works applied on MAR

and the applications of MAR in Lebanon in section 2-2.1&B, and a summary of numerical

models performed to date on Lebanese groundwater basins in section II-C. The study site

expands on the catchment area, including vegetation and soil cover, geomorphological, and

hydrogeological aspects of the catchment area in chapter 3. The methodology describes the

field and laboratory applications conducted for MAR (4), which encompass description of

activities related to a pilot well drilling and aquifer testing. Chapter 5 includes a thorough

description of the set of the numerical model, from preliminary water balance, conceptual

model to model geometry, parameterization, and steady-state and transient simulations.

Results of fieldwork, lab analysis, and numerical modeling are presented in chapter 6. The

discussion in chapter 7 elaborates on the variation in groundwater level heads in the area

since 1970, the availability of water resources under future constraints as well as the

expected interaction between surface and groundwater under future pumping scenarios.

Concluding remarks and recommendations are provided in chapter 8.

CHAPTER 2

REVIEW OF PREVIOUS WORK

The adoption of managed aquifer recharge (MAR) has been increasingly expanding as a full-scale operational scheme, conducted and executed globally (Dillon et al., 2019; Stefan & Ansems, 2018). However, this phenomenon remains at its earliest stages of assessment in developing countries, e.g. Lebanon, where few studies on MAR have been conducted especially when groundwater is subject to contamination and depletion due to over-exploitation and the absence of adequate drainage systems (Konikow & Kendy, 2005). Regional conflicts and the current refugee status have amplified the need for accessible uncontaminated freshwater resources in the semi-arid Bekaa region, where water quality is expected to deteriorate further as dry regions become drier (UNESCO-WWAP, 2019), and water availability poses a challenge on sustainability (Schwabe et al., 2013). Moreover, the Mediterranean Basin is highly vulnerable to climate change resulting from anthropogenic activities, as it faces a projected decrease of 10% in average precipitation, according to the Intergovernmental Panel on Climate Change (IPCC) Synthesis Report 2014 (Pachauri et al., 2014).

Managed Aquifer Recharge may be defined as intentional and enhanced infiltration and treatment of water in an aquifer to be potentially later recovered for different usages (Bouwer, 2002; Dillon, 2005). Due to the availability of diversified MAR projects, professionals have been able to maximize efficiency in utilizing, securing, and

treating water resource potential. Management of groundwater resources using artificial recharge techniques can reduce Lebanon's deficit of 27 Mm^3/yr (Imad, 2003).

MAR encompasses diverse methods that can be classified into techniques aiming at intercepting excess water and infiltrating water. This classification can be further divided into five distinct systems which include wells, shaft, and borehole recharge; spreading methods; induced bank filtration; in-channel modifications; and rainwater and runoff harvesting (Huber & Scheibler, 2013; Ringleb et al., 2016; Sprenger et al., 2017; Table 1). As the implementation of diverse MAR schemes has globally reshaped groundwater storage, maintenance, and supply, there remain site-specific complexities regarding the hydrological system and its processes. The key objective is to gain a comprehensive understanding and characterization of the hydrological system through detailed experimentation and investigation by conducting field and laboratory experiments. However, such experimentation does not yield sufficient information about the boundary conditions and domain-related properties. Therefore, modeling based on the calibration of a detailed data set allows quantifying the available water for recharge, the simulation of different recharge scenarios at a smaller scale, and sensitivity analyses on results to enhance the feasibility and applicability of MAR and its location specification.

2.1 Literature review on MAR

Table 1: Summarized Managed Aquifer Recharge (MAR) classification system (adapted and modified from Brunt et al., 2004; Dillon, 2005; Ringleb et al., 2016; Tuinhof et al., 2003).

	General MAR Methods	Distinct MAR Methods	Definition
MAR Techniques principally directed at water infiltration	Well, shaft and borehole recharge	Aquifer Storage and Recovery (ASR)	Injection of water into a well for storage and recovery from the same well.
		Aquifer Storage, Transfer, and Recovery (ASTR)	Injection of water into a well for storage and recovery from a different well, generally, to provide additional water treatment.
		Dry wells, Shallow well/shaft/pit infiltration	Shallow wells where water tables are very deep, allowing infiltration of very high-quality water to unconfined aquifers at depth.
	Spreading methods	Infiltration ponds & basins	Ponds usually constructed off-stream where surface water is diverted and allowed to infiltrate (generally through an unsaturated zone) to the underlying unconfined aquifer.
		Soil Aquifer Treatment (SAT)	Treated sewage effluent is intermittently infiltrated through infiltration ponds to facilitate nutrient and pathogen removal in the passage through the unsaturated zone for recovery by wells after residence in the unconfined aquifer.
		Flooding; ditch; furrow; drains; irrigation	
	Induced bank infiltration	River/lake bank filtration	Extraction of groundwater from a well or caisson near or under a river or lake to induce infiltration from the surface water body, thereby improving and making more consistent the quality of water recovered.
		Dune filtration	Infiltration of water from ponds constructed in dunes and extraction from wells or

	General MAR Methods	Distinct MAR Methods	Definition
			ponds at a lower elevation for water quality improvement and to balance supply and demand.
MAR Techniques principally directed at water interception	In-channel modifications	Recharge dams	Recharge dams —dams on ephemeral streams are used to detain floodwater and uses may include the slow release of water into the streambed downstream to match the capacity for infiltration into underlying aquifers, thereby significantly enhancing recharge.
		Subsurface dams	Subsurface dams— In ephemeral streams where basement highs constrict flows, a trench is constructed across the streambed keyed to the basement and backfilled with low permeability material to help retain flood flows in saturated alluvium for stock and domestic use.
		Sand dams	Sand dams—built in waddies in arid areas on low permeability lithology, these trap sediment when flow occurs, and following successive floods the sand dam is raised to create an "aquifer" which can be tapped by wells in dry seasons.
		Channel spreading	
	Runoff harvesting	Rooftop rainwater harvesting Barriers and bunds Trenches	Roof runoff is diverted into a well or a caisson filled with sand or gravel and allowed to percolate to the water table where it is collected by pumping from a well.

These methods include injection wells, aquifer storage and recovery (ASR), and infiltration basins (Dillon et al., 2009; Figure 1), with the main goal being a subsequent recovery of stored water and counter-balance of falling water levels. Infiltration techniques are utilized to recharge unconfined aquifers, in contrast to borehole injections, which are suitable for deeper confined aquifers (Dillon, 2005). In the present work, the MAR process referred to is ASR, whereby the dual purpose of the wells used for seasonal storage, such that water is injected in the aquifer during low demand or excessive availability, and is recovered during times of high demand. The same or adjacent pumping wells may be used for recovery and storage simultaneously. The latter method enables great flexibility of water management and distribution in comparison to other infiltration methods. Furthermore, ASR does not require extensive operational infrastructure and is proven to be environmentally and economically favorable. The purpose of this research is to provide a preliminary model of managed aquifer recharge in the Southern-Western Bekaa region, Lebanon.
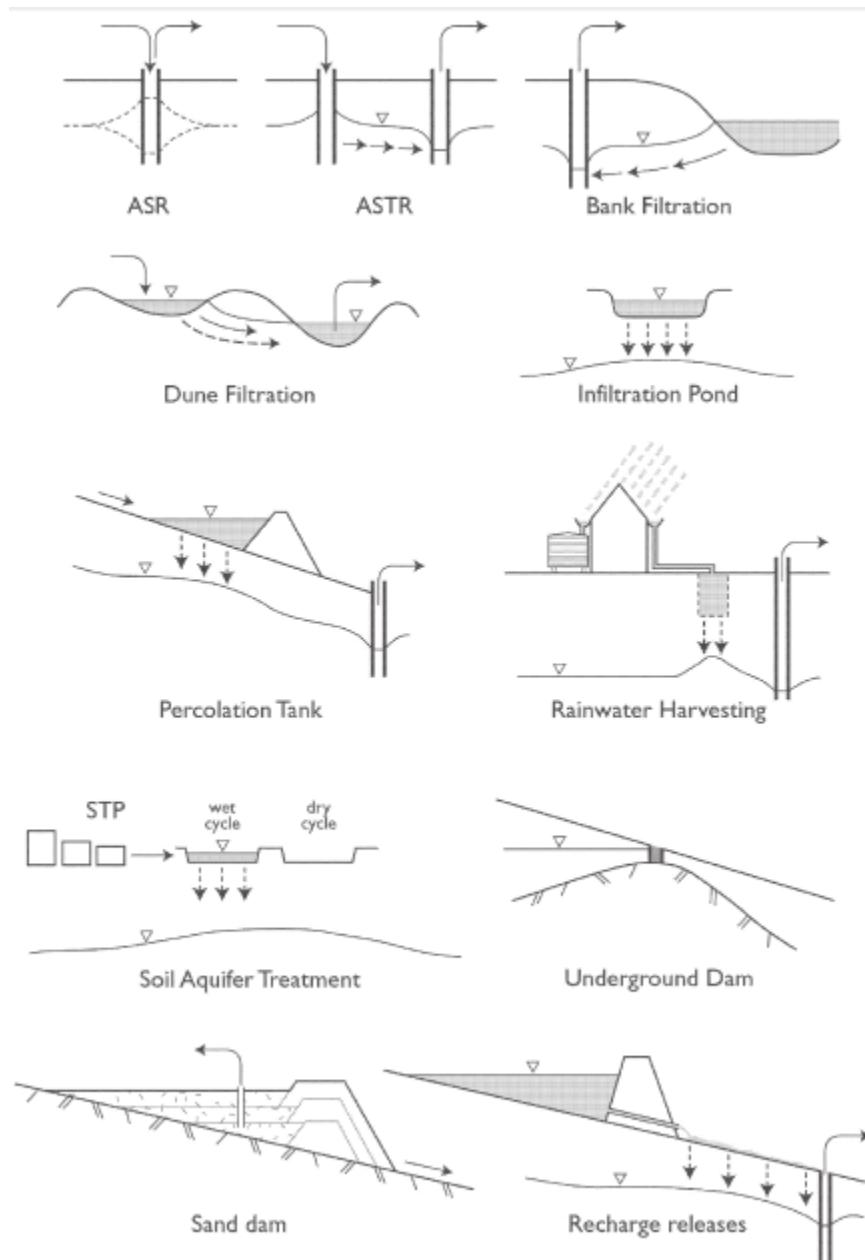
Figure 1: Visual representation of MAR schemes. Adapted from Dillon (2005).

2.2 Applications of MAR in Lebanon

Integrated Water Resources Management (IWRM) research has been conducted since the late 1960s in Lebanon as evident in the work of Massaad (2000), where the

purpose of the research was to mitigate the effects of aquifer salinization as a consequence of saltwater intrusion into the karstified coastal aquifers of Hazmieh-Hadath area. A MAR project was proposed consisting of an Aquifer Storage and Recovery system (ASR) utilizing water from the Beirut river. Preliminary tests were conducted in the early 1970s; however, actual operations did not begin implementation until the early 2000s. Updated information on the current functionality of the system reveals that the system was being operated for 6 months a year with an approximate injection rate of 500 m^3/ hr, according to the Mount Lebanon Water Authority; recently, in 2019 a field visit to the site revealed that the site has been covered and is no longer operational. Back in 2012, a detailed follow-up, and monitoring of the wells in the vicinity of the local well, reveals that salinity levels have not decreased despite the recharge from an upstream source (UNDP, 2014).

Daoud (1973) conducted pilot MAR experiments in the Hazmieh, Beirut area through artificial recharge techniques, which undertakes well injection or infiltration of surface water in existing non-operational or dry wells to deter and reduce seawater intrusion into the karstic limestone Cenomanian aquifer. Methods included four recharge operations with a total recharge volume injection ranging from 400,000 m^3 (12,500 m^3/d) and 852,774 m^3 (16,000 m^3/d). This amounted to more than 1,200,00 m^3 during the period between 1969 -1970, whereas 3,400,000 m^3 was injected during the winter of 1970-1971, with continuous injection ranging from 10 to 210 days. Neighboring observational wells were used to determine the effect of artificial recharge on the aquifer by analyzing piezometric heads, chloride ion concentrations, and water hardness. Despite limitations posed by monitoring constraints, there was a visible reduction of chloride concentrations (by 50%) and an increase of the groundwater table level in the observational wells at a level of 1.2 m

and 450 m distance from the injection wells. Though, there was no perceptible change in groundwater table level at a distance of 5.5 km from the infiltration well. The recovery of recharged water was up to 94% for volumes reaching 400,000 m^3. The recovery rate decreases with increasing recharge volume as a consequence of discharge through springs considered to be a partial loss of the recharge volume. Intermittent borehole injections were conducted within short intervals of the wet period in 2000. Nonetheless, further investigations and recommendations include proper continuous monitoring and pumping tests to accurately evaluate and quantify aquifer properties, the total volume of recovery and storage, recharge capacity of the aquifer, and the influence of saltwater intrusion.

A Water Resources Model (WRM) was designed to assess the efficiency of a baseline model scenario and to optimize different scenarios and processes of the Lower River Litani Basin downstream from the Qaraoun Reservoir (Doummar et al., 2009). The varying simulations and conditions of scenarios were evaluated based on the SWOT analysis (Strengths, Weaknesses, Opportunities, and Threats). Strengths and weaknesses included sufficient capacity of water in the river; however, this is overturned by the inadequate exploitation, unsanitary waste disposal and contamination, and absence of monitoring and regulations. Threats and opportunities include agricultural and hydroelectric prospects and increased pollution, lack of awareness and water quality and quantity deterioration. Two scenarios were simulated based on infrastructural propositions and water-based demand. The proposed infrastructure consists of two dams to allow the retention of water and reduce losses or infiltration to groundwater. Water-based demands include the use of sophisticated irrigation equipment and techniques to consume water more efficiently. Based on this study, it was concluded that combining the scenarios and using

14

multi-disciplinary approaches can proficiently increase the development and sustainability of water resources in order to sufficiently manage the water resources,.

Investigations of MAR in Lebanon by Masciopinto (2013) encompass the examination and design of well barrier to reduce saltwater intrusion in the fractured carbonate coastal aquifers of Damour-Jiyeh area. The groundwater flow and freshwater-saltwater interface were modeled based on the Ghyben-Herzberg theory, and simulations were validated by field transmissivity and depth measurements conducted at 44 wells. A proposed solution of 3 well injection barriers was suggested, where recharge volumes and barrier locations were defined by groundwater flow simulations. Injection of water can remove colloids, however, it may cause clogging and reduction in permeability during water infiltration into the subsoil. Furthermore, MAR and soil aquifer treatments were used to investigate soil-rock interactions, permeability, and mixing of injection water using reclaimed water. Rock permeability reduction varied according to water quality used in injection, recharge rates, and number and frequency of injection wells.

Another investigation conducted by Daher et al. (2011) along the coastline of Damour region undertakes a conceptual methodology for Aquifer Rechargeability Assessment in Karst (ARAK) which determines the most suitable surface sites by which a given karst aquifer can be artificially recharged and maintained since karst conduits pose a challenge of fast drainage without storage and no infiltration. The model is based on four criteria characterizing indices of karst vulnerability, which include the Epikarst, Rock, Infiltration, and Karst. The criteria are distributed along the gridded domain using topographic and geological maps. The intrinsic rechargeability index is computed using a linear expression coupled with a weighting rate and indicates the recharge capacity for a

karst aquifer by firstly considering its occurrence on a regional scale and then by choosing

the most suitable sites. Consequently, an economic and technical feasibility factor is used

for the selected sites and weighted by the operational complications that may be

encountered when surface recharge is functional. The product of these two factors, the

intrinsic rechargeability, and the feasibility index, produces a rechargeability index defining

each site. The ARAK methodology has proved to be a reconciliation between practical and

theoretical complications encountered when analyzing karst aquifer for MAR operations

that may offer solutions to mitigate saltwater intrusion and manage water supplies.

A study conducted by Rolf et al. (2019) considers a MAR pilot system

implemented in the western Bekaa Valley to assess the suitability of MAR techniques in

karst regions as a function of various criteria. The implementation of MAR in karstic

settings requires thorough detailed study, especially with regards to the aquifer storage. A

more promising approach to MAR is its application in alluvial deposits, where a dual

purpose well was set up, however, the scheme remains limited in terms of its functionality,

infiltration, and monitoring activities.

A research work conducted by Khadra & Stuyfzand (2019) discusses the

complexity of the applications of MAR in karstic settings by selecting principal karst

regions in Lebanon through reviewing different MAR systems and approaches. The

proposed methods for potentially effective recharge systems include the riverbank

infiltration by recharging the hydraulically connected karst aquifer by adjacent rivers and a

trench or borehole recharge with the karst aquifer unit by surface water runoff, favorable in

urban areas. Additional techniques in karst units are proposed, which encompass ASTR

(Artificial Storage Transfer Recovery), AR (Artificial Recharge), injection of freshwater

into boreholes in coastal areas vulnerable to saltwater intrusion, along with other techniques and a combination of methods. Bank filtration is defined as groundwater pumping adjacent to or underwater bodies to induce surface water infiltration and establish consistent groundwater quality and flow in the system. Therefore, surface water is subject to natural treatment processes reducing the occurrence of pathogens, turbidity, and contamination.

Furthermore, bank infiltration is characterized by its inexpensive and easy implementation as well as the successful execution of riverbank infiltration in karst, especially along the Damour River. In this area, the river infiltration represents 50% of the water stored in the wells and contributions may increase with increasing number of pumping wells such that it remains below the limit of causing saltwater intrusion. Therefore, the assessment of the Damour area demonstrates the efficiency of the bank filtration system, especially that the karst dominated region improves water quality through filtration, adsorption, and removal of contaminants. Recharge by surface run-off and particularly stormwater in urban areas using infiltration networks interconnected to the karst system has not been prevailingly applied such that there are no existing reports regarding collected volumes of stormwater in Lebanon, but the technique is proposed to be generally feasible with prospective simulation models and pilot sites (Safi et al., 2018). Consequently, numerous managed aquifer recharge techniques coupled with pilot sites and comprehensive research serve as potential and viable applications for the management and conservation of groundwater in karst dominated regions in Lebanon.

2.3 Integrated modeling using MIKE SHE

MIKE SHE (DHI, 2017a) is a modeling simulation tool that accurately integrates flow, processes, and interactions between the groundwater in the saturated and unsaturated zone in subsurface and surface water. Such accuracy and complexity arising from applied modeling dictate detailed hydrological data sets and parameters that will permit adequate determination of the characteristic site parametrization and reduce uncertainty and errors that arise from a complex heterogeneous system. Uncertainty and errors arise from the conceptualization of the model, parametrization, and error in the field and observational measurements (Wu & Zeng, 2013). Therefore, an adequate calibration and a comprehensive conceptualization of the mechanisms and interactions in the natural system define the accuracy and reliability of the modeling output and its representation of the real natural system.

MIKE SHE is characterized by its ability to define certain processes and elements pertaining to the hydrological cycle, encompassing interactive surface and subsurface systems. The cycle is governed by a series of mechanisms that only permit the transformation of the physical state water void of loss or gain in the system. The cycle is characterized by rainfall and snow cover at the surface, infiltration to the saturated zone, evaporation, and transpiration from water bodies, canopy and soil, and discharge in the form of springs. Freeze & Harlan (1969) described the hydrological cycle processes and elements through a series of partial differential equations and in 1977, the Système Hydrologique Européen (SHE) (Abbott et al., 1986) established by the European consortiums formed the integrated numerical hydrological modeling MIKE SHE. Through further development and progression by DHI (Dansk Hydraulisk Institut) Water &

Environment, MIKE SHE has become a more advanced tool used to integrate the different

pre- and post-processing components and establish a basis for the interactions between the

evapotranspiration, overland flow, unsaturated/ saturated zone modules. The physically

based deterministic and distributed model solves partial differential equations defining

momentum transfer and mass flow, such as Darcy's equations, St. Venant's equation etc.

such that parameters integrated into the model are observational and field measurements.

Based on the model's comprehensive framework of temporal and spatial distribution, and

available detailed time series data, the user is able to incorporate input from GIS and build

their conceptual watershed and domain.

The systems encompass a six process-oriented Water Movement component

system characterizing key surface and subsurface level physical processes of the

hydrological cycle, which include (Figure 2): The Evapotranspiration/Interception,

Saturated/Unsaturated zone, Overland/Channel Flow, Precipitation/Snow Melt, and Aquifer

Interchange/Rivers (Keilholz *et al.*, 2015).
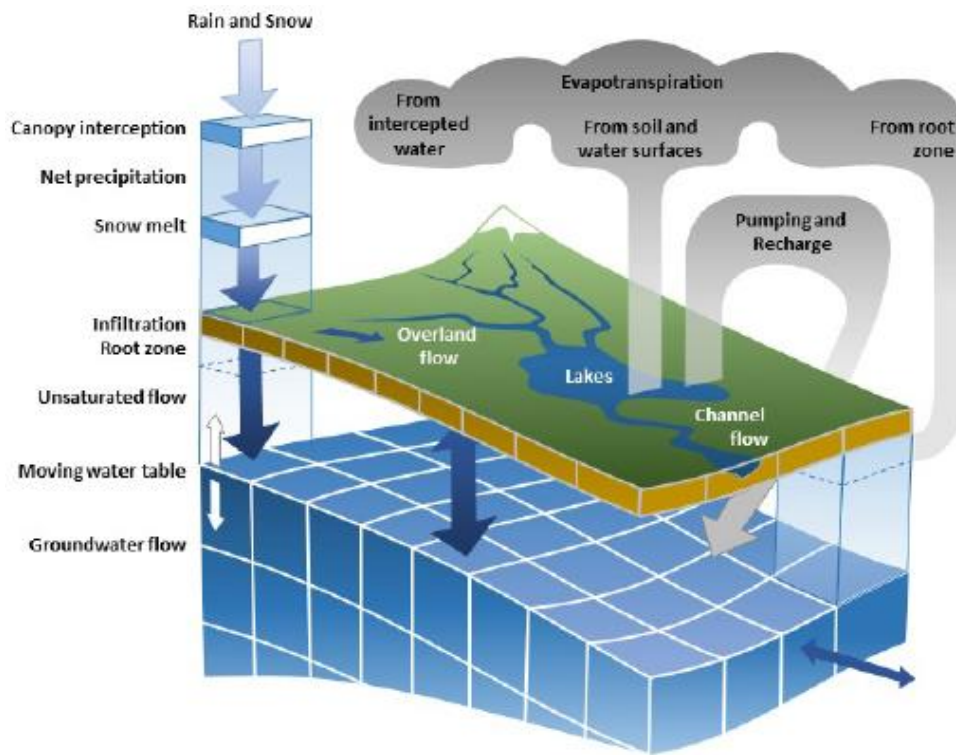
Figure 2: Schematic view of the MIKE SHE modules (DHI, 2017c).

MIKE SHE Modules:

    1.3 The (ET) Climate component: Evaporation, Transpiration, Interception,

    Snow Melt, Precipitation rates as input data.

    2.3 The (OL) Overland Flow component: Modelling Surface runoff and

    interaction with surface water.

    3.3 The (UZ) Unsaturated Zone component: Modelling surface water

    infiltration through the soil profile. The component is also defined by land

    use/ land cover (LU/LC) and irrigation factors.

    4.3 The (SZ) Saturated Zone component: Modelling the aquifers and

    interaction with drainage.

2.4 Numerical simulation of flow in aquifer sites in Lebanon: A review

Groundwater models for management purposes were implemented in Lebanon only in a few catchment areas in a consolidated equivalent porous medium (Litani basin or Akkar plain) or in other karst catchment areas. Groundwater models require high-resolution data for a relatively long period (3-5 years) for calibration and validation (Sonnenborg et al., 2003). Additionally, the karst nature of most of Lebanon's aquifer makes conventional modeling a challenging task, because of the duality of flow and infiltration that requires specific types of models (non-distributed lumped models) and sufficient knowledge of the subsurface geometry and flow (Doummar et al., 2012).

A study conducted by Doummar et al. (2018) on the flow in a snow governed karst system in Lebanon (Aassal Spring), illustrates the significance of using a quantitative model for the adequate management and practice of water resources in semi-arid regions. In this study, a spatially distributed integrated numerical model is constructed and calibrated based on high-resolution flow time-series (2010-2015) and validated based on the years 2015-2017. The effect of climate change was shown by a sensitivity analysis of climatic parameters and their effect of model output. Furthermore, climatic parameters extracted from a climatic scenario IPSL_CM5 global climate model (GCM) were used in the model to predict discharge variations for 2021-2099. The assessment of climate change was done through the evaluation of important hydrograph output such as recession coefficients recession intervals, and lag time responses of springs discharge with respect to snowmelt. The sensitivity analysis revealed temperature to have a great impact on model output by influencing snowmelt, flow level, and the period of recession. In response to the

precipitation and temperature trends, it is predicted that spring recharge and annual volumes have a negative trend by the year 2070, in response to a decline in snow cover and the early arrival of long recession periods. The study concludes that climate change has an impact on spring volume, recession period and coefficient, flowrates, snow cover. Under future scenarios, it is anticipated that demand rates exceed the available volume during dry periods which require that decision-makers implement adequate management practices and pose further investigations and solutions through either managed aquifer recharge, water reallocation, or storage in stressed semi-arid regions of the Mediterranean.

In Kassem (2020), a sensitivity analysis of the model in Doummar et al., (2018) was conducted to determine the most influential parameters on the model output to assess quantitative vulnerability. This study helped identify the most influential parameters and to rank them with a weight that defines their effect on model output. This study revealed that soil thickness and soil and rock hydraulic conductivity were the most impacting parameters in addition to aquifer properties. Such research allows stakeholders and decision-makers to undertake a comprehensive stance towards groundwater resources management and vulnerability assessment in light of the consequences of climate change, particularly in complex heterogeneous karst systems forming most of Lebanon's aquifer systems.

In Dubois (2017), a semi-distributed lumped model of the Qachqouch catchment (in Mount Lebanon) using Mike She was calibrated and validated (DHI, 2017a) against discharge data over the years 2014-2017. The goal of modeling was to calibrate the model based on a detailed statistical and correlative analysis of time series to unravel information about the subsurface saturated zone and hydraulic parameters in a typically poorly investigated karst. The linear reservoir model takes into consideration the calibration of the

saturated zone and flow only. The system was hypothesized to have three different reservoirs draining into each other presenting depletion and recession phases.

Safi et al. (2018) assessed the dynamics of saltwater intrusion of a fractured and heterogeneous aquifer underlying the city and suburbs of Beirut by developing a multi-objective 3D variable-density flow and solute transport model (SEAWAT; MODFLOW 2010) to evaluate the influences of global environmental stresses and local anthropogenic activities and offer a better understanding and possible mitigation strategies for saltwater intrusions in coastal aquifers. The response of the aquifer was reviewed under different scenarios based on population growth, consumption rates, abstraction rates, and sea-level rise with a comparable assessment of the significance of the impacts on aquifer response. It was concluded that saltwater encroachment was influenced by anthropogenic abstraction as water consumption and seasonality proved to be significantly sensitive in comparison to sea-level rise in association with environmental climate stresses.

A 3D groundwater flow model for the Upper Litani Basin was developed using MODFLOW 2005 (UNDP, 2014) was developed to predict the effect of climate change and the expected total precipitation decrease of the Akkar Quaternary-Neogene Basin. The steady-state model was calibrated based on 1969 water level measurements (Food and Agriculture Organization of the United Nations (FAO), 1970) and the transient state model was based on 2013 simulated water level measurements to investigate the evolution of the groundwater levels from 2013 till 2030 taking into consideration the effects of climate change, the decline in total precipitation and increase in abstraction. A 12% decline in total precipitation in 2030 will yield a 2-meter drop in groundwater level and a 1.4 MCM deficit

in aquifer storage coupled with an increase in the propagation of saltwater intrusion into the coastal aquifer as a result of increasing abstraction rates and decrease in recharge rates.

A groundwater model representing a 3D volume of different aquifers using GMS (MODFLOW Groundwater Modeling System), based on MODFLOW 2005, with calibration at steady state on 2010 groundwater level measurements and simulated at transient state for 2010-2011 to estimate future groundwater levels over a 20-year forecast based on four (4) different scenarios (IRG, 2013). The scenarios considered the effects of increasing pumping abstraction rates owing to increasing urbanization and agricultural land use growth and decline in rates of recharge due to climate change. Regardless of which scenario was selected, a general trend in the depletion of the groundwater resources of the upper Litani River in various locations was observed which necessitates detailed planning and monitoring strategies for sustaining and improving the management of water resources in the Litani Basin. The latter model did not account for an integrated approach, as it only considered recharge to the saturated zone. Additionally, the model was run on a 6- month basis for transient simulations to provide simplistic results for water level decline expected in the future.

CHAPTER 3

STUDY SITE

The investigated catchment area consists of the Upper Litani Basin (ULB) in Lebanon. The Aana wetland is located within the ULB and hosts the MAR site, which is located 33°41'4.70"N 35°46'2.73"E, with an elevation of 885m asl. The wetland is located 2 km from the western side of the southern Bekaa Valley flank. The average annual temperature in the Bekaa Valley is 16 °C, with 26 °C in the summer and 5 °C in winter, mean annual potential evapotranspiration of 1,200 mm and mean annual rainfall in the southwest of the Bekaa Valley ranges between 700-900 mm (Food and Agriculture Organization of the United Nations (FAO), 2008). The predominant lithology of the MAR site zone is composed of Middle Miocene lacustrine and fluvial deposits consisting of coarse-grained clastic deposits and gravels (Dubertret, 1955). This section presents the main geomorphological, geological, and hydrogeological characteristics of the Basin (Figure 3).
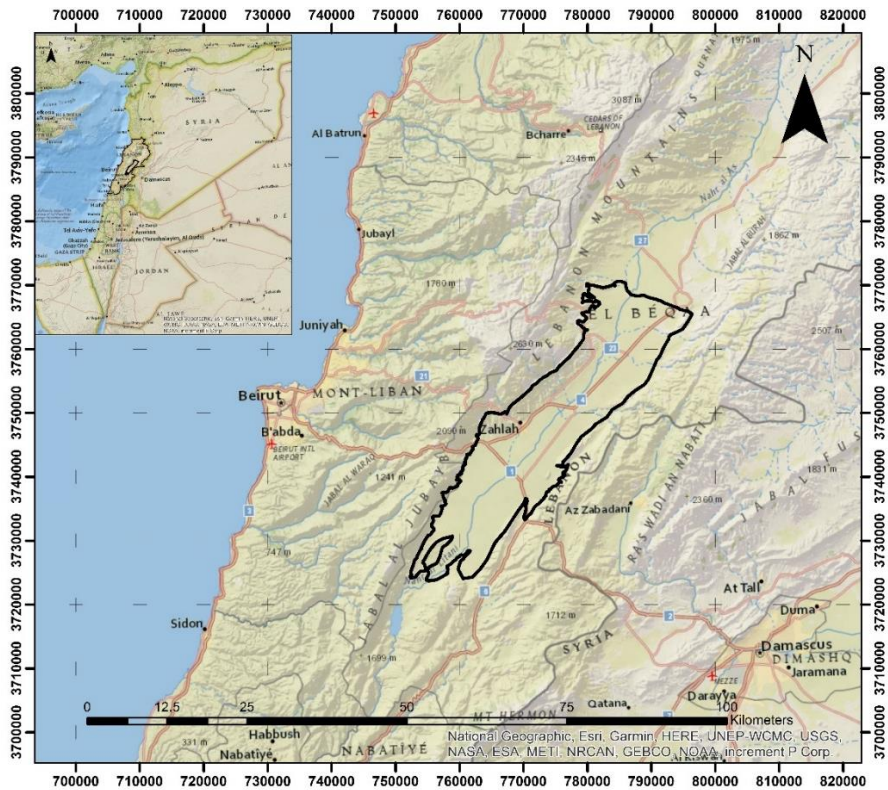
Figure 3: Location of the investigated site in the Upper Litani Basin (ULB).

3.1 Topography and Extent

The Upper Litani Basin covering an area of approximately 636 km^2, has an average elevation of 971 m asl, bounded by the Mount Lebanon range on the eastern and Anti-Mount Lebanon along the western flanks, with topographic elevations of 2,620 and 2,440 m asl respectively. The basin is bounded on the north by Baalbeck city and on the south by the Qaaroun Lake, whereby the drainage system that encompasses the Litani River and its tributaries, flows 170 km downstream to the south to the Qaaroun Lake, with a mean elevation of 830 m asl.

26

3.2 Land Use/Land Cover

The basin encompasses around 85 villages consisting of small to medium-sized populations, in which domestic water supply is provided by the regional water establishment, operating 107 public water wells. The area is characterized by agricultural fields and is cultivated and irrigated by using surface water, by means of ditches and tributaries from the Litani river network and by groundwater well abstraction through private and public wells, and springs. A land use/Land cover map of the Upper Litani Basin is presented in Figure 4 and Figure 5, and were compiled based on the soil resources of Mediterranean countries report (Yigini et al., 2013), centered on maps by Darwish (1999) and Darwish et al., (2002, 2006) ranging in scale from 1:50,000 to 1:200,000 and CNRS (2010). The description of the soil map textures were qualitatively assessed based on Torrent (2005).
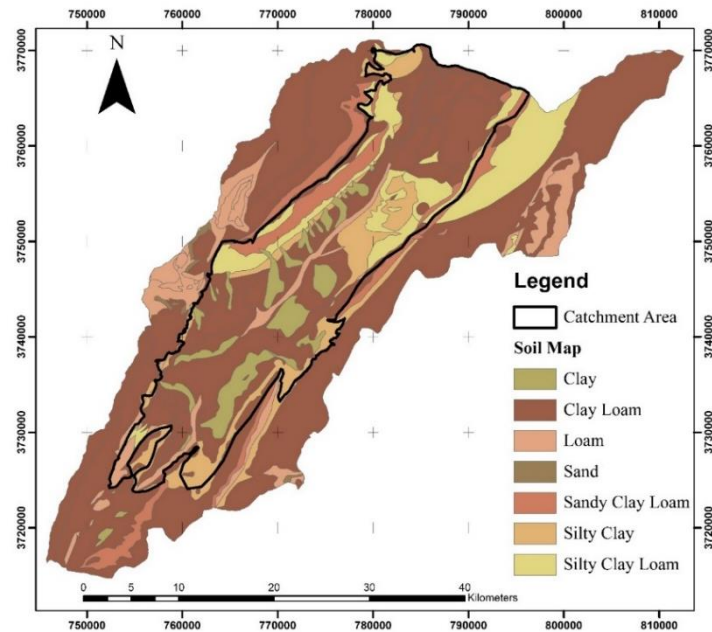
Figure 4: Soil map of ULB depicting the various soil textures ranging from clays to sands, and loams.

27
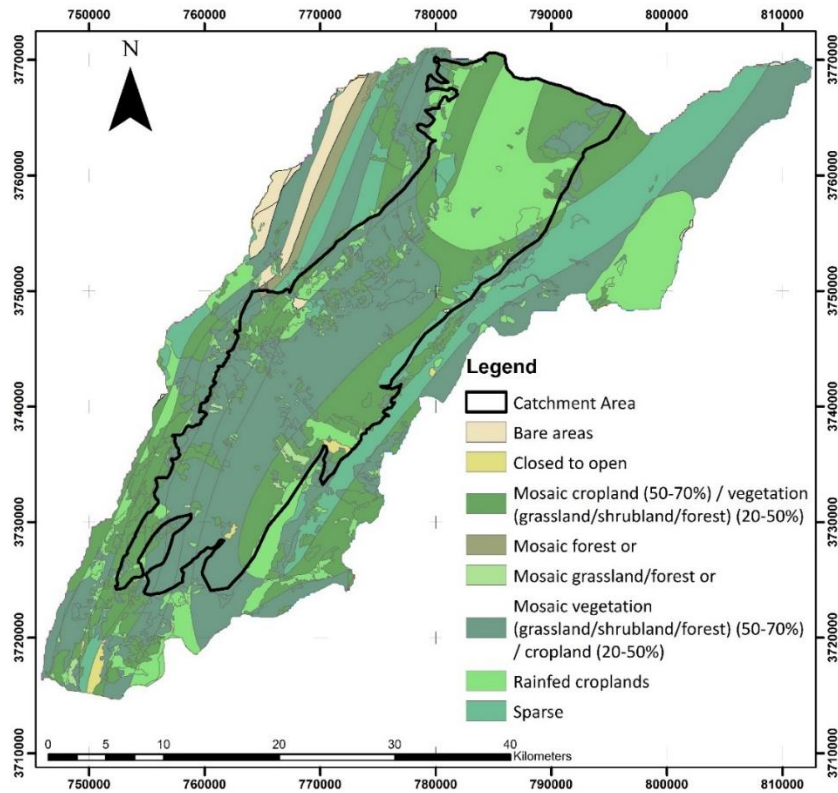
Figure 5: Vegetation map of ULB depicting the distribution of various land covers ranging from bare areas to diverse croplands.

3.3 Regional geological and geomorphological setting

The three principle morphological structures of Lebanon are Mount (Mt.) Lebanon, Bekaa Valley, and Anti-Lebanon Mountain. The Bekaa valley is bounded by the Mt. Lebanon and anti-Mt. Lebanon mountains on the west and east respectively, with the southern Yammouneh fault, a segment of the Levant Dead Sea Transform fault system stretching NNE-SSW (Walley, 1996, 1998), delimiting the western side south of the Bekaa valley (Gomez et al., 2007). The Lebanon Mountain formations predominately comprise Cretaceous and Jurassic limestones (Edgell, 1997; Walley, 1996), along with distinctive local basal Cretaceous sandstone at the base of the Jabal Barouk and Jabal Niha (Walley,

28

1996). The Anti-Lebanon Mountains are dominated by anticlines, outcropping Mesozoic formations in the SSW-NNE direction. The structural nature of the Bekaa valley can be characterized as a synclinorium bounded in between the Lebanese restraining bend comprising the Mt. Lebanon and Anti-Mt. Lebanon ranges (Gomez et al., 2007) and is classified into three structural basins which consist of the Northern, Middle, and Southern basins (Figure 6).
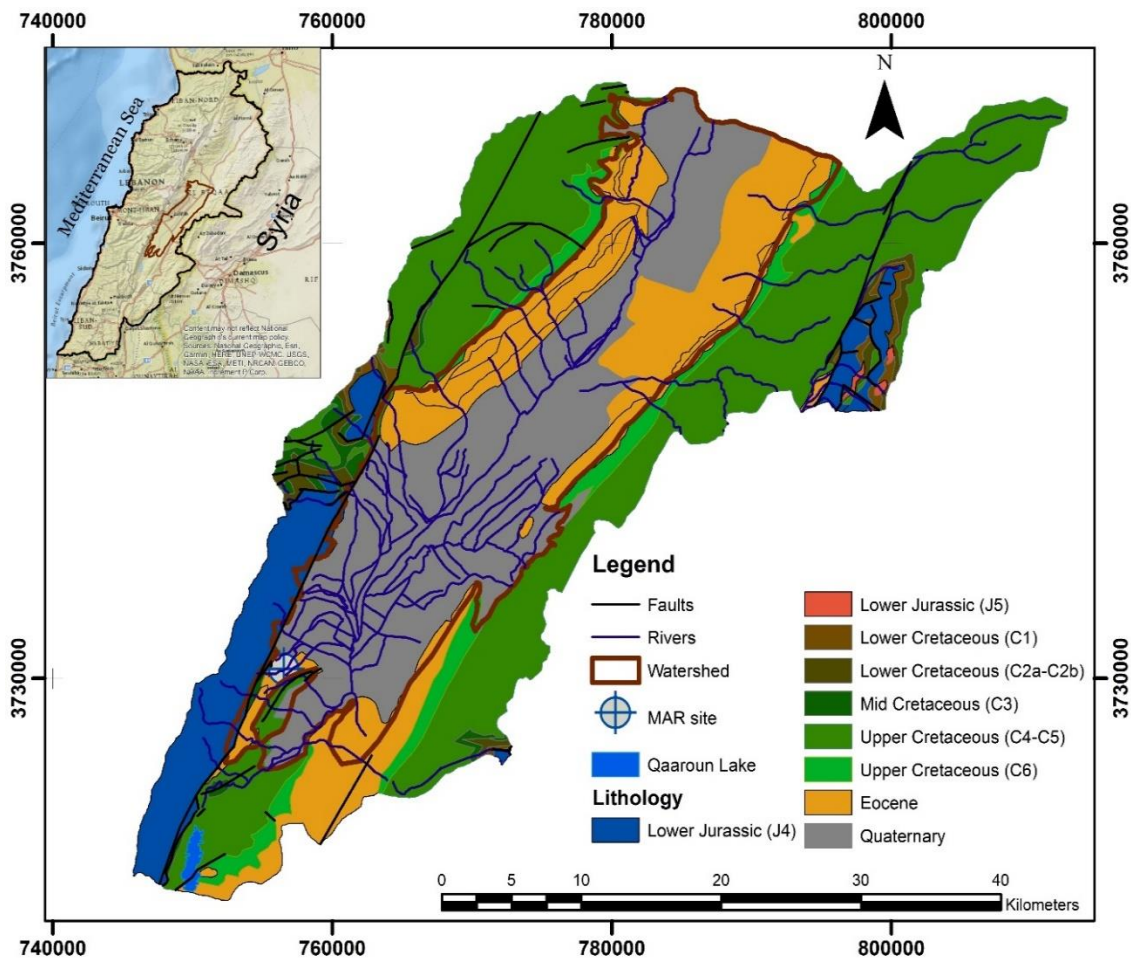
Figure 6: Geological map of the catchment area depicting the predominant lithology.

The SSW-NNE trending Bekaa Valley is delimited by major faults which include the Yammouneh fault in the Southern flanks of the Lebanon Mountain, and the Rachaya and Serghaya faults along the base of the Anti-Lebanon Mountain.

The study area was assessed based on the compiled hydrogeological and geological maps by Dubertret (1955), UNDP (1970), and IRG (2013).

The formations of the Bekaa valley consist of the Upper Cretaceous limestones and dolomites, and Neogene lacustrine and alluvial deposits and conglomerates. The Southern basin encloses several hundred meters thick continental Neogene to Quaternary deposits along the synclinal axis. The major aquifers of the Bekaa valley include a greater than 800 m thickness of Upper Cretaceous limestones and dolomites along the eastern and western flanks, and Neogene–Quaternary deposits within the plain, consisting of conglomerates and alluvial sediments. A comprehensive description of the geological formations from the Middle Jurassic to recent Quaternary deposits is provided in Appendix A.

3.4 Hydrostratigraphy

The following section defines the hydrogeological aspects of major geological formations, i.e. the characterization of lithological units based on their relative physical properties (Table 2).

The basin is characterized by three main aquifer units: The Quaternary, Neogene, and Eocene, which are bounded between two other aquifer systems, the Cretaceous and Jurassic.

The aquifer system consists of the following:

a. Jurassic (J4) deposits: Consists of fractured limestone and karsts along the west side of the basin from Chtaura to south of the Qaraoun reservoir (up to 1000 m thickness).

b. Cretaceous (Sannine-Maameltain) system: Consists of marls, fractured limestone notably as mountainous ranges on opposite borders of the basin, and well-developed karsts along the eastern margin (600-900m thickness).

c. Eocene (e2a-e2b): Consists of well-developed karstified marly limestone along the eastern and western boundary of the basin consisting of thinly outcropped belts (bands range in width of 1000 m and less, an area of 56 km^2, and 250-600 m thickness).

d. Neogene (mL-mL1): Consists of alluvial deposits and conglomerates outcropping at the center of the basin and along the western edge of the mountain base of Chtaura-Chmistar area and stretching from Baalbeck to Rayak (179 km^2- with thickness up to 300 m).

e. Quaternary Deposits (Q): Consists of fine-grained silts and clays with sand and gravel alluvial deposits that predominantly outcrop in the center of the basin and north from Joub Jennine (404 km^2- with thicknesses ranging up to 200 m).

Table 2: Modified stratigraphy and hydrostratigraphy of Lebanon, (adapted from Abbud & Aker, 1986; Cadham et al., 2007; Walley, 1997).

Period / Age				Formation Name/ Code	Thickness (m)	Lithology	Hydrostratigraphy	
							Aquifer type	Description
Quaternary	Quaternary			Q	<100	Coastal Sand, detrital limestone, conglomerates, volcanic or alluvial deposits	Aquiclude / Porous medium semi-aquifer	Low permeability, high porosity. Most percolation occurs in Bekaa plain.
Tertiary	Neogene	Pliocene	Pliocene	Pl	50-100	Volcanics with marls and conglomerates	Aquiclude	Volcanics act as aquiclude, but water is present in fractures in Bekaa Plain
		Miocene	Upper	m$_{cg}$	50-100	Conglomerates, Sandy, silty marly deposits	Aquiclude	Porous medium aquifer, possibility of water percolation, possible presence of springs
			Middle-Lower	mL	300 – 400	Reef, marly limestone, continental conglomerates, sequences of thick fractured limestone	Karstic aquifer-	Water is transmitted through conduits and fissures. Presence of springs

Period / Age			Formation Name/ Code	Thickness (m)	Lithology	Hydrostratigraphy	
						Aquifer type	Description
	Paleogene	Eocene	e2b	200 – 600	Marly, chalky, cherty, nummulitic limestone	Karstic aquifer	High permeability, medium porosity. Well-developed karstification and recharge, especially in South Lebanon
Cretaceous	Upper	Maastrichtian -Coniacian	C6	100 – 500	White and marly chalks with phosphate & chert bands	Aquiclude	Low permeability, medium porosity
		Turonian-Cenomanian	C4-C5	700-900	Massive to thin-bedded limestone and marly limestone Marls and dolomites	Aquifer to Karstic aquifer	Major karstification and fracturing, GW is transmitted through conduits and fissures, Presence of Springs
	Lower	Albian	C3	100 – 400	Marls, limestones, sandstones, lower basalt member	Aquiclude	Low permeability, medium-high porosity, GW trapped in impermeable layers of marls and volcanics
		Aptian	C2b	50	Massive and fractured limestone	Karst Aquifer	karst aquifer, percolation through conduits and fractures

Period / Age			Formation Name/ Code	Thickness (m)	Lithology	Hydrostatigraphy	
						Aquifer type	Description
		Berremian	C2a	50-170	Sandy limestone, argillaceous marls, and limestone	Aquitard-aquiclude	Under favorable conditions, acts as aquifer-aquitard
		Hauterivian-Valanginian	C1	10-300	Coarse to fine Sandstone, with localized lignite and basal basalts	Aquifer to aquitard	Permits minor percolation and flow of GW through the porous medium aquifer, Perched aquifers form above impermeable volcanics
Jurassic	Upper	Tithonian – Oxfordian	J7 – J5	100 – 400	Oolitic/Massive/ dolomitized Limestone, marls, shale, chert, basalt, tuffs	Aquiclude or semi-aquifer	Medium permeability, medium porosity, Acts as good karst aquifer under favorable conditions, and due to structural disturbances
	Middle- Lower	Callovian-Pliensbachian	J4	1000 – 1500	Fractured massive limestone and dolomites with localized chert, marls, volcanics	Karstic aquifer	Very high permeability, medium porosity, Well developed karstification, GW transmitted through conduits and fractures

3.5 *Aquifer properties and characteristics*

The main aquifer systems and their respective hydrogeological properties are summarized based on the works of IRG (2013) and UNDP (1970):

- Jurassic aquifer (J4): Defined by dolomitic limestone and massive limestone, thicknesses reaching up to 1000 m, transmissivities (T) ranging between $10^{-3} - 1 \ m^2/s$, and net-rain fall fractions up to 41%.

- Cretaceous aquifer (C4-C5): Massive to thinly interbedded limestone and marly limestone, and dolomites, thicknesses between 750-900 m, T values ranging from $10^{-2} - 1 \ m^2/s$, and net-rain fall fractions up to 41%.

- Eocene aquifer (e2a/e2b): Marly, chalky, cherty, and nummulitic limestone, thicknesses up to 600 m, T values of $10^{-4} - 10^{-2} \ m^2/s$, and net-rain fall fractions up to 38%.

- Neogene aquifer (mcg/ml): Lacustrine sands, silts, conglomerates, limestone, and marls, thicknesses up to 300 m, T values $< 10^{-3} \ m^2/s$, and net-rain fall fractions around 5%.

- Quaternary aquifer (Q): Colluvium and Alluvium deposits and unconsolidated gravels, up to 250 m thick, $10^{-4} - 10^{-3} \ m^2/s$, and net-rain fall fractions around 5%.

The hydrogeological regimes are complicated by the interconnections between subsurface and surface flow and defined by different hydrogeologic units that encompass relief, synclinal structure, water divides, etc. (Khair et al., 1992). These interconnections include groundwater flow discharged at high elevations that recharge aquifers at lower relief, and flow between aquifers and adjacent sub-basins formed by major faulting activity.

The groundwater regime in the Bekaa valley is interconnected with the Upper Cretaceous aquifer exposed at the eastern and western flanks of the southern basin, and represents a depth of several hundred meters. The general groundwater movement in the Bekka valley follows the NNE-SSW trend. The major fault system, the Yammouneh fault, along the eastern slope provides subsurface flow to discharge as large perennial springs in the valley, and also acts as a barrier to groundwater flow at other segments. The shallow lacustrine aquifer system of the Bekaa plain is recharged by surface runoff, baseflow from and lateral inflow from the Upper Cretaceous karstified aquifer.

CHAPTER 4

METHODS AT A PILOT SCALE

4.1 Collection of drilling samples

      The samples were taken at different depths from a drilling site (Figure 7) located in the Edde Farm, Bekaa. The samples underwent a lab preparation to dry the sample for sieve analysis. The procedures for sample preparation and sieve analysis are detailed in Appendix B.

Figure 7: Drilling operations of the borehole for MAR, at Edde Farm, Bekaa.

4.2 Sieve analysis: Inference of hydraulic properties

This section represents the methodology adopted in this research, including field and lab work as well as details of the numerical simulation of flow in the Litani Upper Basin.

The hydraulic conductivity can be determined from empirical formulas relating grain size distribution to other particle properties of the sediments. Vukovic & Soro (1992) summarized the empirical formulae equating K to other particle properties with the following formula (Eq. 1)

$$K = \frac{g}{v} . C . f(n) . d_{eff} \tag{1}$$

Where K = hydraulic conductivity (m/s), g = gravity acceleration (m/s^2), $v = \frac{\mu}{\rho} =$ kinematic viscosity (m^2/s), C = sorting coefficient, f (n) = porosity function, and $d_{eff} =$ effective grain size diameter. The porosity function f (n) may be derived from the uniformity coefficient U (-), where

$n = 0.255$ $(1 + 0.83^U)$, and $U = \frac{d_{60}}{d_{10}}$, d_{60} and d_{10} represent the 60 and 10 % finer grain size diameter of the sample respectively.

Several methods were used to determine hydraulic conductivity which include the analytically derived Kozeny-Carmen equation, originally proposed by Kozeny (1927, 1953) and later modified by Carman (1937, 1956) and is appropriate for silts, sands and gravelly sands (Eq. 2)

$$K = \beta \frac{\rho g}{\mu} \frac{n^3}{(1-n)^2} \, d_{10}^2 \qquad\qquad (1)$$

Where ρ [M/L^3], g [L/T^2], μ [M/L.T], d_{10} is grain size finer than 10% [L], n [-], $\beta=$ 1/180, and is appropriate for silts, sands and gravelly sands (Rosas et al., 2014).

The Beyer equation (Beyer, 1964) is appropriate for heterogeneous and poorly sorted material with 0.06 mm <d10< 0.6mm, $\beta= 6 \times 10^{-4}$, and 1<C<20 (Rosas et al., 2014; Eq. 3)

$$K = \beta \frac{g}{v} \log \frac{500}{U} \, d_{10}^2 \qquad\qquad (2)$$

The Hazen original equation (Hazen, 1892) is appropriate for uniformly graded fine sands to gravels, where 0.1 mm < d_{10}< 3 mm, $\beta= 6 \times 10^{-4}$, and C < 5 (Rosas et al., 2014; Eq. 4)

$$K = \beta \frac{g}{v} \, [\, 1 + 10 \, (n - 0.26)] \, d_{10}^2 \qquad\qquad (3)$$

The estimation of aquifer parameters accurately such as hydraulic conductivity K, transmissivity T, and storativity S is deemed difficult since comprehensive knowledge is required regarding the aquifer's hydrogeological geometry and boundary (Uma et al., 1989).

Both classical analytical methods and statistical analyses were used in this study, in order to estimate and compare the yielded aquifer parameters. The classical analytical methods which include pumping tests provide precise results and reflect the hydraulic boundaries and geometries of the aquifer, while grain size distribution obtained from statistical analyses express the transmissive character of the aquifer without being very contingent on aquifer geometry and boundaries (Alyamani & Şen, 1993).

4.3 Aquifer testing

Aquifer testing and drawdown analysis were conducted at a fully penetrating single well. The well was drilled to a depth of 156.1 m, whereby samples of the geological formations were collected and described lithologically. A geophysical well log was performed by the contractor to provide a preliminary assessment of the grain size, whereby the depth of the well screen was placed at the level at of the coarsest sediments. After drilling and screening, a pump is installed and the well is subject to development, such that cloudy water is initially pumped at a gradually increasing discharge rate, until the discharged water became clear. The discharged water was directed into a ditch, preventing returning recharge. A piezometer well was chosen 1.3 km away from the pumping well. Prior to the pumping test, the water level was recorded with a pressure transducer (Level troll 100_ Brand INSITU) at the pumping and piezometric wells.

4.3.1   Step drawdown

The step drawdown was conducted at increasing discharge increments of 2, 4, 5, and 6 m3/h over 2-3 hours each step. An earlier pumping test performed at 10 m^3/h (~2.7 l/s), yielded a drawdown that exceeds the level of the pump, therefore the selection of pumping rates accounted for a maximum allowed drawdown. The discharge was measured every 30-60 min to ensure the stability of the flow rate. Prior to the start of the test, the level of the test was 64.70 m BG (September 29). The first pumping stage at 2 m^3/h was initiated at 11:00 am.

Table 3: Summary of the discharge and pumping duration of the four steps of the step drawdown test.

Steps	Q (m³/h)	Duration (hours)
1	2	2.58
2	4	2.46
3	5	2.48
4	6	2.53

4.3.2 Long term pumping test

Pumping tests are a conventionally applied technique to estimate aquifer hydraulic properties, transmissivity, and storativity. The drawdown induced by pumping, acting as a system response of the aquifer, is interpreted by the Theis equation (Theis, 1935), which assumes an ideal homogenous, isotropic, and infinite aquifer. Theis-based interpretations have generally described aquifer flow parameters of intrinsic heterogeneous aquifers (Pechstein et al., 2016). The Theis' log-log method was followed by the Cooper and Jacob semi-log approach (Cooper & Jacob, 1946).

The long term pumping test was initiated on Oct 5, 2018, at 6:00 am and stopped on October 6, 2018, at 10:00 am because of an incident in the electric wiring that has occurred in the container. After the electric incident was fixed with the remote assistance of Broere, the pumping test was restarted on Oct 6, 2018, at 11:30 am after the well has recovered to its residual drawdown. The pumping test was conducted at 3 m³/h for 41.5 hours until the pump shut down automatically most probably because the maximum drawdown allowed above the pump was reached (108 m BG). The discharge was measured each 30-60 min to ensure the stability of the flow rate. Water samples were collected for

chemical testing in two HDPE plastic bottles for major cation and anion analysis (500 ml)

and in two glass bottles (330 ml) for stable isotope analysis.

CHAPTER 5

CHARACTERIZATION OF FLOW AT A LARGE SCALE: NUMERICAL MODELING OF THE ULB

5.1 Conceptual model

A well-established conceptual model provides the foundations needed to establish and design a numerical model (Kresic & Mikszewski, 2012) and comprises of data and information of the hydro-stratigraphy and hydrogeological aquifer properties, flow movement and direction, boundary conditions, sources/sinks and a preliminary water balance (Anderson et al., 2015). The groundwater model of the Upper Litani Basin encompasses a 3D representation of aquifer systems and water movement modules (Figure 8). Therefore, the development of a conceptual model is required prior to numerical modeling and consists of the delineation of model geometry (e.g. boundary conditions and major aquifer units) and the characterization of model parameters (e.g. time series and initial hydraulic conditions). Sufficiently detailed groundwater and geological information are needed to characterize aquifer volumes, distributions, and the rate at which water can flow and be stored. Surface processes characterizing the hydrological system which include exchange between the surface water and groundwater by infiltration from rainfall and rivers, and losses by springs and pumping rates also represent critical information needed to fully describe the hydrogeological structure. The model is constructed based on a

predominant abstraction of groundwater ($\geq$ 80 %) from shallow aquifers, i.e., Quaternary

Neogene, and Paleogene aquifers.
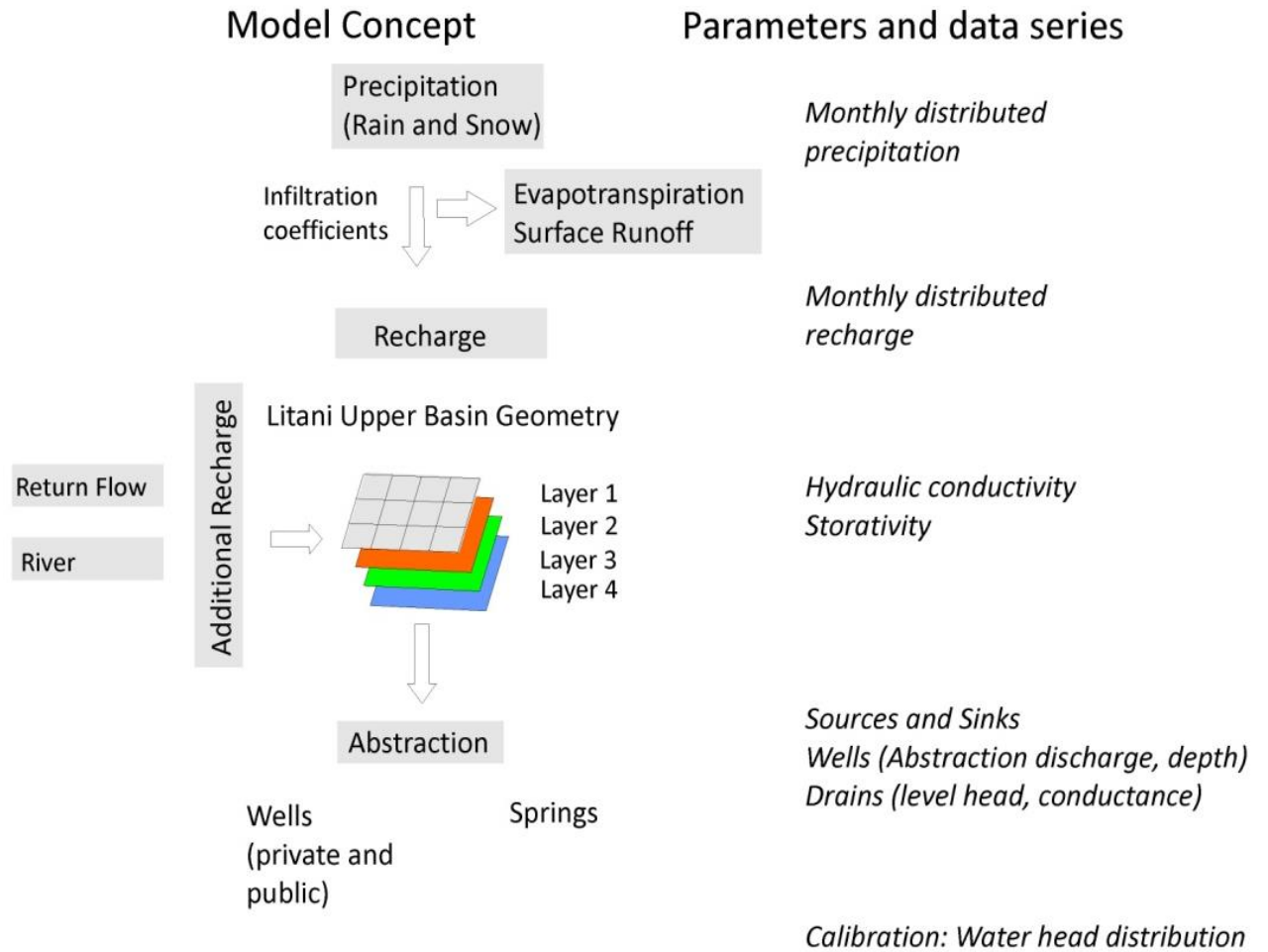
Figure 8: Schematic presentation of a conceptualized model for Mike She (*courtesy of*

Doummar Joanna).

5.1.1   Model geometry and aquiferous layers

The catchment area is characterized by complex geometry and subsurface composition. Model geometry is built based on distinct layers comprising the topography (upper level), the different aquifer units (lower level, bottom of aquifer unit), and the boundaries limiting the study area. The semi-confined leaky aquifer encompassing the Quaternary, Eocene, and Neogene aquifers consists of conglomerates and alluvial sediments for the Quaternary formation, unconsolidated gravels and sands and lacustrine limestones and marls for the Neogene formation, and marly and brecciated limestone for the Eocene formation. The hydro-stratigraphic units were based on the geological maps and cross-sections (Dubertret, 1955; UNDP, 1970). These layers showed variable horizontal and vertical extents, and as such, they were delimited into distinct lenses having variable thicknesses.

5.1.2   Sources and Sinks

The direct major source of water for groundwater recharge in the basin is infiltration from precipitation. Precipitation is partially subject to interception by vegetation and canopy and evaporation from the soil. The remainder is subject to infiltration via unsaturated zone for recharge and excess water forms overland flow by means of rivers, lakes, etc. Lateral inflow from the neighboring Jurassic and Cretaceous formations on the Mt. Lebanon and Anti-Mt. Lebanon ranges and return flow from excess water leaked from wells during irrigation (approximately 10% of abstraction) also constitute sources for groundwater recharge in the basin. Groundwater sinks or outflows in the watershed include

45

groundwater evaporation, transpiration, well abstractions, discharge into springs, the

drainage to the Litani River tributaries, and the outflow to the Qaraoun Reservoir.

5.1.3 Boundary conditions

Boundaries of the study area were delimited based on the horizontal extent of the

major aquifer units. The model is delimited by the following boundaries:

- Along the eastern and western margins, the foothills of two mountain

  ranges represent constant flow zones from the Cretaceous and Jurassic

  aquifers respectively;

- The northern boundary, a river divide between the Litani River flowing to

  the South and the Assi-Orontes River flowing to the North, is considered as

  a zero-flow zone;

- The southern boundary, bounded by the immediate Qaraoun Lake, is

  considered a constant head zone attributed to the hydraulic continuity of

  thin Quaternary, Neogene, and Eocene aquifer with the reservoir at an

  estimated elevation of 840 m asl.

5.1.4 Flow direction

The ULB catchment area is situated between the Mount Lebanon and Anti-Mount

Lebanon ranges stretching along the N-S directions of the West and East respectively, with

a consistent decrease in elevation from the north to the south of the basin. The catchment

area is bounded by an anticline at the northern boundary with respect to the UOB and south

of the watershed is bounded by the Qaraoun Reservoir. Therefore, the direction of flow is in

the direction of higher heads in the northern part to the lower heads towards the Qaraoun

dam (at a constant head of 840 m asl). Additional flow lines from the eastern and western

boundaries are expected as lateral flow.

5.1.5   Preliminary water balance

Past hydrogeological investigations of the Upper Litani Basin revealed different

water balances, whereby UNDP (1970) reported infiltration rates of 220 $Mm^{3/}$ yr while

studies done by (Japan International Cooperation Agency (JICA), 2003) showed infiltration

rates of 480 $Mm^{3/}$ yr. The noticeable difference is a consequence of varying approaches of

infiltration rates calculations particularly since karstic systems pose complications in

quantifying recharge rates. The infiltration rates to the aquifers and water budget were

computed based on the conservation of mass, such that the conservation equation is:

Inflows - Outflows = $\pm$ ΔS (Variation of Storage) = 0 (in steady-state)

Where inflows and outflows consist of recharge inflows (precipitation that percolate into

the ground to aquifer), in-and outflow exchanges between rivers and aquifers, and outflows

from springs (groundwater collected from mountains seeping into springs along foothills).

5.1.5.1 Inflow

Inflow to the aquifer units consists of infiltration (I) from precipitation, and

components reflective of the basin influx from aquifers (AI), irrigation return flow (RF),

and infiltration from the principal Litani River and its branches (RI).

$$Inflow = I + AI + RF + RI$$

47

5.1.5.1.1   Infiltration rate or net rainfall fraction (I)

The infiltration rates for the Quaternary, Neogene, and Eocene aquifers in the Upper Litani Basin were derived from the UNDP (1970) and IRG (2013) study, and are considered the lumped amount of precipitation and return flow (RF) infiltrated. The net rainfall fraction is considered 15% for the Neogene and Quaternary aquifer and 38% for Eocene aquifers.

5.1.5.1.2 River exchange (RI)

The Litani River and its tributaries can either receive discharge from underlying aquifer systems (gaining streams) or provide recharge to the aquifer units (losing streams). The river in this study was considered as a special boundary condition for drainage in the saturated zone in which water was removed out of the system as a function of groundwater head and drainage level. Conceptually, as groundwater recharges the river, an equivalent amount of water will be discharged out of the opposite periphery of the river since water is incompressible and there is no additional storage space in the river.

5.1.5.1.3   Aquifer Interaction (AI)

Aquifer interaction is bounded by the Cretaceous and Jurassic aquifers of the eastern and western flanks of the mountain ranges in direct contact with the Quaternary, Neogene, and Eocene aquifer systems. The groundwater flux recharging the Quaternary, Neogene, and Eocene aquifers were based on the work of IRG (2013) and UNDP (1970) where lateral influxes to groundwater from the Cretaceous and Jurassic is approximately 0.75 m^3/s and influx from the Eocene formation is approximately 0.5 m^3/s

5.1.5.2 <u>Outflow</u>

Outflow includes abstraction from wells (QW) only without springs (QS) as there are no major springs discharging the Quaternary-Neogene-Eocene aquifers.

$$Outflow = QS + QW$$

There are 1184 wells distributed throughout the basin, with average daily abstraction rates from IRG (2013), of 426 m^3/day for the Quaternary, 373 m^3/day for the Neogene, and 916 m^3/day for the Eocene aquifer. However, USAID-LRBMS (2012) reported that between 5,000 to 10,000 wells exist in the ULB with 2,000 private registered wells while UNDP (2014) estimated the number of private non-registered wells as 18,228. Therefore, the number of wells used in the model does not accurately represent the actual figures, and thus represents an underestimation of well abstractions. The current model considers pumping at the full potential rate during the dry summer seasons (June till August) while only 40% of the pumping rate values are applied during the wet winter seasons.

5.2 Numerical model set up

5.2.1 <u>Spatial Discretization</u>

The catchment area is represented by an orthogonal network of 3D gridded cells. Each cell is defined by vertical variations in soil and geological characteristics over several successive horizontal layers of variable depths and extents. A single input value is assigned for each computational grid cell during the pre-processing stage of modeling. The model consists of a cell size of 235 m and a catchment size of 200 x 200 cells in the horizontal

direction (NX) and in the vertical direction (NY), with the vertical layer thicknesses varying according to lithological depths.

5.2.2 External boundary conditions

The explanatory boundary conditions defined in the conceptual model are presented in Figure 9, where the north boundary of the basin is described by a no-flow zone due to the syncline, the western and eastern boundaries were defined as constant flux boundaries due to incoming lateral inflow from the Jurassic and Cretaceous formations recharging aquifers respectively, and the southern boundary was defined as a constant head due to the aquifer being in hydraulic continuity with the Qaraoun reservoir.
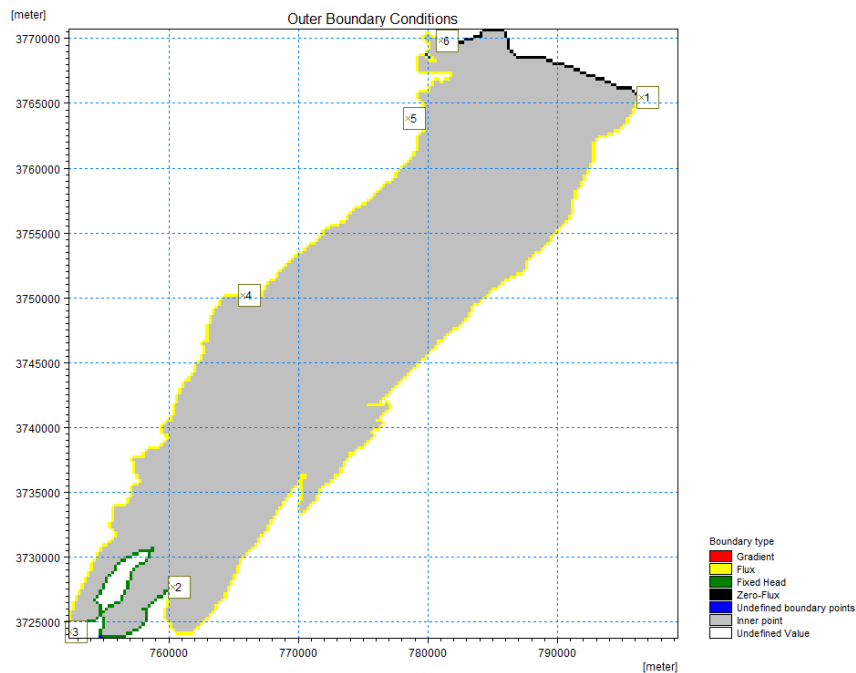
Figure 9: External boundary conditions, with constant fluxes along the western and eastern boundaries, a no-flow zone to the north, and a constant head zone to the south.

5.2.3 Model Geometry: Saturated zone

The saturated zone consists of geological layers and lenses where each is defined by an upper and lower level, horizontal and vertical hydraulic conductivities, and specific yield and storage values. The geological layer encompasses the main Quaternary-Neogene-Eocene aquifer unit. Due to the variability of the hydraulic conductivities and thicknesses in the horizontal and vertical extents, the aquifer is divided into six lenses; each lens describing a specific set of aquifer properties that will facilitate the auto-calibration process (Figure 10).
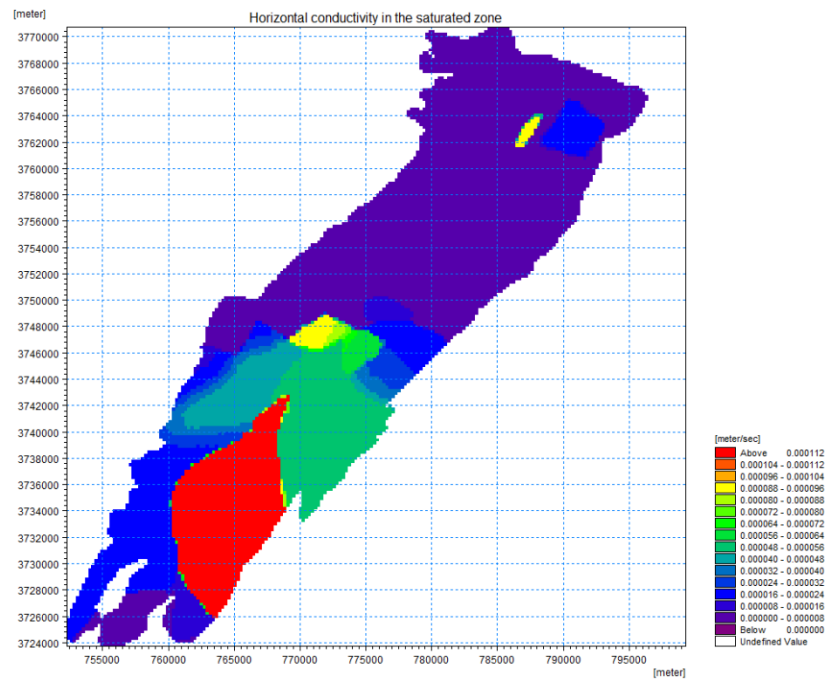
Figure 10: Distributed six lenses showing the highest conductivities from the central part of the basin to the southern part, while lower conductivities to the north.

5.2.4   <u>Sources and sinks</u>

- Input: Recharge to saturated zone and net-rainfall fraction

The precipitation rate was defined by a uniform rate of 1.8 mm/day for the steady-state models, while daily precipitation data according to several climate stations namely Kherbet Qanafer, Talya, Tal Ammara, Bar Elias, and Kferdane dispersed representatively within the basin were used during transient state modelling. The net rainfall fraction is the percentage of rainfall that is available for infiltration and overland flow (DHI, 2014a). The percentage of infiltration is dependent on the hydrogeological characteristics of the aquifers, and as such the catchment area was assigned different infiltration rates as a function of the exposed aquifer units. The fractions for infiltration for the Quaternary and Neogene aquifers are 0.15, and 0.38 for the Eocene aquifer (IRG, 2013; UNDP, 1970; Figure 11).
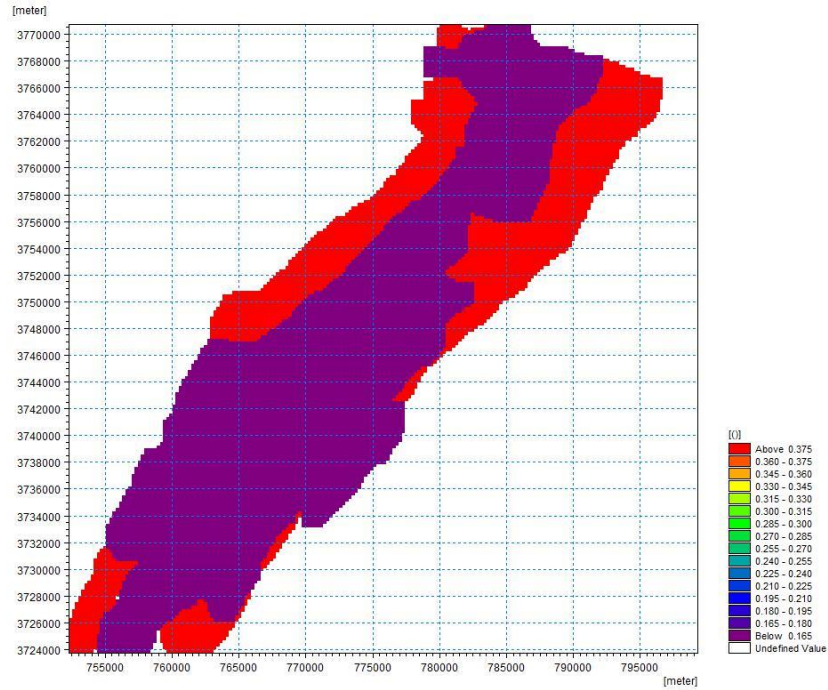
Figure 11: Map of net rainfall fraction over the basin, with higher infiltration rates attributed to Eocene formations, compared to Neogene-Quaternary formations.

- Input: Lateral flow and return flow

Lateral inflow is described by constant fluxes as a function of lithology type, where transfers to groundwater estimates range between 0.4-0.2 m^3/sec for Jurassic and Cretaceous formations, while 0.05-0.2 m^3/sec for Eocene formation. Return flow is the excess volume of water from agricultural activities, broken pipes, and excess pumping that recharges groundwater.

- Output: Pumping

Data on abstraction rates for private and public wells were obtained from UNDP (1970) and IRG (2013) for the years 1970 and 2010. There are approximately 107 public wells and 1109 licensed private wells, without taking into account the number of unlicensed private wells. Average daily pumping rates were taken as 426 m^3/day for the Quaternary, 373 m^3/day for the Neogene, and 916 m^3/day for the Eocene aquifer (IRG, 2013) for the dry months (June, July, and August) due to high dependence on groundwater for irrigation, while 40% of these values were used to the remaining wet months where there is less dependence on groundwater resources and direct irrigation from surface ditches and water bodies (Figure 12).
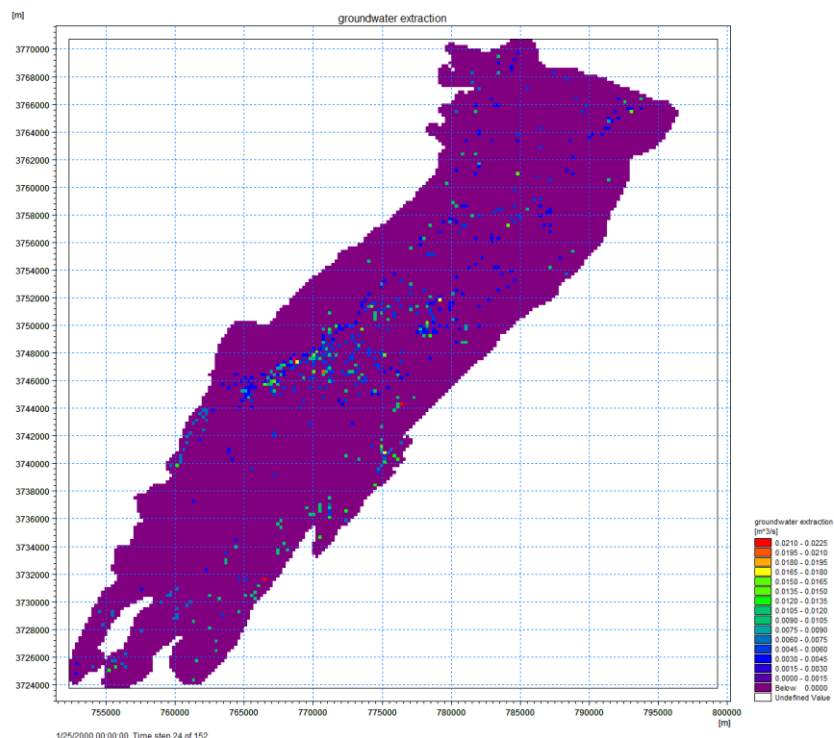
Figure 12: Locations of well abstractions with higher pumping rates for wells penetrating the Eocene formation in comparison to the Neogene and Quaternary formation.

54

- Exchange: Drainage

Drainage flow characterizes natural and artificial routes, and the module becomes active when the simulated water table ascends to a certain level (Zhou et al., 2013). The drainage time constant parameter in MIKE SHE describes the permeability and the density of the drainage system to estimate the velocity of subsurface drainage flow (DHI, 2014b). Drain flow is used to define the natural drainage of the Litani River and is simulated by attributing to each cell a drain level and a time constant (leakage factor) (DHI, 2014a). Both drain levels and time constants are spatially defined and recommended values (DHI, 2014a; Refsgaard, 1997) were used with a drainage level of 1m BG and a time constant between $1e^{-6}$ and $1e^{-8}$ s^{-1} for the conductive alluvial deposits and the surrounding sediments, respectively (Figure 13). The reference system used in the current model is a head-dependent boundary that removes the drainage water from the model omitting routing. As such, the drainage flow is solved implicitly using the Preconditioned Conjugate Gradient solver (PCG) by being directly added in the matrix calculations Eq.(5):

$$q = (h - Z_{dr})\ C_{dr} \tag{5}$$

Where h= head in drain cell (m)

Z_{dr} = drainage level (m)

C_{dr} is the drain conductance or time constant (s^{-1})
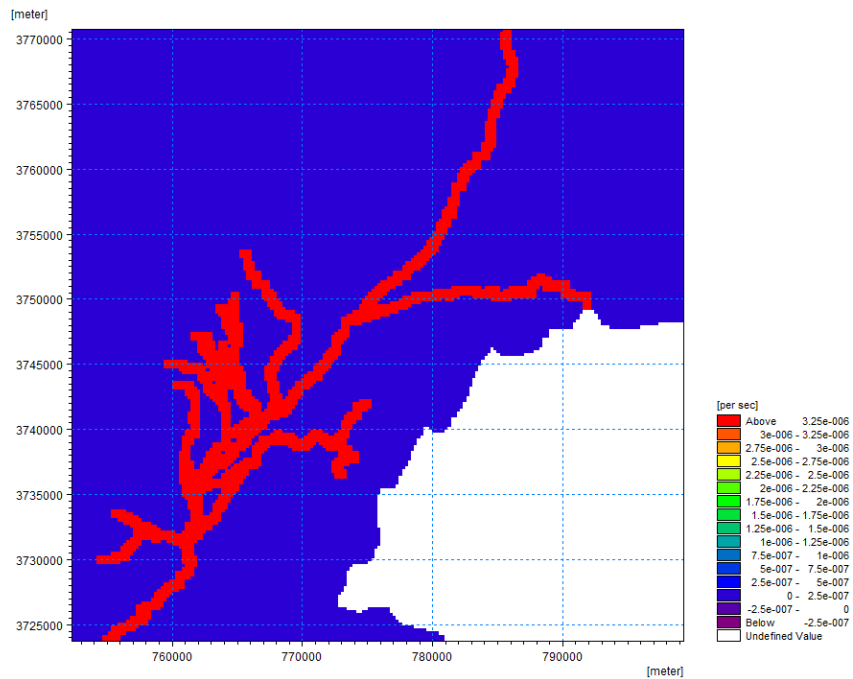
Figure 13: Drainage time constant distribution which is higher for the alluvial deposits in comparison to surrounding deposits.

5.3 Flow simulations

5.3.1   Steady-State Simulations

Steady-state simulation is characterized by its ability to remain constant as a function of time and the conditions which define the steady-state are implicitly reached after an extensive period. This can be further elaborated by Gedeon et al. (2007) where steady-state conditions can be defined by a system's response with respect to a specific set of boundary conditions and present sources and sinks. Therefore, variations in the system occurring, in the long run, can be evaluated by assessing the sensitivity towards variable boundary conditions, and inflow and outflows.

At steady state (under Equilibrium conditions), the flow of groundwater is described by the Laplace equation (Eq. 6):

$$K_x \frac{d}{dx}\left(\frac{dh}{dx}\right) + K_y \frac{d}{dy}\left(\frac{dh}{dy}\right) + K_z \frac{d}{dz}\left(\frac{dh}{dz}\right) - Q = 0 \qquad (6)$$

Where K_x, K_y, and K_z = hydraulic conductivities in the x, y and z directions respectively [m/s]

Q = source or sink [m/s]

Variables defining groundwater systems such as aquifer properties hydraulic conductivity and recharge cannot be obtained easily and directly through field measurements. Consequently, steady-state simulation allows the estimation of aquifer properties and boundary conditions which can be conveyed to transient modelling further simplifying the model calibration process (Hill, 2006; Sonnenborg et al., 2003).

Parameters that were assumed to remain constant for the 1970 and 2010 models were used concurrently such as drainage time constant, geological layers and lenses hydraulic conductivities, and boundary conditions. On the other hand, pumping rates for 1970 were reduced from 2010 abstraction rates in such a way as to mimic the rates obtained in 1970, ie. an extraction rate close to 36.7 Mm^3/yr (IRG, 2013; UNDP, 1970). Variations in groundwater levels surveyed by piezometric wells in 1970 and 2010 were spread out evenly in the basin.

The saturated zone module in MIKE SHE is composed of computational layers and parameters describing the hydrogeological and geological data and in turn, the model interacts with the ET, OL, and UZ components. Groundwater flow in the SZ can be modelled by a fully distributed 3D finite difference approach or by a conceptual linear reservoir scheme.

The linear reservoir method consists of subdividing the catchment area into smaller catchments comprising deep, serial, and shallow base flow reservoirs such that each base flow reservoir is additionally divided to represent the dual storage and discharge slow/fast mechanisms.

5.3.2   Auto-Calibration

The user-defined parameters input into the hydrological modelling system MIKE SHE during model setup are extracted from field measurements and experiments, such as geological and geophysical logs, pumping test analyses, soil, and vegetation types and distribution, etc. As such, several parameters may be directly evaluated and estimated from field data whereas other parameters are calibrated. Therefore, a balance must exist between constructing a well-defined model with intricate parameterization to accurately describe the pronounced variability and fluctuations while simultaneously retaining its relative simplicity for the purpose of smooth calibration (Refsgaard, 1997). The auto-calibration's configuration is based on the evaluation and comparison of the field observations' values with those equivalent to the model's simulations by means of optimization of objective functions, i.e. numerical measures (Madsen and Jacobsen, 2001).

The numerical measures are characterized by the objective function $F(\theta)$, which determines the goodness-of-fit of the models simulated values in reference to a parameter set θ. The optimal parameter set, θ_{opt}, is obtained by solving the optimization problem confined by the constraints of θ to the possible parameter space Θ through the following Eq. (7):

$$\theta_{opt} = Min\{F(\theta)\} \quad \text{such that} \quad \theta \in \Theta \tag{7}$$

Θ = space or hypercube defined by upper and lower boundaries of each parameter such that

the boundaries are based on the understanding of mathematical and physical limitations,

and characteristics.

The sum of squared errors of the simulated vs observed responses, SSE, is the most

frequently employed objective function for automatic optimization procedures of the model

responses

Such a physically-based distributed model is subject to error and uncertainty due to

the nature of the mathematical characterization that does not necessarily reflect processes

and mechanisms occurring in nature. Errors can also be exaggerated by inaccurate

observational and field measurements, insufficient parameter and grid characterization and

definition, and imprecise initial boundary conditions and domain. The calibration process

was based on MIKE SHE's auto-calibration mechanism, AUTOCAL, centered on the

Population Simplex Evolution (PSE) method as the global parameter optimization

algorithm. The method is suitable for parallel executions and the evolution of a population

of points based on contraction and reflection operators with an added mutation component

to reduce premature convergence (DHI, 2017b).

5.3.3   Manual Calibration and Validation

The collected data comprising the most detailed and continuous groundwater flow

characterizing the basin is defined for the years 1970 and 2010, such that the data was

divided into sample calibration and sample validation technique. The calibration sample

period was chosen for the year 1970 and the validation sample was defined by the year 2010. The initial groundwater levels defining the beginning of the simulation were estimated over the region from primary available water level observations and measurements (IRG, 2013; UNDP, 1970). The foundation for this technique is to assess and analyze the simulated groundwater piezometric levels and compare them to the observed groundwater piezometric levels illustrating localized variations and fluctuations within the basin. The available measurements comprise groundwater level data distributed representatively over the catchment area and the following objective function can be written as follows (Eq. 9)

$$F_h(\theta) = \frac{1}{M} \sum_{j=1}^{M} \sqrt{\frac{1}{n_i} \sum_{i=1}^{n_i} [h_{obs\ i,j} - h_{i,j}(\theta)]^2} \qquad (9)$$

Which represents the average root mean squared error (RMSE) of the groundwater levels (h) with M being the number of locations.

The piezometric head data for 1970 are based on groundwater level flow lines (UNDP, 1970), whereby several locations representative of the basin were chosen as the observed head measurements to calibrate the steady-state model. The model was run for 12 months to assimilate the natural values of the saturated zone where default estimates were used, therefore ensuring that the initial values estimated in the steady-state better represent the conditions of the watershed and are transferred into the transient model (Sonnenborg et al., 2003).

5.3.4 Transient Flow simulations

The effect of transient stresses on groundwater movement is crucial in understanding the aquifer system response. The model was run daily from 2010-2019 under transient state, providing the ability to assess the relationship between the spatio-temporal changes of the groundwater level and movement, and transient stresses. As such, values of specific yield and specific storage can be estimated and varied by modeling the temporal fluctuations in groundwater levels. The initial head conditions computed under steady-state were input into the transient model and then run on daily periods until 2019 in order to simulate the influence of abstraction and recharge with shifting seasons while keeping other parameters of the hydrogeologic zone constant.

5.3.4.1 Atmosphere

The Climate component in MIKE SHE functions through evapotranspiration and precipitation input data and is connected to the UZ module. The daily precipitation data was based on several climate stations distributed in the basin. However, cyclic bi-annual time series data was used due to gaps present, resulting in an unrealistic representation of climate conditions.

5.3.4.2 Calculation of reference Evapotranspiration

The basis of the evapotranspiration module in MIKE SHE is centered on the Kristensen & Jensen (1975) empirically derived equations, which is dependent on climate data such as ET_0 and land cover data such as vegetation and related information; Leaf Area

Index (LAI) and Root Depth (RD; Refsgaard & Storm, 1995) which define the land use module and vegetation sub-module. According to DHI (2014b), in order to estimate the total ET and Net Rainfall, several parameters are taken into consideration which include evaporation/interception of rainfall from canopy, drainage from canopy surface to soil, evaporation of soil and root absorption of water and transpiration, as defined by the unsaturated zone soil moisture.

The ET parameters are then modelled in a series of steps; net rainfall is intercepted by canopy surfaces, of which a proportion is subject to evaporation. The other proportion then ponds or represents surface runoff on the surface at the ET_0 rate and/or a fraction infiltrates into the soil profile of the unsaturated zone. A portion of the infiltrating water is subject to evaporation and/or transpiration depending on the soil moisture content, field content, and wilting point in the upper plant root zone if insufficient ET_0 takes place. In addition, the dissemination of evapotranspiration is a function of the vertical distribution of the root properties encompassing root depth and shape factor in the upper root zone. The remaining part of percolating water recharges the groundwater in the saturated zone. The reference evapotranspiration was calculated based on data from Qaa climate station.

The reference evapotranspiration, ET_o [mm day^{-1}], is calculated based on the FAO-56 Penman-Monteith equation as recommended by (DHI, 2014a) and several authors (Allen et al., 1998) and is defined as reference surface that is not short of water (Eq. 10)

$$ET_0 = \frac{0.408\,\Delta \cdot (R_n - G) + \gamma \cdot \frac{900}{T+273} \cdot u_2 \cdot (e_s - e_a)}{\Delta + \gamma(1 + 0.342\,u_2)} \tag{10}$$

Where R_n = net radiation at the crop surface [MJ m^{-2} day^{-1}], G = soil heat flux density [MJ m^{-2} day^{-1}],

T = average daily air temperature at 2 m height [°C], u_2 = wind speed at 2 m height [m s^{-1}],

e_s = saturation vapor pressure [kPa], e_a = actual vapor pressure [kPa], e_s - e_a saturation

vapor pressure deficit [kPa], Δ = slope vapor pressure curve [kPa °C^{-1}], γ = psychrometric

constant [kPa °C^{-1}].

The transpiration and canopy interception, and evaporation from soil calculations

were based on recommendations by DHI (2014a) and Doummar et al. (2012).

5.3.4.3   Unsaturated Zone

The unsaturated zone characterized by its heterogeneous nature serves as a

connection between processes occurring at the ground level surface and processes at the

subsurface level and is defined by cyclic soil moisture fluctuations due to the removal of

water by evapotranspiration processes and percolation to the saturated zone countered by

replenishment through snowmelt and precipitation.

There are three proposed methods of calculation of vertical flow in the unsaturated

zone (DHI, 2014a, 2014b) where the gravity flow method was chosen and accounts for a

uniform vertical gradient whilst disregarding effects of the capillary zone and processes.

The flow in the unsaturated zone is essentially estimated in the vertical direction in

1D in the soil profile, therefore flow in the unsaturated zone is predominantly governed by

changes in hydraulic head (h) [m] that is a function of gravimetric head (z) [m] and pressure

head (ψ) [m] coefficients (Eq. 11)

$$h = z + \psi \tag{11}$$

Using Darcy's equation, the water flux (q) [m/s] can be estimated

$$q = -K(\theta)\frac{dh}{dz} \tag{12}$$

Where $K(\theta)$ = unsaturated hydraulic conductivity is a function of volumetric content.

      With the assumption that the soil matrix incompressibility and constant soil water density the following continuity equation can be deduced as follows, where Eq. 13 solves in the vertical downward direction from the uppermost level of the soil column:

$$\frac{d\theta}{dt} = -\frac{dq}{dz} - S(z) \tag{13}$$

Where t= time [s]

θ = volumetric water/moisture content [-]

z = depth [m]

S = sink term for root extraction [s^{-1}]

      The user specifies the initial conditions of the UZ by setting the initial matrix or water content, or initial conditions may be defined by software generating equilibrium pressure or soil moisture profiles at no-flow conditions. The present model represents user-specified initial conditions based on several sources providing vegetation, LULC, soil distribution data.

The retention curves and hydraulic conductivities were determined for each soil classification by the van Genuchten equations (Eqs 14 & 15)

$$\theta(\psi) = \theta_r + \frac{\theta_s - \theta_r}{[1 + (\alpha \cdot \psi)^n]^m} \qquad (14)$$

$$K(\psi) = K_s + \frac{\left((1 + |\alpha \cdot \psi|^n)^m - |\alpha \cdot \psi|^{n-1}\right)^2}{[1 + (\alpha \cdot \psi)^n]^{m(l+2)}} \qquad (15)$$

Such that: ψ = suction pressure [L]; θ (ψ) = the soil moisture retention curve [-]; K(ψ) = hydraulic conductivity [m/s]; θs = saturated water content [-]; θr = residual water content [-]; α, n, m, l = empirical constants [-]; Ks = saturated hydraulic conductivity [m/s]; K(ψ) = hydraulic conductivity [m/s].

A more complex model that is presently employed describes the variations in hydraulic heads is characterized by the mathematical governing 3D Darcy's equations of the saturated zone flow in a heterogeneous and anisotropic porous media under non-equilibrium conditions, and is solved numerically and iteratively by finite difference approach, and is represented by equation (16). The storage coefficient varies under confined and unconfined aquifer situations whereby under confined aquifer conditions the storage coefficient changes to specific yield under unconfined aquifer conditions and equations become non-linear.

$$K_x \frac{d}{dx}\left(\frac{dh}{dx}\right) + K_y \frac{d}{dy}\left(\frac{dh}{dy}\right) + K_z \frac{d}{dz}\left(\frac{dh}{dz}\right) - Q = S \frac{dh}{dt} \qquad (16)$$

K_x, K_y, and K_z = hydraulic conductivities in the x, y and z directions respectively [m/s]

Q= source or sink [m/s]

h = hydraulic head [m]

S= storativity [-] = S_s b + S_y

Where S_s is the specific storage [L^{-1}]

b= thickness of aquifer [L]

S_y = Specific yield [-]

For an unconfined leaky aquifer, the water stored in interstitial openings is yielded by the effect of gravity drainage as a result of water table decline. Therefore, water table aquifer expansion and aquifer compression release little water from storage in comparison to gravity drainage, the equation (4) becomes $S \cong S_y$ since $S_y \gg S_s b$.

MIKE SHE proposes the SOR and PCG solution techniques whereby SOR solves by successive over relaxation and PCG allows selecting either a steady or unsteady state model by applying a preconditioned conjugate gradient technique.

CHAPTER 6

RESULTS

6.1 Grain size distribution analyses

In calculating the hydraulic conductivities through empirical methods, theoretical assumptions for the grain size and the coefficient of grain uniformity (*U*) were satisfied for all methods applied. The hydraulic conductivity values determined from grain-size distribution analyses based on empirical methods are not representative of the spatial aquifer properties but only localized disturbed samples at various depths. Generally, the yielding values are less accurate than values estimated by pumping tests as a result of the disturbance and alteration in texture of the representative sample subject to processes of extraction, and preparation (Uma et al., 1989). Table 4 represents a sample that was subject to sieving showing the percent finer grains that have passed the mesh, plotted against a semi-log plot against grain diameter size, in order to have a better understanding of the distribution of the passing grains with size (Figure 15). The compiled percent finer grain size as a function of depth of the borehole can be summarized in Figure 14, where gravels and sand-sized grains are predominant over clays and silts in the localized area, and in order to better understand the particle size classification, Table 5 shows the distribution and definition of one sample analyzed, with more than 70% of the sample being gravel and coarse gravel size.

Kozeny-Carman (1927, 1953) and Hazen (1892) take into consideration porosity (n) and grain size in estimating K while Beyer only considers grain size and the coefficient

of uniformity (*U*). On the other hand, the Kozeny-Carman method is based on the total

particle shape and size distribution which is more accurate in comparison to Hazen which

only accounts for particle size distribution for d_{10} (Carrier, 2003). Accounting for only d_{10}

grain size distributions disregards the finest fraction of samples that may decrease hydraulic

conductivity estimates (Gentry et al., 2006; Kasenow, 1997) and tight sediments consisting

of fractions of less than 2% silt and clay (Eggleston & Rojstaczer, 2001).

a)   b)
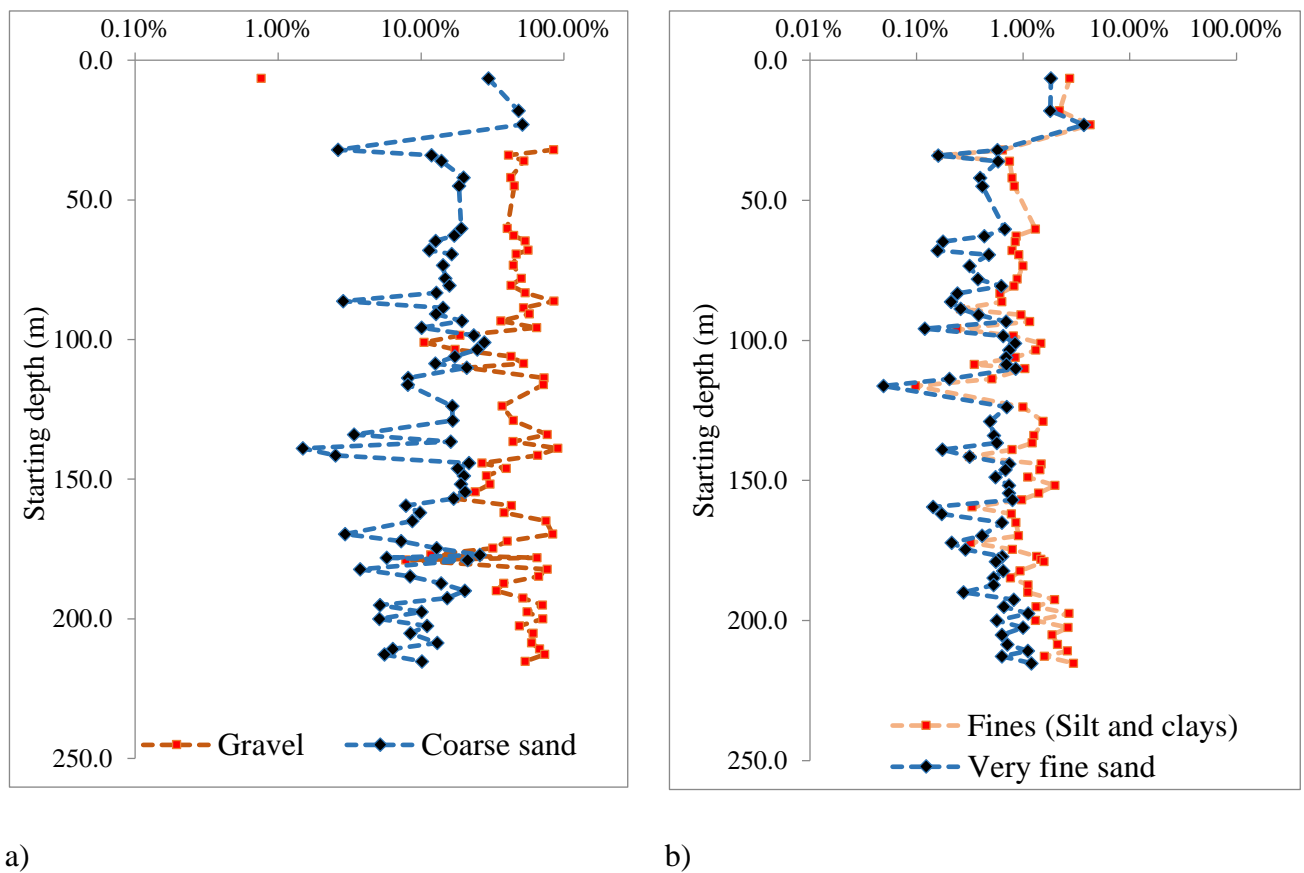
Figure 14: Percent of passing grain sizes as a function of depth, a) for gravel and coarse
sand sized sediments; b) for very fine sand and silt, and clay sediments.

Table 4: Table showing calculation and distribution of % finer particles.

Sieve size (mm)	Sieve #	Sieve size (μm)	Mass of each sieve (g)	Mass of each sieve + retained soil (g)	Mass of soil retained-Wn (g)	% on each sieve Rn	Cumulative percent retained ΣRn	% finer (100- ΣRn)
2	10	2000	460	507.2	47.2	36.22	36.22	63.78
0.85	20	850	390.2	438	47.8	36.68	72.91	27.09
0.42	40	420	536.8	556.9	20.1	15.43	88.33	11.67
0.3	50	300	503.1	508.1	5	3.84	92.17	7.83
0.18	80	180	462.3	467.1	4.8	3.68	95.86	4.14
0.15	100	150	367.8	369.2	1.4	1.07	96.93	3.07
0.125	120	125	313.9	314.9	1	0.77	97.70	2.30
0.106	140	106	450.9	451.2	0.3	0.23	97.93	2.07
0.09	170	90	317.7	318	0.3	0.23	98.16	1.84
0.075	200	75	338	338.9	0.9	0.69	98.85	1.15
0.01	Pan	-	352.9	354.4	1.5	1.15	100.00	0.00
ΣWt$_1$					130.3	100		
% Error Mass lost during sieve analysis $= \dfrac{Wt_{sample}-Wt_1}{Wt_{sample}} \cdot 100$						0.53%		

Table 5: Interpretation and classification of sample results.

Particle Size (mm)	Classification	%
>2.0	Gravel	36.22
2.0-1	V. Coarse sand	36.68
1-0.5	Coarse sand	15.43
0.5-0.25	Medium Sand	3.84
0.25-0.1	Fine sand	3.68
0.1-0.05	V. Fine sand	1.07
less than 0.05	Silt and clays	0.77
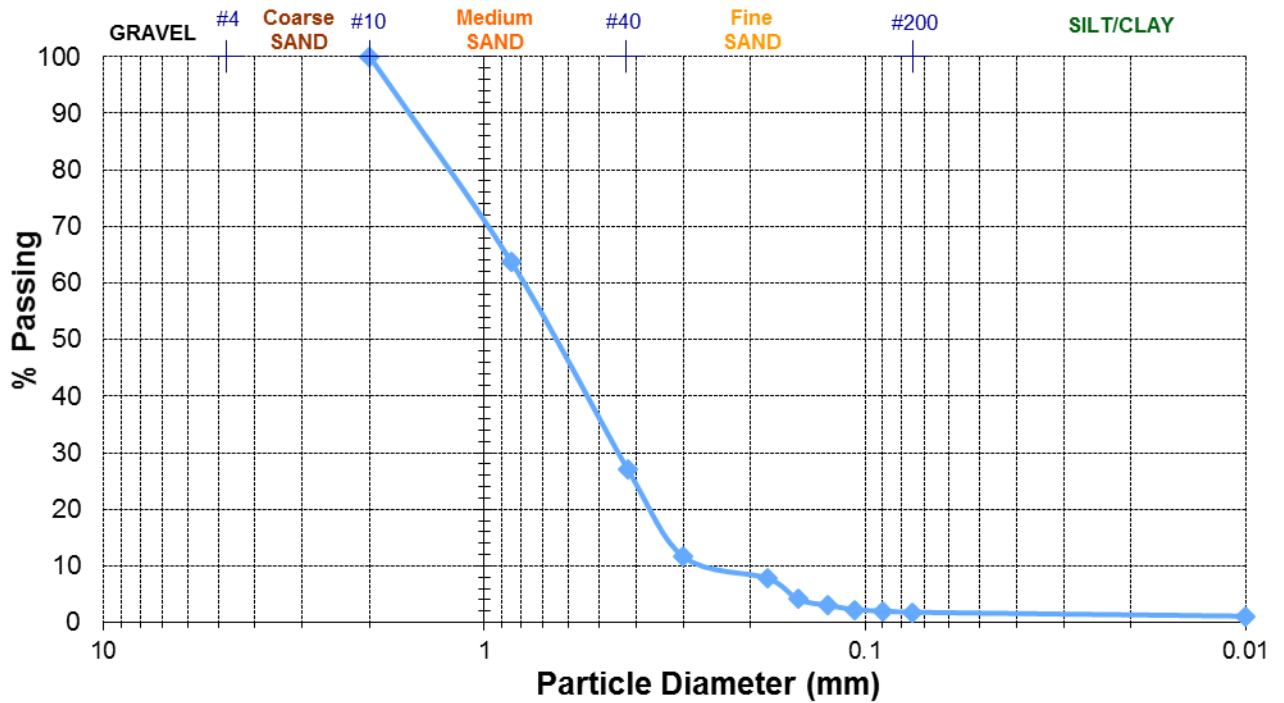
Figure 15: Grading curve of log sieve size (mm) vs. % finer size particles.

6.2 Aquifer test results

Data were processed and analyzed graphically and with the numerical tool

AQTESOLV (Version 4.5 professional; Duffield, 2007) according to the most appropriate

pumping test solution.

6.2.1   Step drawdown

Step drawdown data was downloaded from the pressure transducer at the end of

the test. The total drawdown observed reached 34.05 m. The incremental drawdown in each

step along with pumping conditions is shown in Table 6.

Table 6: Drawdown data for respective pumping steps.

Steps	Q (m³/h)	Q (m³/d)	Cumulative drawdown s (m)	Drawdown Δs (m)
1	2.0	48.00	8.415	8.415
2	4.0	96.00	20.97	12.55
3	5.0	120.0	29.20	16.65
4	5.6	134.4	34.06	17.40

6.2.1.1 Calculation of well efficiency: well and aquifer losses

The plot of Q versus s allows constructing the well capacity curve that shows the expected discharge for a certain amount of drawdown (Figure 16).
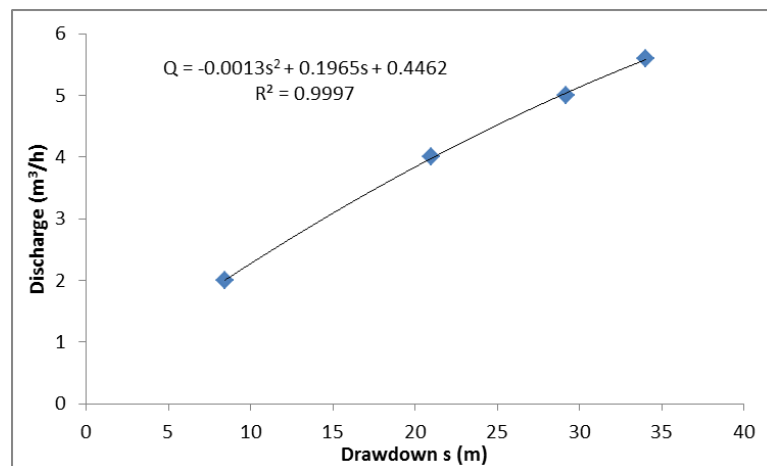
Figure 16: Specific Capacity curve: Plot of discharge versus drawdown Q(s).

Hantush-Cooper solution (Hantush & Jacob, 1955)) for step drawdown was used to calculate the borehole efficiency and aquifer laminar losses (B) and turbulent well losses (C) according to the following

71

$$sQ = \mathbf{B}Q + \mathbf{C}Q^2 \qquad (17)$$

Where s [L] is the drawdown observed for a pumping rate Q [L/T], B [T/L^2] is the aquifer laminar losses and C is the well turbulent losses [T^2/L^5].

Based on the plot of s/Q versus Q, the calculated slope represents the turbulent losses C and the intercept is the laminar losses B. The efficiency of the well was calculated based on:

$$E = \frac{\mathbf{B}Q}{\mathbf{B}Q + \mathbf{C}Q^2} \qquad (18)$$
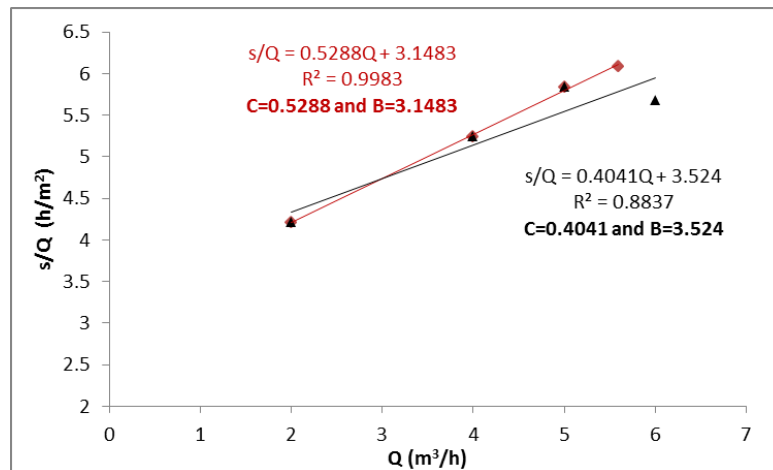
Figure 17: Plot of s/Q versus Q to calculate the slope C and the Intercept B for the step drawdown tests with the last two steps at 5.6 m^3/h (red) and 6 m^3/h (black).

For a better fit of s versus Q for the last step, the average pumping rate in step 4, was closest to 5.6 m^3/h rather than 6 m^3/h, even though the flowmeter was displaying a 6 m^3/h. Therefore, well efficiency was calculated for both scenarios (Table 7). The well efficiency over the four steps ranged between 51-81% ($\pm$ 7%). Well efficiency was highest (closest to 75%) at 2 m^3/h. The borehole losses effects on drawdown are illustrated in

Figure 19. Therefore it was decided that the pumping test be conducted at 3 m^3/h since it

was considered to be in the range of highest efficiency and within the ranges of maximum

allowed drawdown.

Table 7: Results of the step drawdown analysis.

Steps	Q m^3/h	Q m^3/d	s (m)	ΔS	s/Q	E	Error
1	2	48.00	8.415	8.415	0.175313	81.34%	-4.16%
2	4	96.0	20.97	12.552	0.218406	68.55%	-6.81%
3	5	120.0	29.20	16.652	0.243367	63.56%	-7.81%
4	6	134.4	34.06	17.403	0.236493	59.24%	-6.96%
	B=3.524 h/m^2 ±5%		**C=0.404 h^2/m^5 ±13%**				

Table 8: Results of step drawdown test with the corrected discharge in the last step.

Steps	Q m^3/h	Q m^3/d	s (m)	ΔS	s/Q	E	Error
1	2	48.00	8.415	8.415	0.1753	74.85%	4.16%
2	4	96.0	20.97	12.55	0.2184	59.81%	6.81%
3	5	120.0	29.20	16.65	0.2433	54.35%	7.81%
4	*5.6*	**134.4**	**34.06**	**17.40**	**0.2533**	**51.53%**	6.96%
	B=3.148 h/m^2 ±5%		**C=0.529 h^2/m^5 ±13%**				
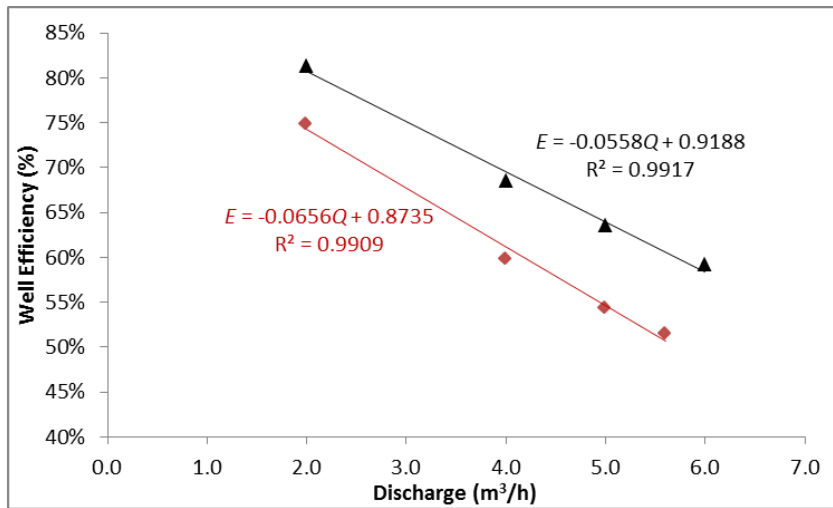
Figure 18: The percentage in Efficiency versus discharge rate to determine the most suitable flowrate for the long term pumping test.
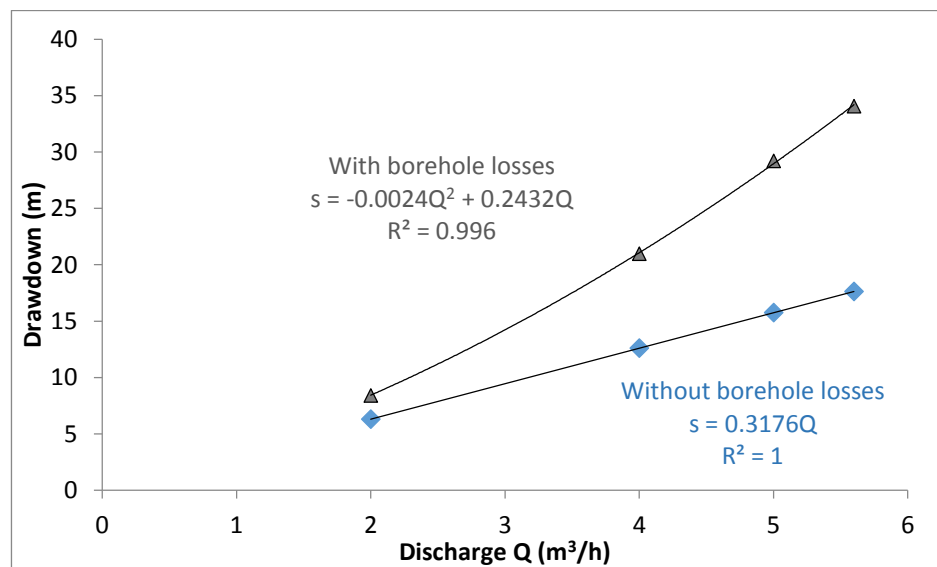
Figure 19: Effect of borehole losses CQ^2 on drawdown.

6.2.1.2 Estimation of transmissivity (T) and storativity (S) from the step drawdown

The plot of S versus T allows the estimation of transmissivity and storativity for consecutive discharge steps (Figure 18) using Hantush-Jacob (1955) for unconfined

74

aquifers. An average Transmissivity was estimated at **T=1.7 x 10^{-5} m^2/s**. Consequently a

hydraulic conductivity (T=Kb) of **K= 1.2 x 10^{-7} m/s** for 145 m of saturated thickness**.**

Specific yield (S_y) for this unconfined aquifer was estimated at **0.13**. These values are in

concordance with a relatively low- yield aquitard.

Estimated Parameters		
Parameter	Estimate	
T	1.702E-5	m^2/sec
S	0.1327	
r/B	0.1	
Sw	0.0005875	
C	0.01	sec^2/m^5
P	1.5	
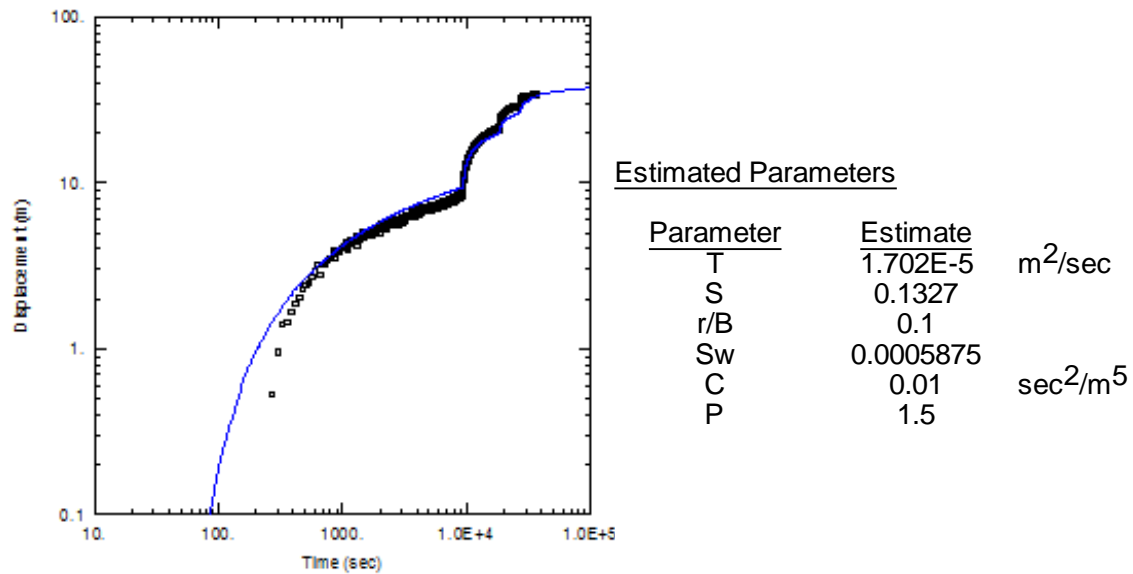
Figure 20: Hantush-Jacob solution for the Step drawdown with AQTESOLV.

6.2.2   Long term Pumping test

Pumping test data were downloaded from the pressure transducer at the end of the

test. The total drawdown observed at Q= 3 m^3/h reached 17.5 m and 16.8 m for the 41.5 and

12.75-hour pumping tests, respectively. The slight shift observed in the two curves in

Figure 21 is due to residual drawdown after recovery from the 12.75 hrs pumping test.

Figure 21 shows the plot of drawdown versus time for the two pumping tests (12.75-hr and

41.50-hr). A diagnostic plot of the derivative of drawdown versus time [ds/d(log(t))] allows

to highlight the type of aquifer and the most appropriate solution, which revealed to be a

leaky aquifer with an aquitard (Renard et al., 2009).
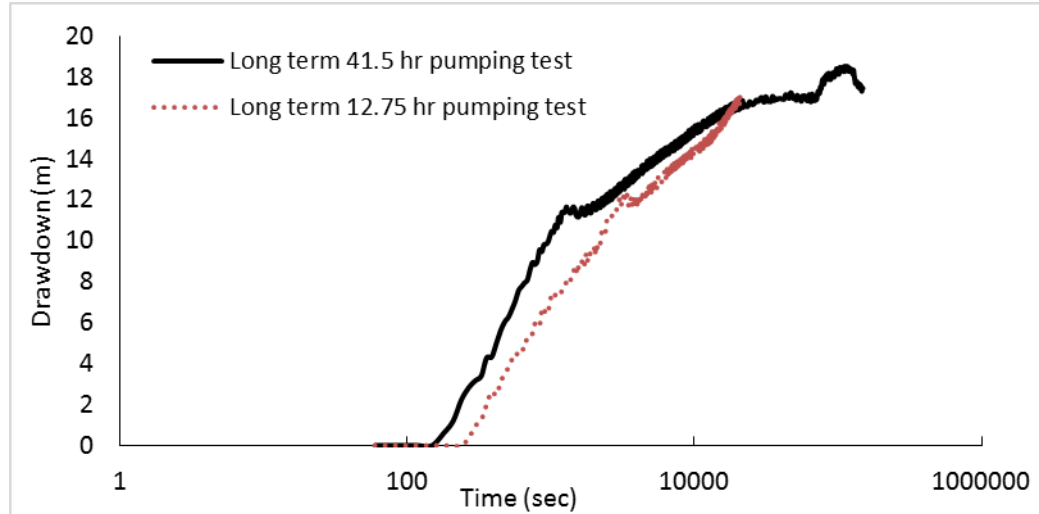
Figure 21: Plot of drawdown versus time (s(t)) observed in the two long term pumping tests (12.75 hrs and 41.5 hrs).

The most appropriate mathematical solution by Hantush and Jacob (1955) was

used to estimate the hydraulic properties; Transmissivity and Storativity of leaky confined

or (semi-confined) aquifers (21). The analysis involves matching the Hantush-Jacob W

(u,r/B) well function for leaky confined aquifers to drawdown data collected during a

pumping test.

$$ s = \frac{Q}{4\pi T} W(u,r/B) \quad \text{where } u = \frac{r^2 S}{4Tt} \text{ and } B = \sqrt{\frac{Tb'}{K'}} \tag{19} $$

Where s is drawdown [L], Q is pumping rate [L³/T], T is transmissivity [L²/T], S is

storativity [dimensionless], w (u,r/B) is the Hantush and Jacob well function for leaky

confined aquifers, the leakage parameter r/B [dimensionless], where B is in [L]. b′ is the

76

aquitard thickness [L], and K′ is the vertical hydraulic conductivity of the aquitard [L/T].

In this case, the hydraulic properties of the aquitard through which leakage is occurring

cannot be estimated due to the lack of observation well data.

6.2.2.1 Estimation of Transmissivity and Storativity

The plot of S versus T allows the estimation of transmissivity (T) and storativity

(S) for 41.5-hr pumping test (Figure 22). Values of Transmissivity $T=1.5 \times 10^{-5} \, m^2/s$, a

hydraulic conductivity (T=Kb) of $K= 1.1 \times 10^{-7} \, m/s$ for 145 m of saturated thickness were

estimated for this pumped aquifer. Specific yield (S_y) for this unconfined unit was estimated

at 0.10. Modeled results are most sensitive to each of T and S in this solution. Specific

Storage (S_s) was estimated at $6.9 \times 10^{-4} \, 1/m$. Other parameters such as thickness and

hydraulic conductivity of aquitard (b' and K') are not estimated due to the absence of

drawdown data from observation wells. The estimated parameters are in concordance with

the ones calculated in the step drawdown test.
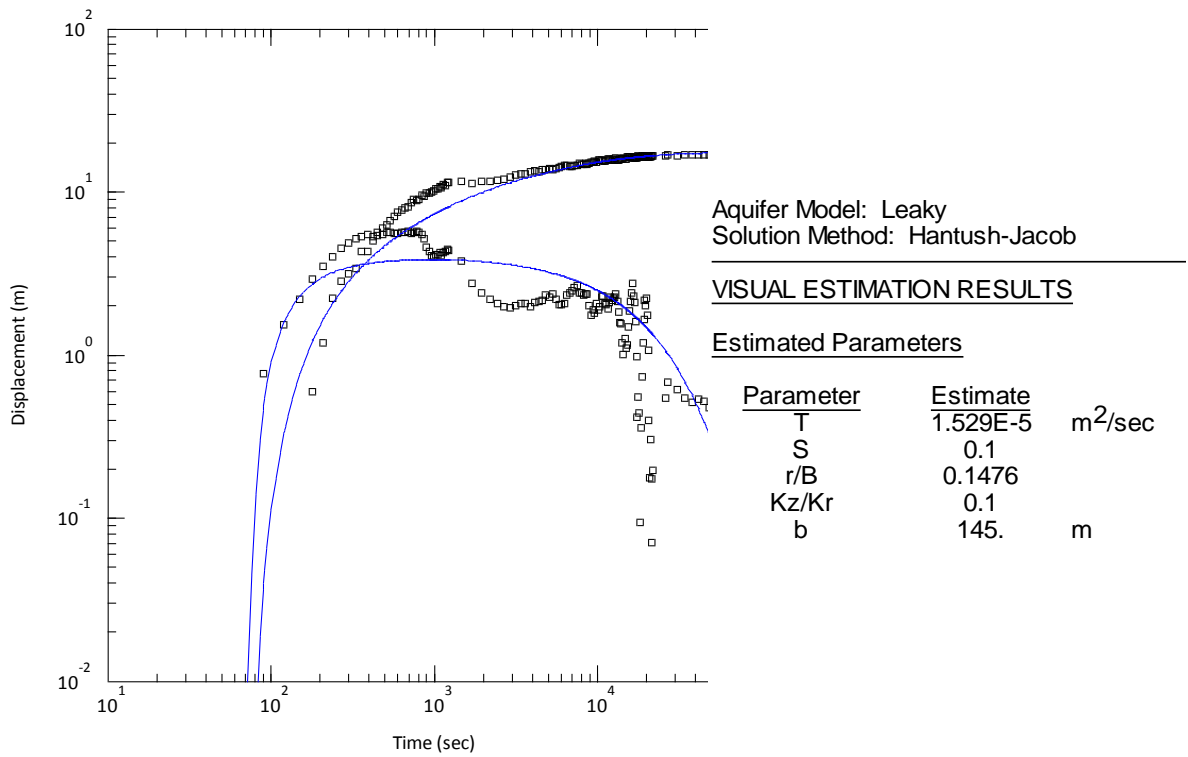
Figure 22: Plot of modeled and observed data using the Hantush-Jacob solution for leaky confined aquifers (Upper Left), and diagnostic plot ds/dln T vs T of observed data used to estimate the most appropriate pumping test solution (Bourdet et al., 1983, 1989; Lower Right).

6.3 Steady-State Model

6.3.1 Calibrated Parameters

The horizontal hydraulic conductivity ranged from 0.068 m/day to 8.64 m/day and vertical hydraulic conductivity ranged from 0.000147 m/day to 0.069 m/day, with an anisotropy ratio ranging between 0.01-0.1. The hydraulic conductivities are a function of lithology, such that the lens with the highest conductivity is to the southern section of the

basin attributed to the Eocene formation in contrast to the northern part of the basin mainly

consisting of Neogene deposits (Table 9).

Table 9: Various model parameters that were measured or fitted during the set-up and calibration of the steady-state model.

Component		Parameters	Unit	Type of Data	Range	Calibrated Value
Atmosphere and Surface	Climate data	Precipitation (P)	mm/day	Measured	1.7 - 2	1.8
		Net Rainfall Fraction	%		15 - 38	-
Saturated Zone	Geological Layers	Vertical Hydraulic conductivity (K_{yy})	m/s	Fitting	$1 \times 10^{-9} - 1 \times 10^{-6}$	-
		Horizontal Hydraulic conductivity (K_{xx})	m/s		1×10^{-7}	-
		Specific yield (S_{yc})	-		$1 \times 10^{-5} - 1 \times 10^{-3}$	-
		Specific Storage (S_{sm})	1/m		0.1-0.3	-
	Geological Lenses	Vertical Hydraulic conductivity (K_{yy})	m/s	Fitting	-	$1 \times 10^{-9} - 1 \times 10^{-6}$
		Horizontal Hydraulic conductivity (K_{xx})	m/s		-	$1 \times 10^{-6} - 1 \times 10^{-5}$
		Specific yield (S_{yc})	-		-	0.2
		Specific Storage (S_{sm})	1/m		-	1×10^{-4}
		1 to 2[1]	m^3/s	Fitting	0.1-0.4	0.25

---

[1] Constant flux from eastern Cretaceous boundary.

Boundary conditions	2 to 3[2]	m		840	-
	3 to 4[3]	m³/s		0.1-0.4	0.25
	4 to 5[4]	m³/s		0.05-0.2	0.1
	5 to 6[5]	m³/s		0.1-0.4	0.25
	6 to 1[6]	m		0	-
Drainage	Time Constant	/s		5×10^{-6} - 3×10^{-8}	-

6.3.2 <u>Calibrated and validated heads and error evaluation</u>

The piezometric heads were assessed for both steady-state models 1970 and 2010, by calculating mean errors, mean absolute error, root mean square error, and coefficient of determination R^2 (See Appendix D). The simulated water level for 1970 and 2010 show that the water table has dropped severely, as evident from the potentiometric maps (Figure 24 a,b). The flow direction in 1970 is more evident, as the flow is from the north of the basin to the south, in contrast to 2010 where flow direction is not as apparent, which may in turn affect the drainage to rivers and the Qaraoun reservoir.

---

[2] Constant head boundary with Qaraoun reservoir.
[3] Constant flux boundary from western Jurassic boundary.
[4] Constant flux from western Eocene boundary.
[5] Constant flux from western Cretaceous boundary.
[6] Zero flux boundary due to water divide.
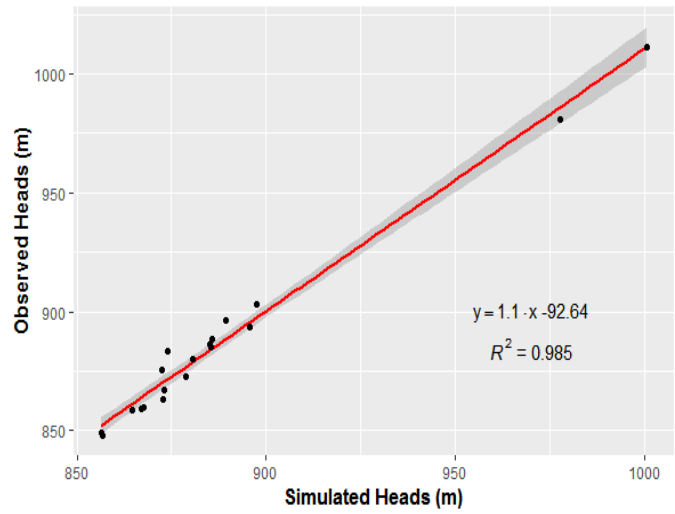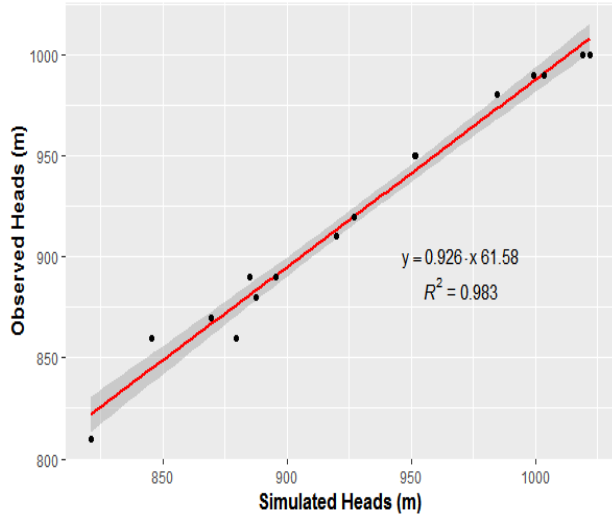
Figure 23: a) Observed vs. Simulated heads for 1970.

b) Observed vs. Simulated heads for 2010.
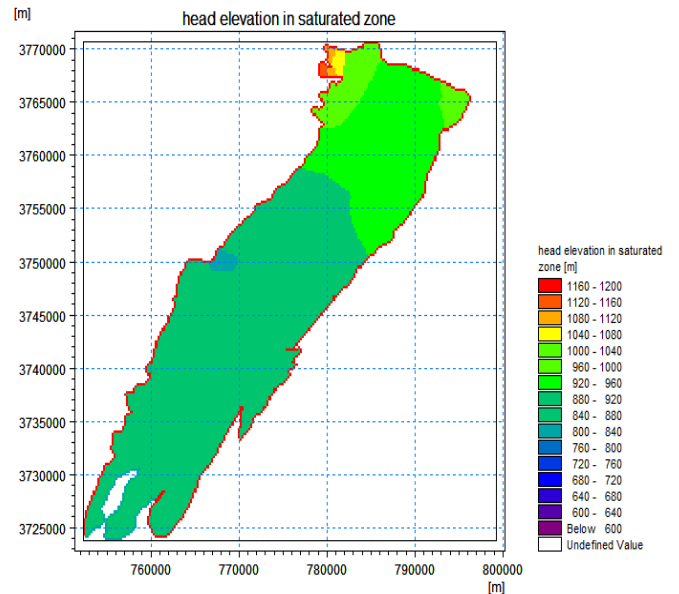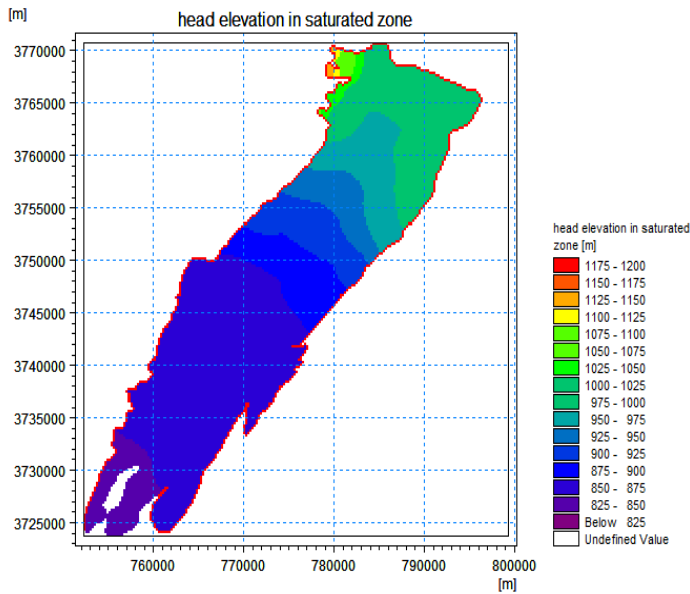
Figure 24 a): Head elevation of the saturated zone for 1970 steady-state model.

b) Head elevation of the saturated zone for 2010 steady-state model.

The potentiometric levels of 1970 and 2010 were overlaid to estimate the hydraulic head difference (Figure 25). The highest difference is to the upper western zone of the basin, along the Eocene boundary, with head drops up to more than 40 m. This is due to the excessive pumping and lower lateral influx from the Eocene formation. The differences in head decrease from the northern part of the basin, where declines in groundwater levels range from 20-30m towards the central part, up to 10-20 m drops, reaching the southern zone with differences less than 10 m and less than 5 m near the constant head boundary.
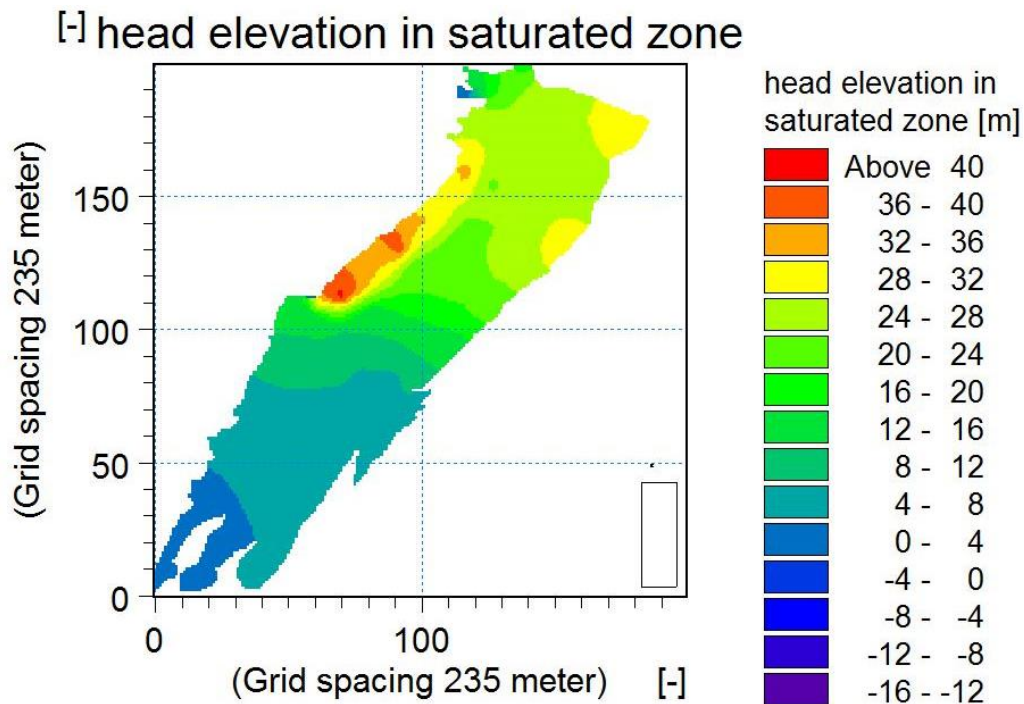
Figure 25: Distribution of hydraulic heads by overlaying 1970 simulated potentiometric levels over 2010 simulated potentiometric levels.

6.3.3   Water budget

The estimated water budget signifies water availability and storage within the ULB as climatic conditions and anthropogenic activities influence the area. Table 10 depicts the water budget components for the ULB at steady-state for 1970. Assuming recharge and return flow remain the same for 1970-2010, pumping has significantly impacted the water budget, as a result of approximately ~200% increase in pumping rate, assuming that during wet months only 40% of the pumping rate values for Quaternary, Neogene and Eocene are used compared to pumping during the dry summer season. As such, the output from pumping increased form 37 Mm^3 to 105 Mm^3. This in turn has affected lateral inflow and drainage to rivers. This is validated by the resulting aforementioned simulated flow levels and directions showing the significant effect that pumping has on the water table.

Table 10: Preliminary groundwater balance for 1970.

Source	Input (Mm^3)	Output (Mm^3)	Total (Mm^3)
Wells	0	-37.84	-37.84
River	0	-33.38	-33.38
Recharge/Return flow	87.49	0	87.49
Inflow from adjacent boundaries	27.43	0	27.43
Outflow from adjacent boundaries	0	-43.69	-43.69
Error			0.01

6.4 Transient Simulations

Transient simulations are conducted based on the introduction of individual stresses, such as variations in recharge and well abstractions, affecting the transient solutions, whereas boundary conditions influence the steady-state solution. Generally, a steady-state flow model is achieved following the introduction of stresses after an adequate interval. In order to run transient simulations, several requirements should be satisfied which include the setup of initial conditions, spatio-temporal discretization, sufficient simulation time for complete termination of iterative solving, and use of appropriate hydraulic head distributions at steady state (Anderson et al., 2015).

Having satisfied these requirements, transient simulations were run from 2010-2019, with initial conditions from the validated steady state 2010 model used as hot-start data, using cyclic bi-annual meteorological data for the area due to the absence of times series data and gaps. The total and annual water budgets were estimated for the transient model, showing the response of the model to fluctuations of precipitation and evapotranspiration and variations in recharge and drainage (Table 11). The recharge to saturated zone appears to have decreased over the years, attributed to the high pumping rates in comparison to the precipitation and constant lateral boundary inflows, in turn affecting the exchange with the Litani River. This can be further explained by Figure 26, that the main temporal decrease in drainage and recharge occurred during the dry summer months, which are consistent with the drop in precipitation, and the increased abstraction.

Table 11: Annual water budgets for the transient model.

Date	Recharge to SZ (mm)[7]	Net Precipitation (mm)	Evapo-tranpiration (mm)[8]	Subsurface boundary inflow (mm)	Subsurface boundary outflow (mm)	Pumping (mm)	Drainage outflow + Storage (mm)	Error of WB (mm)
2013-2014	-192.28	-291.84	197.18	-43.24	100.12	200.04	-64.61	-0.34
2014-2015	-179.13	-428.74	290.09	-43.24	93.34	202.60	-73.53	-0.18
2015-2016	-172.79	-295.33	183.77	-43.36	88.62	202.90	-75.34	-0.14
2016-2017	-167.20	-291.45	197.23	-43.24	86.31	203.20	-79.05	-0.09
2017-2018	-164.50	-429.13	291.64	-43.24	84.31	203.54	-80.08	-0.04
2018-2019	-161.05	-295.33	183.09	-43.24	82.03	203.92	-81.64	-0.06

---

[7] Negative signs indicate downward movement and positive recharge.

[8] Positive signs indicate upward movement and negative discharge.
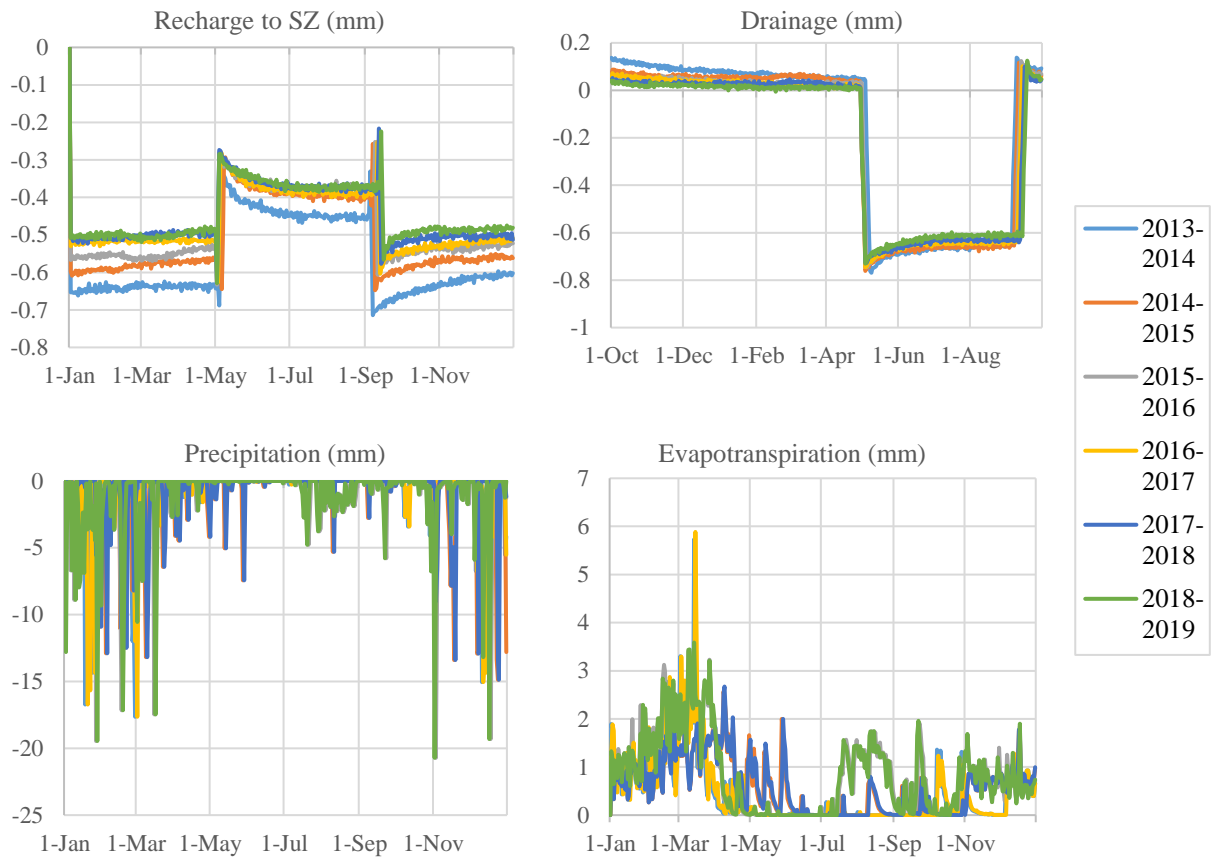
Figure 26: Annual variations in a) recharge to saturated zone (negative sign indicate downward movement and positive recharge), b) lumped drainage , c) cyclic bi-annual precipitation data, d) cyclic bi-annual evapotranspiration data.

Certain parameters were increased and decreased within an acceptable range in order to check the sensitivity of the model towards these parameters. The horizontal conductivities, precipitation rates, and pumping rates were increased and decreased by 20%, and specific yield S_y was varied between 0.05 and 0.3. The majority of simulated hydraulic heads fall within ± 10 m error of the observed 2010 head data (Figure 27). The model's sensitivity towards the parameters is influenced by the location of the piezometer.

Observation wells near the western Cretaceous boundary show moderate model sensitivity with respect to the varying parameters, with head differences ranging between 10-20 m, with the observed heads less than the simulated heads. The simulated heads are larger than the observational heads, this can be a result of the high lateral influx from the Cretaceous boundary and the location of the piezometric wells from the high abstraction of clustering. In contrast, well #48 located close to the Eocene boundary, shows the highest deviation in ME of 74 m of the simulated head with respect to the observed head, as a result of lower subsurface influx from the Eocene boundary in comparison to higher influx rates from the Jurassic and Cretaceous boundaries. Observational wells located at the center of the basin show a ME of 5-10m extending to the southern part of the basin with a decrease in a difference of less than 5m. This can be attributed to the remote location of the observational wells from the effect of the pumping wells.
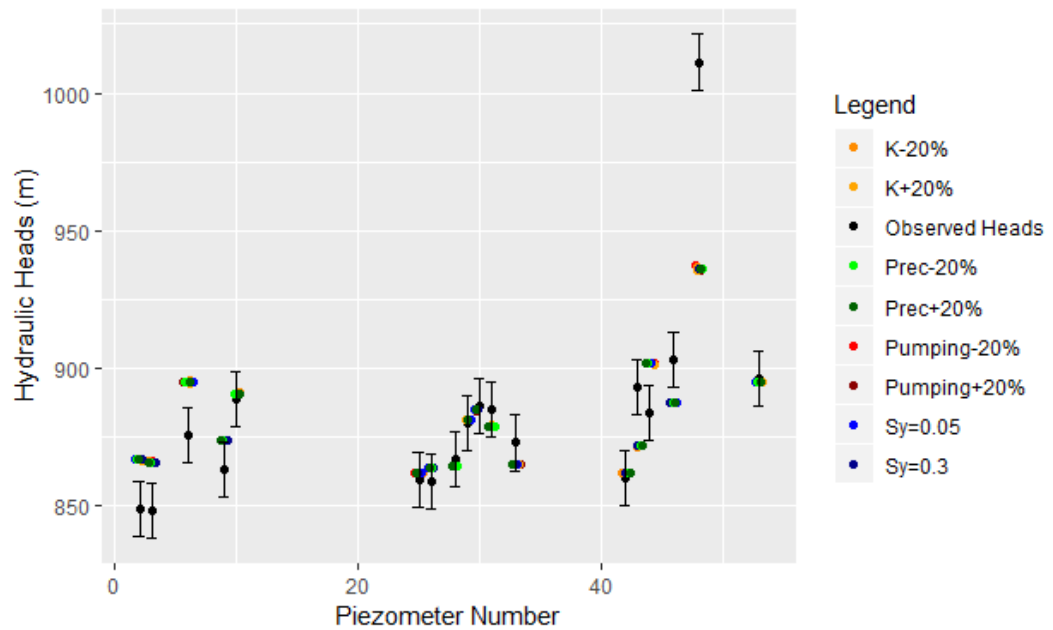
Figure 27: Observed head intervals of ±10 m according to the piezometer number, and the distribution of the simulated heads with varying parameter ranges with respect to the 2010 observational head measurements.

The model's sensitivity towards precipitation was evaluated based on running 2 additional transient models with precipitation data derived from Zahle and Kherbet Qanafer climate stations. The water budgets were computed for the respective climate stations, assuming pumping, and lateral inflows are constant Table 12 and Table 13. The average precipitation rates in Zahle are higher compared to those of Kherbet Qanafer, ranging between 600-700 mm/yr. It can be noted that the difference in precipitation has in turn affected the infiltration to the saturated zone, and consequently affected recharge and drainage to rivers.

Table 12: Water budget for the transient model with precipitation data from Zahle climate station.

| | mm | | | | | | | | | |
Date	Total Precipit-ation	Net Precipit-ation.	Infiltr-ation	Recharge	Evapo-transpiration	Subsurface Boundary Inflow	Subsurface Boundary Outflow	Pumping	SZ Drain Outflow + Storage	Error of WB
2013-2014	-705.29	-618.35	611.83	-365.64	282.03	-43.24	98.36	200.08	105.06	-0.29
2014-2015	-678.29	-562.18	550.07	-292.98	422.54	-43.24	89.77	202.62	35.51	-0.20
2015-2016	-705.29	-623.46	616.94	-348.01	285.02	-43.36	85.50	202.93	94.06	-0.08
2016-2017	-678.29	-560.02	552.53	-304.40	375.10	-43.24	86.03	203.27	52.04	-0.12
2017-2018	-705.29	-621.07	614.50	-354.71	291.69	-43.24	85.62	203.80	102.64	0.00
2018-2019	-678.29	-567.04	560.56	-306.51	387.23	-43.24	82.86	204.36	54.48	-0.09

Table 13: Water budget for the transient model with precipitation data from Kherbet Qanafer climate station.

| | mm | | | | | | | | | |
Date	Total Precipit-ation	Net Precipit-ation.	Infiltr-ation	Recharge	Evapo-transpiration	Subsurface Boundary Inflow	Subsurface Boundary Outflow	Pumping	SZ Drain Outflow+ Storage	Error of WB
2013-2014	-438.81	-363.69	-360.59	-240.20	263.72	-43.24	103.77	200.06	-14.95	-0.37
2014-2015	-662.52	-533.93	-520.96	-223.70	461.11	-43.24	98.12	202.61	-25.41	-0.20
2015-2016	-691.29	-599.30	-591.27	-290.80	289.79	-43.36	94.39	202.92	45.77	-0.08
2016-2017	-617.59	-511.27	-504.18	-275.26	314.82	-43.24	92.35	203.25	29.24	-0.07
2017-2018	-622.41	-503.12	-494.66	-261.35	381.45	-43.24	91.52	203.73	15.27	-0.05
2018-2019	-604.19	-495.56	-491.96	-249.09	383.98	-43.24	90.92	204.24	5.25	-0.08

Each component was calculated as a percentage of total precipitation and recharge, in order to show much each component is representative of the total water budget (Table 14Table 15). The net-precipitation represents around 80-88% of the total precipitation in the hydrological system, while recharge to the SZ represents around 50% of total precipitation. The ETP can range between 40-60% of the total precipitation. From the volume of water recharging the system, a portion is removed by subsurface flows, SZ

storage change, drainage, and pumping. Pumping represents one of the highest sinks in the

system, where the volume of groundwater removed from recharge ranges from 54-90%.

There is an apparent decreasing trend in drainage over the years, assuming pumping and

lateral inflows are kept constant.

Table 14: The percentages of net-precipitation, recharge, and ETP from total precipitation for the respective climate stations.

	Zahle Climate Station From Total Precipitation			Kherbet Qanafer Climate Station From Total Precipitation		
Date	Net precipitation	Recharge	Evapotranspiration	Net precipitation	Recharge	Evapotranspiration
2013-2014	87.67%	51.84%	-39.99%	82.88%	54.74%	-60.10%
2014-2015	82.88%	43.19%	-62.30%	80.59%	33.76%	-69.60%
2015-2016	88.40%	49.34%	-40.41%	86.69%	42.07%	-41.92%
2016-2017	82.56%	44.88%	-55.30%	82.78%	44.57%	-50.98%
2017-2018	88.06%	50.29%	-41.36%	80.84%	41.99%	-61.29%
2018-2019	83.60%	45.19%	-57.09%	82.02%	41.23%	-63.55%

Table 15: The percentages of subsurface flows, pumping, and drainage + SZ storage from recharge for the respective climate stations.

	Zahle Climate Station From Recharge			Kherbet Qanafer Climate Station From Recharge		
Date	Δ Subsurface Flows	Pumping	Drainage + Storage	Δ Subsurface Flows	Pumping	Drainage + Storage
2013-2014	-16.55%	-54.72%	-28.73%	-22.95%	-83.29%	6.22%
2014-2015	-18.73%	-69.16%	-12.12%	-20.80%	-90.57%	11.36%
2015-2016	-14.66%	-58.31%	-27.03%	-14.49%	-69.78%	-15.74%
2016-2017	-16.13%	-66.78%	-17.10%	-15.55%	-73.84%	-10.62%
2017-2018	-13.61%	-57.46%	-28.94%	-16.21%	-77.95%	-5.84%
2018-2019	-15.56%	-66.67%	-17.78%	-15.91%	-81.99%	-2.11%

CHAPTER 7

DISCUSSION

7.1 Pumping Test analysis and Empirical methods

Hantush-Cooper (1955) solution for step drawdown was used to calculate the borehole efficiency and aquifer laminar losses (B) and well losses turbulent losses (C), and to estimate storativity and transmissivity for the tested unit. The overall efficiency E was the highest (above 75%) for $Q = 2\text{-}3 \ m^3/h$. Above this rate, not only is the borehole efficiency non-satisfactory, but a maximum allowable drawdown below the pump level would be expected.

Values of T and S from the step drawdown test are in concordance with those calculated from pumping test results. T values range between $1.5\text{-}1.7\text{x} \ 10^{-5} \ m^2/s$, while K is estimated at $1.1\text{-}1.5\text{x} \ 10^{-7} \ m/s$ for a saturated thickness between 100-145 m. The values of storativity (S equivalent to Sy) can be considered valid for the area close to the borehole and range between 0.10 and 0.13. A longer-term pumping test is needed in order to verify the presence of a barrier boundary condition that may yield a drastic increase of drawdown after a certain time (>42 hours). The pumping test can be repeated at a later stage once the level of the pump is regulated to account for further drawdown.

The hydraulic conductivity values estimated by empirical methods are greater by orders of magnitude $10^3\text{-}10^4$ in comparison to values obtained by step drawdown and pumping tests. Estimates of hydraulic conductivity based on grain-size results range from $2.1 \ x \ 10^{-3}$ to $7.1 \ x \ 10^{-4} \ m/s$. The overestimation can be attributed to the fact that the grain

size analyses represent disturbed and distorted samples lacking intrinsic structural or aquifer defining properties signifying unspecific directional hydraulic conductivities (unlike that of aquifer tests indicating directional horizontal conductivities). Therefore, empirical methods reflect very localized zones and are limited in reflecting properties such as pore shape, packing, anisotropy that can affect hydraulic conductivity estimates and present inaccurate overestimations (Gentry et al., 2006). Contrariwise, pumping test and step drawdown analyses yielding low horizontal hydraulic conductivity values may be a result of insufficient well development, formation disturbance during drilling, or the use of drilling fluids (Gentry et al., 2006).

Nonetheless, there is great capacity and potential for using the well for the purpose of MAR and for the collection of observational information with time that can be used to show the influence of MAR on modelling current and future scenarios. Currently, the water level is being monitored in the borehole to display the response to recharge from a nearby channel through infiltration and the response to discharge by pumping. In order to achieve a detailed response and highlight the impact of aquifer storage and recovery, the characterization of the borehole and its surroundings should be done on a locally discretized and refined scale model to accurately emphasize the application of MAR as a viable option to remedy groundwater quality and quantity deterioration at a finer scale.

7.2 Comparison with other models

There is a general consensus in previous and current studies conducted over the ULB that there has been a decline in groundwater levels, and projections that current resources will continue to deteriorate and become depleted without proper intervention and

92

governance, and that the water balance for the various aquifers is not precisely known. There have been several models proposed and approximations made with respect to recharge, hydraulic conductivity, subsurface boundary inflow, and drainage. The study conducted by UNDP (1970) was the first comprehensive groundwater resources assessment on a national scale, especially in the collection of spring discharge data. The water balance for the ULB was estimated to be 220 Mm^3/yr. JICA (2003) estimated groundwater recharge to the ULB to be 484 Mm^3/yr. The DAI (2003, 2005) assessed groundwater vulnerability of the various aquifer systems based on a conceptual approach, such that model boundaries were extended in the SE direction assuming there was groundwater outflow to the Hasbani basin, and potentiometric data and aquifer hydraulic properties were not employed in setting up and calibrating the model. The estimated groundwater recharge to the basin is 388 Mm^3/yr. The JICA (2003) and DAI (2003, 2005) recharge approximations are considered overestimates compared to other studies as a result of the larger catchment area (1,500 km^2 in comparison to 655-700 km^2) and consequently interception of larger inputs from rainfall and precipitation of 1100 Mm^3/yr. On the other hand, the LRBMS (2011) have presented that the adjacent groundwater boundaries are in continuum with the surface water divides based on the groundwater level head distributions collected from the field. The estimated recharge is 210 Mm^3/yr with annual depletion of the Neogene-Quaternary aquifer up to70 Mm^3 while that of UNDP (2014) shows annual Quaternary-Neogene aquifer depletion amounting to 45.7 Mm^3. USAID-LRBMS (2014) reported that the mean decrease in groundwater levels from 1970 to 2010 is 14 m at a rate of 0.35 m/yr. Moreover, recharge to the Quaternary-Eocene aquifer is estimated to be 80 Mm^3 for LRBMS (2011), and pumping is estimated to be 120 Mm^3 and the lateral transfers to groundwater are 17 Mm^3.

On the other hand, the IRG (2013) study developed a groundwater model at steady-state for November 2010 and a transient state model from November 2010- May 2011 using GMS Modflow. The steady-state model for 2010 was based on the calibration of the hydraulic conductivity ranging between 10 m/day to 0.002 m/day, with higher conductivities to the south of the basin and conductivities to the north of the basin, in addition to adjusting recharge from precipitation and river conductance to be approximately 10 Mm^3/yr.

The steady-state models set up for 1970 and 2010 show similar results with respect to models proposed by IRG (2013). The current model estimates recharge from precipitation and return flow of 87.5 Mm^3 for 1970 and 2010, while that of IRG is 88.5 Mm^3 for 1970 and 95.6 Mm^3 for 2010. Abstraction rates of the current model are 37.8 and 105 Mm^3 for 1970 and 2010 respectively, in comparison to 36.7 and 112.3 Mm^3.

7.3 Model uncertainties

On the other hand, major uncertainties lie in the accurate characterization of the parameters in the model. Some parameters were calibrated since they cannot be measured directly in the field (e.g. hydraulic conductivity), providing a range of estimates, while measurable data and observational data are subject to inherent inaccuracies, calibration, and measurement errors, and intervals of missing data. There is uncertainty regarding pumping rates for the 2010 steady-state model, whereby the currently used values do not account for unlicensed wells that are estimated to pump 5 times more than the registered wells (IRG, 2013), which are located at the center of the basin. Therefore, the current model

overestimates the probable groundwater level, and the drainage to rivers and aquifer-river interchange. Uncertainties pertaining to coarse grid size and coarse DEM may have also affected the differences between topography and aquiferous layering that define the aquifer-river interchange boundary, impacting the gains or losses to the river. The coarse topography also lead to a series of unnatural sinks that in turn affected drainage flow and direction. Unlikely natural sinks that were less than 5 m different than the topography, assumed not to be part of the river tributary, were removed by filling sinks tool in ArcGIS, thereby reducing the error in the propagation of ponding and appropriately conveying river drainage direction and flow in the basin. Moreover, the current models assume a recharge by precipitation and return flow from agricultural practices in a lumped sum, since there is no accurate distinction with regards to the percentage of recharge by infiltration from precipitation and return flow. Regarding transient modelling, inevitably missing meteorological data lead to the use of cyclic precipitation and evapotranspiration data, which do not reflect realistic climate conditions. Moreover, better characterization of the unsaturated zone should be conducted, whereby soil parameter calibration is accompanied by sensitivity analysis to simulate representative unsaturated zone processes and overall interactions with the saturated zone.

CHAPTER 8

CONCLUSION

The focus of this research was to evaluate the ability of the physically based, hydrological model, MIKE SHE, to simulate at regional scale the groundwater flow in the Upper Litani Basin in order to estimate the water balance and highlight the significance of applying Managed Aquifer Recharge as a means to reduce anticipated groundwater level drops as a result of increasing well abstraction and climate change. A steady-state model was calibrated for the year 1970, based on hydraulic head distributions, where optimal parameter estimates of horizontal and vertical hydraulic conductivities of the saturated zone, and boundary conditions were estimated using auto-calibration based on the population simplex evolution algorithm. The simulated hydraulic heads were within range of the observed groundwater levels with a mean of less than 10m difference for 1970, and the fitted parameters were within acceptable physical ranges. The validation was based on 2010 hydraulic head distributions, and the estimated error of simulated vs observed heads was also within acceptable limits with a mean of ~5m difference. The estimated water budgets show that the drainage of the river has decreased from 1970 to 2010 due to drops in groundwater level as a consequence of excess well abstractions. The simulated models from 1970 to 2010 show a drop in potentiometric head ranging from ± 40 m along the western Eocene boundary and a ± 30 m decline along the eastern Cretaceous boundary. In the center of the basin to the north, there is a 25 m drop, and the potentiometric head decline decreases southern to the basin, where the center of the basin shows a 10-15 m drop, arriving at a constant head boundary there is a less than 5 m decline. As such, MAR shows

promising results in reducing groundwater quality and quantity deterioration as a function

of abstractions and global warming. Anticipated decline in potentiometric levels and

groundwater resources depletion promptly calls for monitoring and adequate water

governance strategies to be undertaken to sustain and manage current and future resources,

where MAR can be seen as a viable alternative to reduce excessive unsupervised and

unlicensed pumping and in regulating pumping durations and rates in the Quaternary and

Neogene aquifers. Further refinement of model parameterization is needed for more

accurate model simulations and projections. These include measurements of hydraulic

heads regularly, a routine survey of well pumping, detailed characterization of the

unsaturated zone and continuous climate records for precipitation, and evapotranspiration.

Recommendations within the scope of this thesis include a sensitivity analysis of the

transient model in order to understand the effects of various model parameters and stresses

on the groundwater model's response by identifying potential sensitive parameters through

systematic variation of the calibrated values (Anderson et al., 2015). Furthermore, after

having accurately calibrated and validated both steady-state and transient models, the

finalized transient model may be utilized as a tool for back- and forecasting predictions. It

may also be used to generate several scenarios depicting the effect of MAR if it were to be

applied on a regional scale. Recommendations beyond the scope of the thesis include

establishing a continuous model from 1970-2010 with available data and data gap filing

methods thus, considering the model as a tool to undertake future simulations (2020-2099)

based on downscaled time series of forecast climatic data (Global Climatic Models GCM;

IPS_CMP5; Dufresne et al., 2013) to highlight the impact of concrete climate change

scenarios on hydraulic head variations, and river groundwater interaction within the various

compartments in the system.

REFERENCES

Abbott, M. B., Bathurst, J. C., Cunge, J. A., O'connell, P. E., & Rasmussen, J. (1986). An
introduction to the European Hydrological System—Systeme Hydrologique
Europeen,"SHE", 2: Structure of a physically-based, distributed modelling system.
Journal of Hydrology, *87*(1–2), 61–77.

Abbud, M., & Aker, N. (1986). The study of the aquiferous formations of Lebanon through
the chemistry of their typical springs. *Lebanese Science Bulletin*, *2*(2), 18.

Allen, R. G., Pereira, L. S., Raes, D., & Smith, M. (1998). *Crop evapotranspiration-
Guidelines for computing crop water requirements-FAO Irrigation and drainage
paper 56. Fao, Rome, 300(9), D05109.*

Alyamani, M. S., & Şen, Z. (1993). Determination of hydraulic conductivity from complete
grain- size distribution curves. *Groundwater*, *31*(4), 551–555.

Anderson, M. P., Woessner, W. W., & Hunt., R. J. (2015). Applied groundwater modeling:
simulation of flow and advective transport. *Academic Press*.

Assaf, H., & Saadeh, M. (2006). *Development of an Integrated Decision Support System for
water quality control in the Upper Litani Basin*.

Assaf, H., & Saadeh, M. (2009). Geostatistical Assessment of Groundwater Nitrate
Contamination with Reflection on DRASTIC Vulnerability Assessment: The Case of
the Upper Litani Basin, Lebanon. *Water Resources Management*, *23*(4), 775–796.
https://doi.org/10.1007/s11269-008-9299-8

Bachelor, C., Cain, J., Farquharson, F., & Roberts, J. (1998). Improving water utilization from a catchment perspective. *SWIM Paper 4, International Water Management Institute, Colombo, Sri Lanka.*

Beyer, W. (1964). Kornverteilung, Zur Bestimmung der Wasserdurchlässigkeit von Kiesen und Sanden aus der Wasserwirtsch. *Wassertech. WWT, Berlin Ost*, 165–169.

Bourdet, D., Ayoub, J., & Pirard, Y. (1989). Use of pressure derivative in well test interpretation. *SPE Formation Evaluation*, *4*(2), 293–302. https://doi.org/10.2118/12777-PA

Bourdet, D., Whittle, T. M., Douglas, A. A., & Pirard, V. M. (1983). A new set of type curves simplifies well test analysis. *World Oil*, *196*(6), 95–106.

Bouwer, H. (2002). Artificial recharge of groundwater: Hydrogeology and engineering. *Hydrogeology Journal*, *10*(1), 121–142. https://doi.org/10.1007/s10040-001-0182-4

Brunt, R., Vasak, L., & Griffioen, J. (2004). *International Groundwater Resources Assessment Centre (IGRAC) Report nr. SP, 1(15)*.

Cadham, J. S., Litani River Authority, & Development Studies Association. (2007). *Towards an ecosystem approach to the sustainable management of the Litani watershed-Lebanon: final technical report to IDRC*.

Carman, P. (1937). Fluid flow through granular beds. *Trans. Inst. Chem. Eng.*, *15*, 150.

Carman, P. (1956). Flow of gases through porous media. *Butterworths Scientific Publications, London.*

Carrier, W. D. (2003). Goodbye, Hazen; hello, Kozeny-Carman. *J. Geotech. Geoenviron.*

Eng., *129*(11), 1054.

Chamber of Commerce Industry & Agriculture Zahle & Bekaa (CCIAZ). (2014). *Annual*
Report. http://www.cciaz.org.lb/english/reports.php?menu=132-local

CNRS. (2010). Land cover map of Lebanon. *Beirut, Lebanon.*

Cooper, H. H., & Jacob, C. E. (1946). A generalized graphical method for evaluating
formation constants and summarizing well- field history. *Eos, Transactions American*
Geophysical Union, *27*(4), 526–534.

Daher, W., Pistre, S., Kneppers, A., Bakalowicz, M., & Najem, W. (2011). Karst and
artificial recharge: Theoretical and practical problems. A preliminary approach to
artificial recharge assessment. *Journal of Hydrology*, *408*(3–4), 189–202.
https://doi.org/10.1016/j.jhydrol.2011.07.017

Danish Hydraulic Institute (DHI). (2014a). *MIKE SHE User Manual, Volume 1: User*
Guide.

Danish Hydraulic Institute (DHI). (2014b). *MIKE SHE User Manual, Volume 2: Reference*
Guide.

Danish Hydraulic Institute (DHI). (2017a). *MIKE SHE*.

Danish Hydraulic Institute (DHI). (2017b). *MIKE SHE AutoCal, Autocalibration Tool:*
Reference Guide.

Danish Hydraulic Institute (DHI). (2017c). *MIKE SHE User Manual, Volume 1: User*
Guide.

Daoud, A. (1973). *Groundwater recharge in the Beirut Area*. American University of Beirut.

Darwish, T. (1999). Mapping of natural resources using remote sensing for soil studies. *National Forum on Support of Remote Sensing Techniques to Planning and Decision-Making Processes for Sustainable Development. CTM, ERS/RAC, UNEP and NCSR/NCR, Beirut,* 36–41.

Darwish, T., Khawlie, M., Jomaa, I., Abou Daher, M., Awad, M., Masri, T., Shaban, A., Faour, G., Bou Kheir, R., Abdallah, C., & Haddad, T. (2006). Soil Map of Lebanon 1/50000. *CNRS-Lebanon, Monograph Series 4, p-367.*, undefined.

Darwish, T., Khawlie, M., Jomaa, I., Awad, M., Abou Daher, M., & Zdruli, P. (2002). A survey to upgrade information for soil mapping and management in Lebanon. *Options Mediterannéennes, Series A: Mediterranean Seminars*, *50*, 57–71.

Development Alternatives Inc. (DAI). (2003). *Water Quality Assessment of the Upper Litani River Basin and Lake Qaraoun, Lebanon. USAID*.

Development Alternatives Inc. (DAI). (2005). *BAMAS Project. Groundwater Flow Modeling and Vulnerability Mapping.Litani Water Quality Management Project. USAID*.

Dillon, P. (2005). Future management of aquifer recharge. *Hydrogeology Journal*, *13*(1), 313–316. https://doi.org/10.1007/s10040-004-0413-6

Dillon, P., Pavelic, P., Page, D., Beringen, H., & Ward, J. (2009). Managed aquifer recharge: An Introduction. In *recharge.iah.org*. www.ag.gov.au/cca.

Dillon, P., Stuyfzand, P., Grischek, T., Lluria, M., Pyne, R. D. G., Jain, R. C., & Stefan, C. (2019). Sixty years of global progress in managed aquifer recharge. *Hydrogeology Journal*, *27*(1), 1–30.

Doummar, J., Kassem, A. H., & Gurdak, J. J. (2018). Impact of historic and future climate on spring recharge and discharge based on an integrated numerical modelling approach: Application on a snow-governed semi-arid karst catchment area. *Journal of Hydrology*, *565*, 636–649. https://doi.org/10.1016/j.jhydrol.2018.08.062

Doummar, J., Massoud, M. A., Khoury, R., & Khawlie, M. (2009). Optimal water resources management: Case of lower Litani River, Lebanon. *Water Resources Management*, *23*(11), 2343–2360. https://doi.org/10.1007/s11269-008-9384-z

Doummar, J., Sauter, M., & Geyer, T. (2012). Simulation of flow processes in a large scale karst system with an integrated catchment model (Mike She) - Identification of relevant parameters influencing spring discharge. *Journal of Hydrology*, *426–427*, 112–123. https://doi.org/10.1016/j.jhydrol.2012.01.021

Dubertret, L. (1955). Carte Geologique du Liban au: 1: 200,000 et notice explicative. *Republique Libanaise, Ministere Des Travaux Publics*.

Dubois, E. (2017). *Analysis of high resolution spring hydrographs and climatic data: application on the Qachqouch spring (Lebanon). Unpublished master's thesis. American University of Beirut-Lebanon*.

Duffield, G. M. (2007). *AQTESOLV for Windows Version 4.5 User's Guide. HydroSOLVE, Reston, VA*.

Dufresne, J. L., Foujols, M. A., Denvil, S., Caubel, A., Marti, O., Aumont, O., Balkanski, Y., Bekki, S., Bellenger, H., Benshila, R., Bony, S., Bopp, L., Braconnot, P., Brockmann, P., Cadule, P., Cheruy, F., Codron, F., Cozic, A., Cugnet, D., … Vuichard, N. (2013). Climate change projections using the IPSL-CM5 Earth System Model: From CMIP3 to CMIP5. *Climate Dynamics*, *40*(9–10), 2123–2165. https://doi.org/10.1007/s00382-012-1636-1

Edgell, H. (1997). Karst and hydrogeology of Lebanon. *Carbonates Evaporites*, *12*(2), 220–235. https://doi.org/10.1007/BF03175419

Eggleston, J., & Rojstaczer, S. (2001). The value of grain-size hydraulic conductivity estimates: Comparison with high resolution in-situ eld hydraulic conductivity. *Geophys. Res. Lett.*, *28*(22), 4255–4258.

Evaluation of UNICEF WASH Programme in Lebanon – Final Report. (2017). *Evaluation of the Water, Sanitation and Hygiene (WASH) Programme within the UNICEF Country Programme in Lebanon (2013-2016).*

Food and Agriculture Organization of the United Nations (FAO). (1970). Projet de Développement Hydro-Agricole: Etude Hydrogeologique De La Plaine D'Akkar. *République Libanaise, Ministère Des Ressources Hydrauliques et Électriques, Beyrouth, Liban.*

Food and Agriculture Organization of the United Nations (FAO). (2008). Irrigation in the Middle East region in figures–AQUASTAT Survey 2008. In *Land and Water Division*.

Freeze, R. A., & Harlan, R. L. (1969). Blueprint for a physically-based, digitally-simulated hydrologic response model. *Journal of Hydrology*, *9*((3)), 237–258.

Gedeon, M., Wemaere, I., & Marivoet, J. (2007). Regional groundwater model of north-east Belgium. *Journal of Hydrology*, *335*(1–2), 133–139.

Gentry, R., McKay, L., Thonnard, N., Larsen, D., & Anderson, J. (2006). Novel techniques for investigating recharge to the Memphis aquifer. *American Water Works Association*.

Gomez, F., Nemer, T., Tabet, C., Khawlie, M., Meghraoui, M., & Barazangi, M. (2007). Strain partitioning of active transpression within the Lebanese restraining bend of the Dead Sea Fault (Lebanon and SW Syria). *Geological Society, London, Special Publications*, *290*(1), 285–303.

Hantush, M. S., & Jacob, C. E. (1955). Non-steady radial flow in an infinite leaky aquifer. *Trans. Am. Geophys. Union*, *36*(1), 95–100.

Hazen, A. (1892). Some physical properties of sands and gravels, with special reference to their use in filtration. *24th Annual Rep., Massachusetts State Board of Health*, *34*, 539–556.

Hill, M. C. (2006). The practical use of simplicity in developing ground water models. *Groundwater*, *44*(6), 775–781.

Huber, A., & Scheibler, F. (2013). *Development of a Catalogue on European MAR Sites—Documentation. Report DEMEAU Project.*

Imad, E. (2003). Prevention of seawater intrusion by the artificial recharge of groundwater

on the Lebanese coast. In *Thses et Masters (CIHEAM)*.

International Resources Group (IRG). (2013). *Litani River Basin Management Support Program Groundwater Modeling Within the Upper Litani Basin Report*.

Jaafar, H., King-Okumu, C., Haj-Hassan, M., Abdallah, C., El-Korek, N., & Ahmad, F. (2016). *Water resources within the Upper Orontes and Litani Basins*. https://doi.org/10.13140/RG.2.2.14793.34401

Japan International Cooperation Agency (JICA). (2003). *The Study on Water Resources Management Master Plan in the Republic of Lebanon (draft)*.

Kasenow, M. (1997). Applied Groundwater and Well Hydraulics. *Water Resources Publications*.

Kassem, A. H. (2020). *Sensitivity Analysis of an Integrated Numerical Flow Model Output to Key Model Parameters Used in Common Qualitative Vulnerability Assessment Methods*. American Univeristy of Beirut.

Kayal, D., Bou Jaoude, I., Karam, F., Berger, E., Tezcan, L., Ekmekci, M., Merheb, F., Najem, W., Ghanem, R., Balmert, D., Abdallah, C., Doumar, J., Makhoul, G., Saab, M., Idriss, B., Shamas, B., Matar, A., Machtoub, T., & Khayat, Z. (2014). *Assessment of the Groundwater Resources of Lebanon*.

Khadra, W. M., & Stuyfzand, P. J. (2019). Problems and promise of managed recharge in karstified aquifers: the example of Lebanon. *Water International*, 1–16. https://doi.org/10.1080/02508060.2019.1682910

Khair, K., Aker, N., & Zahruddine, K. (1992). Hydrogeologic units of Lebanon. *Applied*

Hydrogeology, *1*(2), 34–49.

Kløve, B., Ala-Aho, P., Bertrand, G., Gurdak, J. J., Kupfersberger, H., Kværner, J.,
Muotka, T., Mykrä, H., Preda, E., Rossi, P., Uvo, C. B., Velasco, E., & Pulido-
Velazquez, M. (2014). Climate change impacts on groundwater and dependent
ecosystems. *Journal of Hydrology*, *518*, 250–266.
https://doi.org/10.1016/j.jhydrol.2013.06.037

Konikow, L. F., & Kendy, E. (2005). Groundwater Depletion: A Global Problem. *Article in
Hydrogeology Journal*, *13*(1), 317–320. https://doi.org/10.1007/s10040-004-0411-8

Kozeny, J. (1927). Uber kapillare leitung der wasser in boden. *Royal Academy of Science,
Vienna, Proc. Class I*, *136*, 271–306.

Kozeny, J. (1953). Hydraulik: Ihre Grundlagen und praktische Anwendung. *Springer-
Verlag, Vienna.*

Kresic, N., & Mikszewski, A. (2012). *Hydrogeological conceptual site models: data
analysis and visualization*. CRC press.

Kristensen, K. J., & Jensen, S. E. (1975). A model for estimating actual evapotranspiration
from potential evapotranspiration. *Hydrology Research*, *6*(3), 170–188.

LRBMS Program. (2011). *Water Balance Report, August 2011*.

Masciopinto, C. (2013). Management of aquifer recharge in Lebanon by removing seawater
intrusion from coastal aquifers. *Journal of Environmental Management*, *130*, 306–312.
https://doi.org/10.1016/j.jenvman.2013.08.021

Massaad, B. (2000). *Salt Water Intrusion in the Hadeth Aquifer: Groundwater*

Rehabilitation Techniques, Expert Group Meeting on Implications of Groundwater Rehabilitation Fro Water Resources Protection and Conservation.

MOE/UNDP/ECODIT. (2011). *State of the Environment report in Lebanon, 3rd Edition*.

Pachauri, R. K., Allen, M. R., Barros, V. R., Broome, J., Cramer, W., Christ, R., Church, J. A., Clarke, L., Dahe, Q., Dasgupta, P., & Dubash, N. K. (2014). Climate Change 2014: Synthesis Report. Contribution of Working Groups I, II and III to the Fifth Assessment Report of the Intergovernmental Panel on Climate Change. In *Ipcc*.

Pechstein, A., Attinger, S., Krieg, R., & Copty, N. K. (2016). Estimating transmissivity from single-well pumping tests in heterogeneous aquifers. *Water Resources Research*, *52*(1), 495–510. https://doi.org/10.1002/2015WR017845

Refsgaard, J. C. (1997). Parameterisation, calibration and validation of distributed hydrological models. *Journal of Hydrology*, *198*(1), 69–97. https://doi.org/10.1016/S0022-1694(96)03329-X

Renard, P., Glenz, D., & Mejias, M. (2009). Understanding diagnostic plots for well-test interpretation. *Hydrogeology Journal*, *17*, 589–600. https://doi.org/10.1007/s10040-008-0392-0

Ringleb, J., Sallwey, J., & Stefan, C. (2016). Assessment of Managed Aquifer Recharge through Modeling—A Review. *Water*, *8*(12), 579.

Rolf, L., Burger, S., De Vries, A., & Wiersma, A. (2019). Implementing an energy-neutral ASR system in a complex setting in Lebanon. *Proceedings of the International Symposium on Managed Aquifer Recharge (ISMAR 10)-Managed Aquifer Recharge:*

Local Solutions to the Global Water Crisis, 725–735.

Rosas, J., Lopez, O., Missimer, T. M., Coulibaly, K. M., Dehwah, A. H. A., Sesler, K., & Mantilla, D. (2014). Determination of hydraulic conductivity from Grain-Size distribution for different depositional environments. *Groundwater*, *52*(3), 399–413. https://doi.org/10.1111/gwat.12078

Safi, A., Rachid, G., El-Fadel, M., Doummar, J., Abou Najm, M., & Alameddine, I. (2018). Synergy of climate change and local pressures on saltwater intrusion in coastal urban areas: effective adaptation for policy planning. *Water International*, *43*(2), 145–164. https://doi.org/10.1080/02508060.2018.1434957

Schwabe, K., Albiac, J., Connor, J. D., Hassan, R. M., & González, L. M. (2013). Drought in arid and semi-arid regions: A multi-disciplinary and cross-country perspective. In *Drought in Arid and Semi-Arid Regions: A Multi-Disciplinary and Cross-Country Perspective*. Springer Netherlands. https://doi.org/10.1007/978-94-007-6636-5

Sonnenborg, T. O., Christensen, B. S. B., Nyegaard, P., Henriksen, H. J., & Refsgaard, J. C. (2003). Transient modeling of regional groundwater flow using parameter estimates from steady-state automatic calibration. *Journal of Hydrology*, *273*(1–4), 188–204. https://doi.org/10.1016/S0022-1694(02)00389-X

Sprenger, C., Hartog, N., Hernández, M., Vilanova, E., Grützmacher, G., Scheibler, F., & Hannappel, S. (2017). Inventory of managed aquifer recharge sites in Europe: historical development, current situation and perspectives. *Hydrogeology Journal*, *25*(6), 1909–1922.

Stefan, C., & Ansems, N. (2018). Web-based global inventory of managed aquifer recharge applications. *Sustainable Water Resources Management*, *4*(2), 153–162. https://doi.org/10.1007/s40899-017-0212-6

Sun, G., Alstad, K., Chen, J., Chen, S., Ford, C. R., Lin, G., Liu, C., Lu, N., Mcnulty, S. G., Miao, H., Noormets, A., Vose, J. M., Wilske, B., Zeppel, M., Zhang, Y., & Zhang, Z. (2011). A general predictive model for estimating monthly ecosystem evapotranspiration. *Ecohydrology*, *4*(2), 245–255. https://doi.org/10.1002/eco.194

Theis, C. V. (1935). The relation between the lowering of the piezometric surface and the rate and duration of discharge of a well using groundwater storage. *Eos, Transactions American Geophysical Union*, *16*(2), 519–524.

Torrent, J. (2005). *Mediterranean soils. In: Hillel, D. (Ed.), Encyclopaedia of Soils in the Environment, vol. 2. , Oxford*.

Tuinhof, A., Olsthoorn, T., Heederik, J. P., & Vries, J. J. de. (2003). *Management of Aquifer Rechange and Subsurface Storage* (pp. 3–18). NNC-IAH publication 4.

Uma, K. O., Egboka, B. C. E., & Onuoha, K. M. (1989). New statistical grain-size method for evaluating the hydraulic conductivity of sandy aquifers. *Journal of Hydrology*, *108*, 343–366. https://doi.org/10.1016/0022-1694(89)90293-X

UNDP. (1970). *Liban Etude Des Eaux Souterraines*. Government of Lebanon, Beirut, Lebanon.

UNDP. (2014). *Assessment of Groundwater Resources of Lebanon, Beirut*.

UNESCO-WWAP. (2019). *The United Nations World Development Report 2019. Leaving*

no one behind. Main Messages. 12. https://doi.org/.1037//0033-2909.I26.1.78

United Nations (UN). (2017). *World Population Prospects: The 2017 Revision, Key Findings and Advance Tables.*

USAID-LRBMS. (2012). *Litani River basin management plan. Volume 1: Current situation. February 2012. USAID.*

USAID-LRBMS. (2014). *Litani River Basin Management Support Program. Project Completion Report. USAID.*

Vukovic, M., & Soro, S. (1992). Determination of hydraulic conductivity of porous media from grain-size analysis. *Littleton, CO: Water Resources Publications.*

Walley, C. D. (1996). *The geology and hydrogeology of the Aammiq Wetland region. ARocha Lebanon.*

Walley, C. D. (1997). The Lithostratigraphy of Lebanon: A Review. In *Lebanese Scientific Research Reports 10.*

Walley, C. D. (1998). Some outstanding issues in the geology of Lebanon and their importance in the tectonic evolution of the Levantine region. *Tectonophysics*, *298*(1–3), 37–62.

World Bank Water Sector. (2009). *Public Expenditure Report, Draft*.

Wu, J., & Zeng, X. (2013). Review of the uncertainty analysis of groundwater numerical simulation. *Chinese Science Bulletin*, *58*(25), 3044–3052. https://doi.org/10.1007/s11434-013-5950-8

Zhou, X., Helmers, M., & Qi, Z. (2013). Modeling of subsurface tile drainage using MIKE

SHE. *Applied Engineering in Agriculture*, *29*(6), 865–873.

https://doi.org/10.13031/aea.29.9568

APPENDICES

APPENDIX A: LITHOLOGY

A.1 Jurassic Formations

The Jurassic formations encompass the Late Jurassic and Middle Jurassic, covering an area of 122 km^2 which bound the basin on the west, and are composed of 119 km^2 dolomitic limestone rocks and about 3 km^2 of basalts and volcanic tuffs. The four formations belonging to the Jurassic are described in detail below.

A.1.a   Kesrouane Fm. (J4)

The Kesrouane Fm. outcrops at the eastern flank of Mount Lebanon and SW with respect to the catchment area and is predominantly composed of massive highly karstified dolomitic limestone and limestone with some marl lenses. The formation is the oldest exposed outcrop in Lebanon of Batholian age; however, its thickness remains undetermined but is anticipated to be around 1000 m.

A.2 Cretaceous Formations

The Cretaceous Fm. are represented from the Late Cretaceous to Early Cretaceous and are primarily composed of sandstone, shales, and limestone.

A.2.a   Chouf Sandstone Fm. (C1)

The Chouf Fm. characterizes the basal Cretaceous rocks and outcrops NE of the basin along the Anti-Lebanon flanks and also forms small patches west of the catchment

area along the Mount Lebanon flanks. It is primarily composed of cross-bedded thick to thin layers with massive sandstone intercalating with silt, clays, and shale horizons that are highly jointed. The thickness of the Chouf Sandstone Fm. has a maximum thickness of 75 m.

A.2.b   Abieh Fm. (C2A)

The Abieh Fm. is exposed west and north-east of the catchment area along the Mount Lebanon range and Anti-Mount Lebanon range flanks respectively, such that the formation is of Barremian-Lower Aptian age and comprises thinly to thickly bedded and jointed clastic limestones.

A.2.c   Mdairej Fm. (C2B)

The Mdairej Fm. is exposed as small patches west and north-est of the basin along the Mount Lebanon and Anti-Mount Lebanon flanks respectively, and is of Upper Aptian Age and primarily composed of medium to thickly bedded and massive karstified limestone that is jointed and partially dolomitized reaching a maximum thickness of 50 m.

A.2.d   Hammana Fm. (C3)

The Hammana Fm. is also exposed in small patches west along the Mount-Lebanon flanks and SE along the Anti-Mount Lebanon flanks with respect to the catchment area. The formation is of Albian age and is predominantly composed of thin to medium jointed beds of fossiliferous and clastic limestones interbedded with calcareous shales, reaching a maximum thickness of 50 m.

A.2.e   Sannine-Maameltein Fms. (C4-C5)

The Sannine-Maametlein Fms. outcrops at the base of the Anti-Mount Lebanon and Mount Lebanon ranges and are of Cenomanian- Turonian age. They are primarily composed of highly karstified and jointed limestone and dolomitic limestone with intermittent intercalating calcareous shale and marl horizons and marly limestones, and reach a thickness of 700 m.

A.2.f   Chekka Fm. (C6)

The Chekka Fm. is exposed NW along the Mount-Lebanon range and east along the Anti-Mount Lebanon range with respect to the catchment area. It is of Senonian age and is primarily composed of thinly to medium bedded and jointed chalky marls and chalky marl limestones with partial siliceous limestone horizons, reaching a maximum thickness of 50 m.

A.3 Tertiary and Quaternary Formations

The Tertiary and Quaternary deposits represent formations ranging from the Eocene to recent deposits and are primarily composed of limestone and fluvial/alluvial deposits.

A.3.a   Eocene Fm. (E2a-E2b)

The Eocene formation is exposed at the base of the Anti-Mount Lebanon and Mount Lebanon flanks east and north of the basin respectively. The Eocene formation is

divided into two sections which include the Upper Eocene (e2b) and the Lower Eocene (e2a), such that the e2b overlies the e2a and is predominantly marly limestone whilst the e2b is primarily composed of brecciated limestone. The karstic limestone formation has a maximum depth of 250 m and appears mainly around Joub Jannine, and in thin bands NE of Anjar and NW of Zahle.

A.3.b   Neogene Fm. (M_L-M_{Ll})

The Neogene formation, also known as the Upper Miocene deposits, is overlain by Quaternary deposits and is of Miocene and Pliocene epoch. The Neogene Fm. is exposed in the west near Chmistar and Chtaura and NE to Rayak and Baalbek, and is composed of unconsolidated gravels and sands, and lacustrine limestones and marls. The aquifer has a maximum depth of up to 300 m supporting hundreds off wells with yields ranging between 10-30 L/s.

A.3.c   Quaternary Deposits (Q)

The Upper Litani Basin mostly consists of unconsolidated Quaternary deposits, whereby the center of the basin is composed of a combination of clays, sands, silts and gravels with varying occurrences over the area. The Quaternary deposits reach a maximum depth of 200 m. Well yields range between 5-10 L/s and 30-40 L/s depending on their locations due to the heterogeneous nature of the Quaternary aquifer.

APPENDIX B: SAMPLE PREPARATION AND SIEVE ANALYSIS

The following steps were performed in order to analyze the % finer grain size distribution with respect to the depths at which they were extracted:

1. Around 150 samples were collected, each defined by the depth at which it was extracted. Small representative samples were taken from each bag brought from Bekaa (Figure 28).

Figure 28: Cuttings samples brought to the lab from Bekaa during borehole drilling operations.

2. Very wet soil samples were first put into centrifuge tubes, in order to separate the water from the soil by centrifugal forces, 2 layers were observed in addition to water; whereby denser conglomerates precipitated at the bottom, overlain by the finer clays (Figure 29).

a   b

Figure 29: a) Wet samples to be separated by centrifuge device, b) Sample showing
precipitated sand and gravel at the bottom, overlain by silts and clays, and water at the top.

3. After removing the liquid, the sediments were spread on a thin aluminum sheet in

   order to dry at room temperature and numbered according to the depth at which they

   were extracted. Other lager samples were dried in the oven, in order to accelerate

   the drying process.

4. After the samples dried, aggregated samples were carefully grounded by a pestle

   and mortar (Figure 30).

a   b

Figure 30: a) Dried samples in the oven and room temperature, b) Sample being carefully grounded by pestle.

Sieve analysis

The sieve analysis protocol was prepared beforehand. The procedure consisted of the following:

a.   Testing objectives & Scope:

The standard grain size analysis test determines the relative proportions of different grain sizes as they are distributed among certain size ranges. The grain size analysis is widely used in the classification of sediments.

b.   Apparatus Used:

- Stack of Sieves including pan and cover

- Balance (error $\pm$ 0.01 g)

- Mechanical sieve shaker

c.   Procedure:

1. Prepare a stack of sieves, making sure the sieves are clean. If many soil particles are stuck in the openings, poking and brushing gently on the opposite side helps remove any clogging. Sieves having larger pore opening (i.e. lower numbers) are placed above the ones having smaller openings (i.e. higher numbers). The very last sieve is #200 and a pan is placed under it to collect the portion of soil passing the #200 sieve (Figure 31).

2. The sieves and pan are weighed individually and reported.

3. A representative oven or room temperature dried sample of soil is weighted and recorded.

4. The sample is poured into the top sieve, and the sieve shaker is adjusted to approximately 10 to 15 minutes.

5. The mass of each sieve and retained soil is then measured.

Figure 31: a) Mechanical sieve shaker. b) Mass of each sieve and retained soil is measured by mass balance.

d.   Calculations:

- Mass of soil retained = Total Mass of each sieve and retained soil - Mass of each sieve

- Percentage on each sieve (Rn) $= \dfrac{\text{Mass of soil retained}}{\text{Total Mass of each Sieve}} \times 100$

- Cumulative percent retained of soil retained on the nth sieve $= \Sigma$ Rn

- Cumulative percent passing through the nth sieve, Percent finer $= 100 - \Sigma$ Rn

- % Error or Mass Loss during Sieving $= \dfrac{\text{Original mass of sample} - \Sigma \text{ Rn}}{\text{Original mass of sample}} \times 100$

APPENDIX C: GRAIN SIZE ANALYSIS

				φ	5	20	40	50	80-140	170-200	Pan			
								Percentages of grain sizes (mm)				Hazen K (m/s)	Kozney-Carman K (m/s)	Beyer K (m/s)
		Depth (m)		Mean d (mm)	>2.0	2.0-1.0	1.0-0.5	0.5-0.25	0.25-0.1	0.1-0.05	less than 0.05			
Sample number	Thickness (m)	from	to		Gravel	V Coarse sand	Coarse sand	Medium sand	Fine sand	Very fine sand	Fines (Silt and clays)			
2	0.50	6.5	7.0	0.17	0.76%	5.02%	29.64%	58.81%	1.22%	1.82%	2.74%	1.957E-04	1.814E-04	3.954E-04
6	3.00	18.00	21.00	0.22	0.00%	7.91%	48.05%	38.94%	1.10%	1.80%	2.20%	2.008E-04	1.534E-04	4.165E-04
8	2.00	23.00	25.00	0.29	0.00%	12.60%	51.10%	27.81%	0.55%	3.70%	4.25%	1.333E-04	8.783E-05	2.868E-04
9	2.00	32.00	34.00	0.60	84.90%	8.51%	2.62%	2.50%	0.26%	0.58%	0.64%	1.864E-03	1.621E-03	3.786E-03
10	2.00	34.00	36.00	0.76	41.03%	44.04%	11.84%	2.69%	0.08%	0.16%	0.16%	1.830E-03	1.400E-03	3.795E-03
11	1.50	36.00	37.50	0.90	52.45%	27.72%	13.86%	4.48%	0.17%	0.58%	0.75%	1.205E-03	7.470E-04	2.641E-03
14	3.00	42.00	45.00	0.74	42.57%	30.19%	19.79%	6.01%	0.25%	0.40%	0.79%	8.056E-04	4.991E-04	1.766E-03
15	2.50	45.00	47.50	0.77	44.89%	30.27%	18.40%	5.01%	0.18%	0.41%	0.83%	1.182E-03	7.804E-04	2.541E-03
21	2.50	60.25	62.75	0.71	40.17%	31.84%	19.08%	6.65%	0.27%	0.67%	1.31%	5.483E-04	3.204E-04	1.226E-03
22	2.00	62.75	64.75	0.77	44.42%	31.31%	17.06%	5.80%	0.11%	0.43%	0.87%	8.611E-04	5.298E-04	1.892E-03
23	2.50	64.75	67.25	0.92	53.54%	29.40%	12.65%	3.21%	0.18%	0.18%	0.85%	1.459E-03	9.403E-04	3.160E-03
24	1.42	67.98	69.40	0.97	56.14%	27.67%	11.40%	3.60%	0.24%	0.16%	0.79%	1.459E-03	9.249E-04	3.176E-03
25	4.00	69.40	73.40	0.80	46.35%	31.19%	16.33%	4.56%	0.17%	0.48%	0.91%	1.212E-03	7.930E-04	2.614E-03
26	2.20	73.40	75.60	0.78	44.32%	35.54%	14.25%	4.31%	0.26%	0.32%	1.00%	1.296E-03	8.802E-04	2.765E-03
28	2.50	78.10	80.60	0.86	50.25%	29.19%	14.77%	4.28%	0.25%	0.38%	0.88%	1.258E-03	8.016E-04	2.734E-03
29	2.62	80.60	83.22	0.76	42.64%	35.13%	15.77%	4.85%	0.16%	0.63%	0.82%	1.248E-03	8.577E-04	2.655E-03
30	2.98	83.22	86.20	0.92	53.46%	28.92%	12.76%	3.65%	0.36%	0.24%	0.61%	1.387E-03	8.830E-04	3.014E-03
31	0.80	86.20	87.00	0.60	85.34%	8.23%	2.85%	2.43%	0.32%	0.21%	0.63%	1.910E-03	1.668E-03	3.879E-03
32	2.14	88.70	90.84	0.43	52.07%	27.85%	14.25%	4.79%	0.52%	0.26%	0.26%	4.935E-04	3.564E-04	1.037E-03

		Depth (m)			φ	5	20	40	50	80-140	170-200	Pan			
									Percentages of grain sizes (mm)				Hazen K (m/s)	Kozney-Carman K (m/s)	Beyer K (m/s)
Sample number	Thickness (m)			Mean d (mm)	>2.0	2.0-1.0	1.0-0.5	0.5-0.25	0.25-0.1	0.1-0.05	less than 0.05				
		from	to		Gravel	V Coarse sand	Coarse sand	Medium sand	Fine sand	Very fine sand	Fines (Silt and clays)				
33	2.46	90.84	93.30	0.99	57.39%	24.87%	12.67%	3.49%	0.24%	0.38%	0.96%		1.337E-03	8.239E-04	2.937E-03
34	2.50	93.30	95.80	0.70	36.22%	36.68%	19.26%	5.76%	0.23%	0.69%	1.15%		8.040E-04	5.305E-04	1.729E-03
35	2.66	95.80	98.46	1.10	64.51%	22.26%	10.05%	2.69%	0.12%	0.12%	0.24%		1.758E-03	1.118E-03	3.822E-03
36	2.54	98.46	101.00	0.58	18.74%	50.63%	23.37%	5.56%	0.24%	0.65%	0.81%		8.807E-04	6.465E-04	1.843E-03
37	2.50	101.00	103.50	0.51	10.51%	50.02%	27.66%	9.25%	0.25%	0.84%	1.47%		3.685E-04	2.330E-04	8.028E-04
38	2.58	103.50	106.08	0.55	17.34%	47.68%	24.70%	7.97%	0.25%	0.74%	1.32%		3.988E-04	2.473E-04	8.741E-04
39	2.52	106.08	108.60	0.75	42.76%	32.43%	17.26%	5.70%	0.31%	0.69%	0.85%		8.387E-04	5.235E-04	1.834E-03
40	1.50	108.60	110.10	0.90	52.26%	29.27%	12.54%	4.88%	0.00%	0.70%	0.35%		1.090E-03	6.608E-04	2.408E-03
41	3.60	110.10	113.70	0.59	20.71%	50.21%	20.85%	6.05%	0.28%	0.85%	1.04%		6.910E-04	4.749E-04	1.469E-03
42	2.50	113.70	116.20	1.20	72.75%	16.00%	8.10%	2.24%	0.20%	0.20%	0.51%		2.005E-03	1.278E-03	4.356E-03
43	2.50	116.20	118.70	1.19	71.81%	17.78%	8.06%	2.01%	0.20%	0.05%	0.10%		2.210E-03	1.446E-03	4.764E-03
46	2.50	123.80	126.30	0.71	36.90%	40.30%	16.50%	4.50%	0.10%	0.70%	1.00%		1.258E-03	9.152E-04	2.639E-03
49	3.56	128.94	132.50	0.77	44.34%	30.81%	16.63%	6.03%	0.16%	0.49%	1.55%		6.708E-04	3.887E-04	1.505E-03
50	2.56	134.00	136.56	0.57	76.29%	12.88%	3.39%	5.44%	0.20%	0.53%	1.26%		1.223E-03	9.924E-04	2.508E-03
51	2.44	136.56	139.00	0.77	44.04%	32.11%	16.12%	5.68%	0.27%	0.56%	1.22%		8.360E-04	5.130E-04	1.839E-03
52	2.50	139.00	141.50	0.61	90.81%	4.55%	1.49%	2.01%	0.18%	0.18%	0.79%		2.867E-03	2.678E-03	5.790E-03
53	2.68	141.50	144.18	0.52	65.41%	29.25%	2.52%	1.57%	0.63%	0.31%	0.31%		1.570E-03	1.372E-03	3.188E-03
54	2.02	144.18	146.20	0.60	26.66%	39.99%	21.66%	8.81%	0.67%	0.74%	1.48%		3.386E-04	1.931E-04	7.640E-04
55	2.60	146.20	148.80	0.70	39.45%	31.80%	18.02%	7.90%	0.72%	0.68%	1.44%		3.372E-04	1.763E-04	7.876E-04
56	3.00	148.80	151.80	0.63	28.73%	43.09%	19.89%	6.63%	0.00%	0.55%	1.10%		5.669E-04	3.589E-04	1.234E-03
57	2.70	151.80	154.50	0.64	30.43%	39.57%	18.98%	7.66%	0.63%	0.74%	1.99%		3.490E-04	1.953E-04	7.933E-04
58	2.40	154.50	156.90	0.60	23.91%	46.14%	20.35%	7.10%	0.37%	0.74%	1.40%		4.565E-04	2.813E-04	1.003E-03
59	2.52	156.90	159.42	0.59	17.22%	54.57%	16.87%	9.27%	0.31%	0.79%	0.97%		3.407E-04	1.997E-04	7.612E-04

Sample number	Thickness (m)	Depth (m) from	Depth (m) to	Mean d (mm)	φ 5 >2.0 Gravel	20 2.0-1.0 V Coarse sand	40 1.0-0.5 Coarse sand	50 0.5-0.25 Medium sand	80-140 0.25-0.1 Fine sand	170-200 0.1-0.05 Very fine sand	Pan less than 0.05 Fines (Silt and clays)	Hazen K (m/s)	Kozney-Carman K (m/s)	Beyer K (m/s)
60	2.58	159.42	162.00	0.78	42.90%	46.52%	7.82%	2.10%	0.19%	0.14%	0.33%	2.441E-03	1.940E-03	5.025E-03
61	3.00	162.00	165.00	0.74	38.07%	48.33%	9.83%	2.56%	0.26%	0.17%	0.78%	1.964E-03	1.561E-03	4.045E-03
62	2.04	165.00	167.04	0.56	74.92%	11.03%	8.68%	3.71%	0.18%	0.63%	0.86%	1.099E-03	8.750E-04	2.262E-03
64	2.54	169.66	172.20	0.59	83.24%	9.58%	2.93%	2.77%	0.17%	0.41%	0.91%	1.716E-03	1.474E-03	3.493E-03
65	2.46	172.20	174.66	0.76	40.11%	49.01%	7.24%	2.68%	0.43%	0.21%	0.32%	2.361E-03	1.880E-03	4.860E-03
66	2.49	174.66	177.15	0.69	31.85%	50.49%	12.86%	3.58%	0.14%	0.29%	0.79%	1.601E-03	1.252E-03	3.305E-03
67	1.00	177.15	178.15	0.54	11.69%	53.99%	25.72%	6.38%	0.25%	0.64%	1.35%	6.164E-04	4.306E-04	1.305E-03
68	0.85	178.15	179.00	0.51	64.90%	20.31%	5.74%	6.33%	0.66%	0.59%	1.47%	9.474E-04	7.493E-04	1.952E-03
69	3.28	179.00	182.28	0.54	7.81%	60.37%	21.21%	7.89%	0.58%	0.55%	1.58%	3.944E-04	2.486E-04	8.599E-04
70	2.52	182.28	184.80	0.57	76.62%	14.50%	3.75%	3.25%	0.29%	0.65%	0.94%	1.443E-03	1.210E-03	2.945E-03
71	2.50	184.80	187.30	0.53	66.43%	13.64%	8.35%	9.99%	0.29%	0.53%	0.76%	3.912E-04	2.519E-04	8.472E-04
72	2.60	187.30	189.90	0.72	37.82%	40.71%	13.81%	5.63%	0.39%	0.53%	1.11%	9.613E-04	6.535E-04	2.050E-03
73	2.70	189.90	192.60	0.66	33.70%	38.12%	20.17%	6.35%	0.28%	0.28%	1.10%	6.874E-04	4.440E-04	1.49E-03
74	2.50	192.60	195.10	0.43	51.70%	20.20%	15.24%	9.18%	0.88%	0.82%	1.97%	3.355E-04	2.220E-04	7.21E-04
75	2.40	195.10	197.50	0.54	70.85%	16.85%	5.16%	4.82%	0.33%	0.66%	1.32%	1.071E-03	8.553E-04	2.20E-03
76	2.50	197.50	200.00	0.46	55.30%	18.37%	10.07%	11.45%	0.99%	1.12%	2.70%	2.423E-04	1.454E-04	5.37E-04
77	2.50	200.00	202.50	0.54	70.98%	14.31%	5.11%	7.33%	0.40%	0.57%	1.31%	7.391E-04	5.447E-04	1.54E-03
78	2.64	202.50	205.14	0.41	48.93%	24.49%	10.99%	11.19%	0.75%	1.00%	2.65%	2.969E-04	1.942E-04	6.40E-04
79	3.46	205.14	208.60	0.49	60.93%	19.75%	8.39%	7.76%	0.66%	0.63%	1.87%	3.923E-04	2.577E-04	8.45E-04
80	2.20	208.60	210.80	0.49	59.40%	15.04%	12.96%	8.69%	1.09%	0.71%	2.11%	3.101E-04	1.938E-04	6.78E-04
81	1.96	210.80	212.76	0.53	67.39%	12.88%	6.35%	8.88%	0.79%	1.11%	2.60%	2.965E-04	1.781E-04	6.57E-04
82	2.49	212.76	215.25	0.56	73.27%	11.12%	5.54%	7.17%	0.69%	0.63%	1.58%	4.118E-04	2.634E-04	8.94E-04
83	2.50	215.25	217.75	0.45	53.49%	20.45%	10.14%	11.03%	0.72%	1.19%	2.98%	2.536E-04	1.553E-04	5.58E-04

APPENDIX D: CALIBRATED AND VALIDATED HEADS AT STEADY-STATE

Table showing the observed and simulated heads for 1970 with their respective mean error (ME), mean absolute error (MAE), and root mean squared error (RMSE).

Well Number	Latitude	Longitude	ME (m)	MAE (m)	RMSE (m)	Observed Heads (m)	Simulated Heads (m)
3	781664	3757880	1.44	1.44	1.44	950	951.44
5	787796	3756980	9.28	9.28	9.28	990	999.28
6	777159	3749130	-4.91	4.91	4.91	890	885.09
7	778700	3749960	9.98	9.98	9.98	910	919.98
8	773921	3748470	5.68	5.68	5.68	890	895.68
9	772203	3744250	11.14	11.14	11.14	810	821.14
10	757043	3725510	19.33	19.33	19.33	860	879.33
11	784425	3764410	13.49	13.49	13.49	990	1003.49
12	783795	3764780	18.77	18.77	18.77	1000	1018.77
13	786990	3760260	21.98	21.98	21.98	1000	1021.98
15	787030	3762260	4.64	4.64	4.64	980	984.64
18	786686	3757340	13.56	13.56	13.56	990	1003.56
19	783614	3752600	1.81	1.81	1.81	950	951.81
22	771626	3747910	7.00	7.00	7.00	920	927.00
23	772497	3746400	7.33	7.33	7.33	880	887.33
24	773226	3747470	-14.46	14.46	14.46	860	845.54
25	769266	3747180	-0.42	0.42	0.42	870	869.58

Table showing the validation of the 1970 steady state model was based on the year 2010, where also the table shows the observed and simulated heads and their respective ME, MAE, and RMSE.

Well Number	Latitude	Longitude	ME (m)	MAE (m)	RMSE (m)	Observed Heads (m)	Simulated Heads (m)
2	767962	3734200	7.32	7.32	7.32	849.14	856.46
3	766134	3732100	8.46	8.46	8.46	848.17	856.63
6	777079	3744750	-3.23	3.23	3.23	875.64	872.41
9	763900	3726910	9.65	9.65	9.65	863.23	872.88
10	776392	3745520	-2.92	2.92	2.92	888.67	885.75
15	772543	3751640	-3.46	3.46	3.46	981.00	977.54
25	762529	3736910	7.71	7.71	7.71	859.27	866.98
26	766676	3739780	5.94	5.94	5.94	858.69	864.63
28	766945	3740280	5.78	5.78	5.78	867.18	872.96
29	773836	3746450	0.26	0.26	0.26	880.35	880.61
30	774538	3747230	-1.05	1.05	1.05	886.15	885.10
31	773819	3745370	0.48	0.48	0.48	885.05	885.53
33	768286	3738200	5.92	5.92	5.92	872.94	878.86
42	761535	3737160	7.82	7.82	7.82	859.93	867.75
43	772478	3744260	2.25	2.25	2.25	893.41	895.66
44	777189	3747980	-9.65	9.65	9.65	883.58	873.93
46	774069	3748530	-5.90	5.90	5.90	903.39	897.49
48	773960	3752110	-10.60	10.60	10.60	1011.25	1000.65
53	776229	3747850	-6.99	6.99	6.99	896.23	889.24